University of Wisconsin Milwaukee
UWM Digital Commons

Theses and Dissertations

August 2018

Optimal Design of Green Roofs: Mathematical Model and Experimental Evidence

Jing Hong
University of Wisconsin-Milwaukee

Follow this and additional works at: https://dc.uwm.edu/etd

 Part of the Architectural Engineering Commons, and the Sustainability Commons

Recommended Citation
Hong, Jing, "Optimal Design of Green Roofs: Mathematical Model and Experimental Evidence" (2018). *Theses and Dissertations*. 1825.
https://dc.uwm.edu/etd/1825

This Dissertation is brought to you for free and open access by UWM Digital Commons. It has been accepted for inclusion in Theses and Dissertations by an authorized administrator of UWM Digital Commons. For more information, please contact open-access@uwm.edu.

OPTIMAL DESIGN OF GREEN ROOFS: MATHEMATICAL MODEL AND EXPERIMENTAL EVIDENCE

by

Jing Hong

A Dissertation Submitted in

Partial Fulfillment of the

Requirements for the Degree of

Doctor of Philosophy

in Architecture

at

The University of Wisconsin-Milwaukee

August 2018

ABSTRACT

OPTIMAL DESIGN OF GREEN ROOFS: MATHEMATICAL MODELS AND EXPERIENTAL EVIDENCE

by

Jing Hong

The University of Wisconsin-Milwaukee, 2018

Under the Supervision of Professor D. Michael Utzinger

Green roofs ease the heat island effect and decrease storm water runoff. Optimizing green roof design helps achieve these goals more efficiently. This dissertation proposes energy and mass models of green roofs and validates them through experimental evidence.

The energy and mass transfer models proposed in this dissertation can be programmed in any simulation tools, and benefits architects and engineers optimizing their green roof design. The mathematical models of green roofs were validated by the measured soil temperature and water content of the Golda Meir Library green roof.

Using energy and mass balance models, this research found the effects of the surface color, soil depth, and plant types on the surface temperature of a green roof. The green roof surface temperature can be reduced by lighter surface colors, shallow soil depth, and the use of plants with lower internal leaf resistance and larger leaf size. It also found the effects of the vegetation coverage, soil porosity and depth and plant

types on storm water runoff reduction. The storm water runoff can be reduced by higher vegetation coverage, larger soil porosity (void fraction) depth, and the use of plants with lower internal leaf resistance and larger leaf size.

© Copyright by Jing Hong, 2018
All Rights Reserved

To my dear family and friends,

I am thankful for each and every person who has contributed to the completion of my dissertation.

TABLE OF CONTENTS

LIST OF FIGURES

LIST OF TABLES

ACKNOWLEDGEMENTS

Special thanks to Professor Michael Utzinger for his wise suggestions and helpful criticisms. Without his guidance, I could not have this research done well.

Professors James Wasley, Filip Tejchman and Alice Yan have also been very helpful. Their comments enhance my dissertation.

I could not have the opportunity to pursue a doctoral degree without the spiritual and financial support given by my Mom and Dad.

I would also like to express my gratitude to Milwaukee Metropolitan Sewage District and University of Wisconsin- Milwaukee for their support of this green roof research.

1 Research Motivation

When I was an undergraduate mechanical engineering student studying HVAC design in 2005, I learned that the two major goals of mechanical engineering are to make the building well insulated while increasing the efficiency of the heating and cooling systems. During my master's degree in architecture, I used thermal simulation tools to study energy consumption of buildings impacted by building envelopes and human behavior. Those experience led me to pursue further studies seeking a better solution to improve a building's energy performance.

I began studying green roofs project on the Golda Meir Library roof supported by UWM and Milwaukee Metropolitan Sewage District (MMSD) and managed by my committee members, Professors James Wasley and Michael Utzinger in 2012. The weather data collected in this project allowed me to validate the green roof mathematical model. In this dissertation, I focused on creating the energy (temperature) and mass (water) model to predict the green roof surface temperature and the rain water retention process to reduce storm water runoff. With appropriate mathematical models, a green roof's ability of reducing heat island effect and storm water runoff can be simulated prior to installation. With the mathematical models proposed in this dissertation, the designer will know if a green roof fits for the location, and which growing medium and plants should be selected for the green roof.

Green roofs are one of the most complex building components and their performance can be hard to predict. This is due to the heat transfer and mass composite in a green roof which are always in an unsteady condition and rely on the

ambient condition. A green roof model is valuable for designers in the schematic design phase and encourage its use more. Therefore, studying the mathematical models of the green roofs with better accuracy than the existing ones became the main driver for my dissertation.

1.1 The Benefit and Limitation of Green Roofs

Green roofs have potential benefits of energy savings, storm water reduction, wildlife habitat, and aesthetic influence. One big contribution of green roofs is the reduction of the heat island effect, an environmental hazard caused by global warming and urban sprawl. It raises the air temperature in densely built-up environments above that of the surrounding countryside (Wong, Akbari, Bell & Cole, 2011). Green roof vegetation reduces the heat island effect at both the urban and building scale (Susca, Gaffin & Dell'Osso, 2011). In the Los Angeles basin, increasing 1% vegetation can significantly reduce the urban heat island effect (Sailor, 1995)

Some researchers argue that green roofs are not better than other cool roofs when it comes to the heat island effect, such as white roof (Sproul, Benjamin& Rosenfeld, 2014). The Berkeley Lab Report- "Economic Comparison of White, Green, and Black Flat Roofs in the United State" explains: "Both white and green roofs do a good job at cooling the building and cooling the air in the city, but white roofs are three times more effective at countering climate change than green roofs". However, it only refers to the fact that the lighter color surface has higher heat reflectivity, and does not take into account the effect that the convective heat transfer and evapotranspiration on

green roof surface can offset heat absorption and reduce the surrounding air temperature (Oke, 2002).

Even though both white roof and green roofs can reduce heat island effect, their approaches are different. Takebayashi and Moriyama (2007) compare the sensible heat flux on the surface of white and green roofs. Both the highly reflective white paint surface and the green roof have small sensible heat flux. However, the surface with highly reflective white paint cools due to high albedo. On the contrary, the green surface cools by evaporation while the net radiation is large.

Apart from reducing heat island effect, green roofs make other important contributions. Scholars demonstrated that green roofs can efficiently retain water (Berndtsson, 2010). Through green roofs, precipitation is drained in three ways: soil absorption, evapotranspiration, and drainage (Oke, 2002). Green roofs reduce storm water runoff, lowering the risk of urban floods, and improving the urban water balance approach to the natural environment (Bengtsson et al., 2005; Mentenset al., 2006; VanWoert et al., 2005).

In addition to reducing heat island effect and storm water runoff, green roofs can help save energy for heating and cooling, especially for the structures with poor insulation. For higher R-value modern buildings, green roofs do not significantly improve thermal resistance, which does not reduce heating and cooling energy (Castleton, Stovin, Beck & Davison, 2010). Additionally, the energy benefits of green roofs depend on the water content and weather. Wet green roofs have better cooling performance and the dryer the roof, the lower the heating demand (Zinzi & Agnoli, 2012).

Some scholars raise reasonable arguments about whether green roofs are the most efficient way to reduce heating and cooling load (Castleton, Stovin, Beck & Davison, 2010). Green roof plants have to survive harsh conditions. However, suitable plants, like sedum, do not absorb water as efficiently as other plant species. Scott MacIver, a biologist at York University, who co-wrote the city's new guidelines for biodiverse green roofs, stated that sedum actually absorbs heat instead of reflecting it. "The problem is that sedum plants aren't really performing on green roofs," he notes. "They're just there." Choosing the appropriate plants is critical to green roof performance.

In addition to the thermal and water retention benefits, green roofs bring their surrounding environments benefits improving water runoff quality, mitigating the heat island effect, creating habitats for wildlife, reducing noise, air pollution, and providing aesthetically pleasing landscapes (Hodo-Abalo, Banna, & Zeghmati, 2012; Van Renterghem and Booteldooren, 2009; Currie and Bass, 2008; Yang et al., 2008; Brenneisen, 2003; Dunnett et al., 2008; Gedge and Kadas, 2005).

1.2 Problem Statement

The goal of this dissertation is to create a complex heat and mass transport model of a vegetated roof with green roof materials and assemblies as parameters and climate data as inputs. Various elements, including weather condition, green roof characteristics, and the insulation underneath roofs, can affect green roofs' performance in the level of energy efficiency and water management (Berndtsson, 2010; Del Barrio,1998; Jim, 2014; Kumar & Kaushik, 2005; Pandey, Hindoliya, & Mod,2013).

However, weather conditions and buildings' genetic envelops shall not be seen as parts of green roof design. Weather conditions cannot be controlled, and a building's original envelopes is out of the scope of a green roof. Only variable elements of green roofs are studied in this dissertation. A model integrating green roofs' variable elements are optimally studied for designing green roofs.

To achieve this goal, following questions need to be answered in this dissertation:

1. What are the problems is the green roof model addressing?

2. How will the model be validated?

3. How will the model be tested for potential error as parameters move further from the specific values of the Golda Meier Library green roof?

4. How would members of the building design team use green roof heat and mass transport model to analyze green roof design?

1.3 Dissertation Structure

This dissertation includes four chapters: 1. Research Motivation. 2. Literature Review. 3. Methodology. 4. Results. 5.Conclusions and Discussion. Chapter 1 summaries the history, functionality and limitations of green roofs. Chapter 2 states the previous studies researching the green roofs' mathematical models and performance. Chapter 3 creates and validates the mathematical models of the vegetated roof heat and mass transport. Chapter 4 studies the relative importance of different green roof parameters. Chapter 5 concludes the findings in this dissertation.

2 Literature Review

To discover the correlation between green roof characteristics and performance, energy and water balance equations are the proper resources to identify and quantify green roofs' characteristics. In this chapter, previous studies presenting the correlations between particular characteristics of green roofs and their performance in the terms of energy performance and water management are discussed.

2.1 Brief History of Green Roofs

A green roof is a roof covered partially or completely by living vegetation. It can include the layers of growing medium, a waterproofing membrane, root barrier, drainage, and irrigation systems.

The green roof is not a new term. People realized urbanization had gradually eliminated vegetation from the earth and began to use green roofs to mitigate the loss of green space. (Vandermeulen, Verspecht, Vermeire, Van Huylenbroeck, & Gellynck, 2011). Especially in high-density cities, green elements can be hard to find. Buildings replaced human and wildlife's habitats. In the past decades, modern architects began realizing the toll of old-fashioned building industry on the natural habitat. They advocated that architects should leave the land no worse than they found it (Wells, 1981). When architects eliminate an area of vegetation, they should replace it. With the trend of growing living materials on architecture, green roofs have become a prevalent alternative passive strategy in sustainable design.

Modern green roof technologies boosted in early 1960s in Germany when the first green roof systems were developed and marketed on a large scale (Kaluvakolanu,

2006). Modern green roofs are an alternative strategy and believed as a new and advanced building technology nowadays. However, the concept of the green roof does not only include the contemporary definition, but also its past vernacular characteristics. Some of the vernacular examples include historic underground buildings, cave-dwellings, vegetated roofs, earth sheltered buildings or earth-covered buildings are the ancient forms of green roofs, which can be traced back to ancient China, Tunisia, Turkey, Italy, and Afghanistan. Contrary to modern green roofs, ancient green roofs are generally not a choice or a style, but a prerequisite to build a reliable and comfortable living space. Ancient green roofs have the same functions as the modern green roofs in respect to their thermal flows and water absorption capacity.

Figure 1. Matmata troglodyte dwelling. Source: http://www.freresdudesert.org

In southern Tunisia, a small village called Matmata has local Berber residents living in traditional underground dwellings. This type of housing is called “Troglodyte Dwelling”, which became prominent by serving as the home for the main characters in Star Wars, as shown in Figure 1. In this region, this type of underground housing appeared for over centuries. The underground buildings in Matmata prevented the dwellers from enemies and reduced the demand of construction materials. At the time, Troglodyte Dwellings provided the residents with comfortable living environments for centuries.

Most of the earth-covered buildings have been abandoned by residents or mandatorily vacated by governments because they are not safe for people to live. However, in China, a particular form of earth-covered building, Yao Dong, was reserved and rehabilitated as a type of modern dwelling in north central China. Yao Dong is the cave dwelling built underground or by cliffs, as shown in Figure 2. Yao Dong has been the typical dwelling in that area since Zhou dynasty (1050-771 BC) due to the semi-arid climate at Loess Plateau and lack of woods (Hou & Wang, 1999). Even though the current economy and technologies allow farmers in that area to build their houses with bricks and concrete, most of them still prefer to live in Yao Dongs. Because the earth that surrounds the indoor spaces serves as an effective insulator to keep the indoor warm in cold seasons and cool in hot seasons, the dwellings maintain a comfortable indoor environment. Yao Dongs are an effective strategy to enhance the building energy performance with less cost for the farmers. The modern Yao Dong brings some sustainable strategies into its design, as shown in Figure 3.

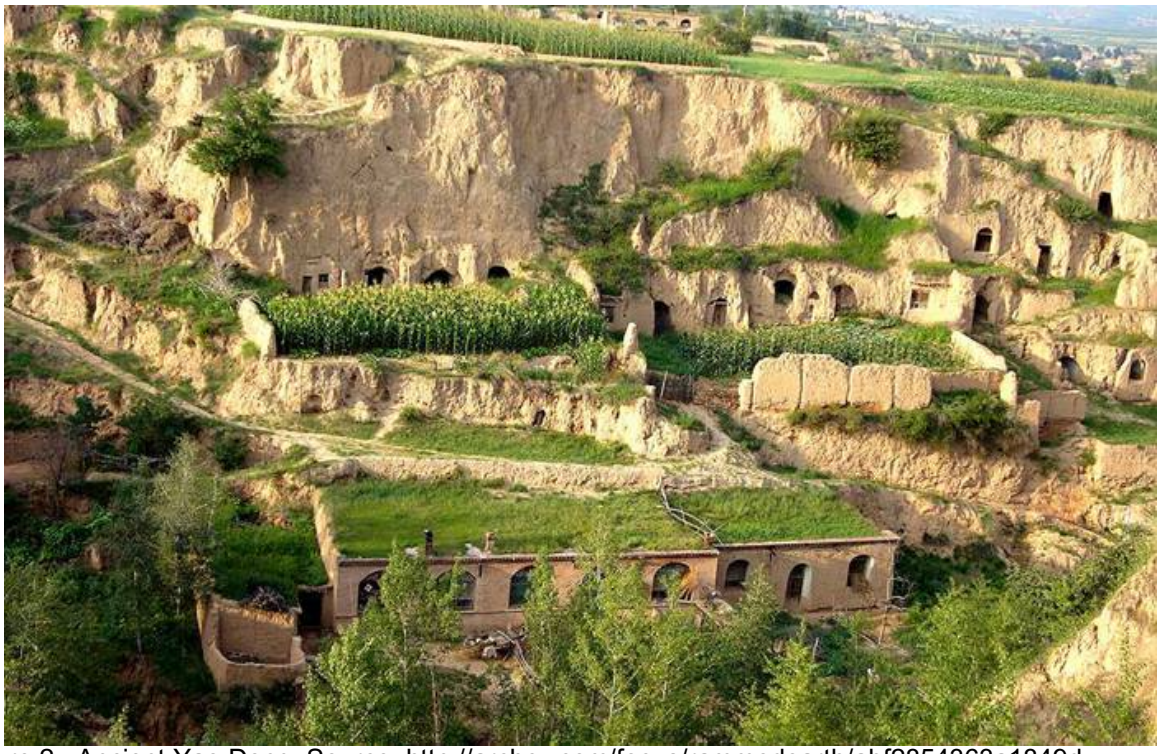

Figure 2. Ancient Yao Dong. Source: http://archcy.com/focus/rammedearth/abf2854363a1849d

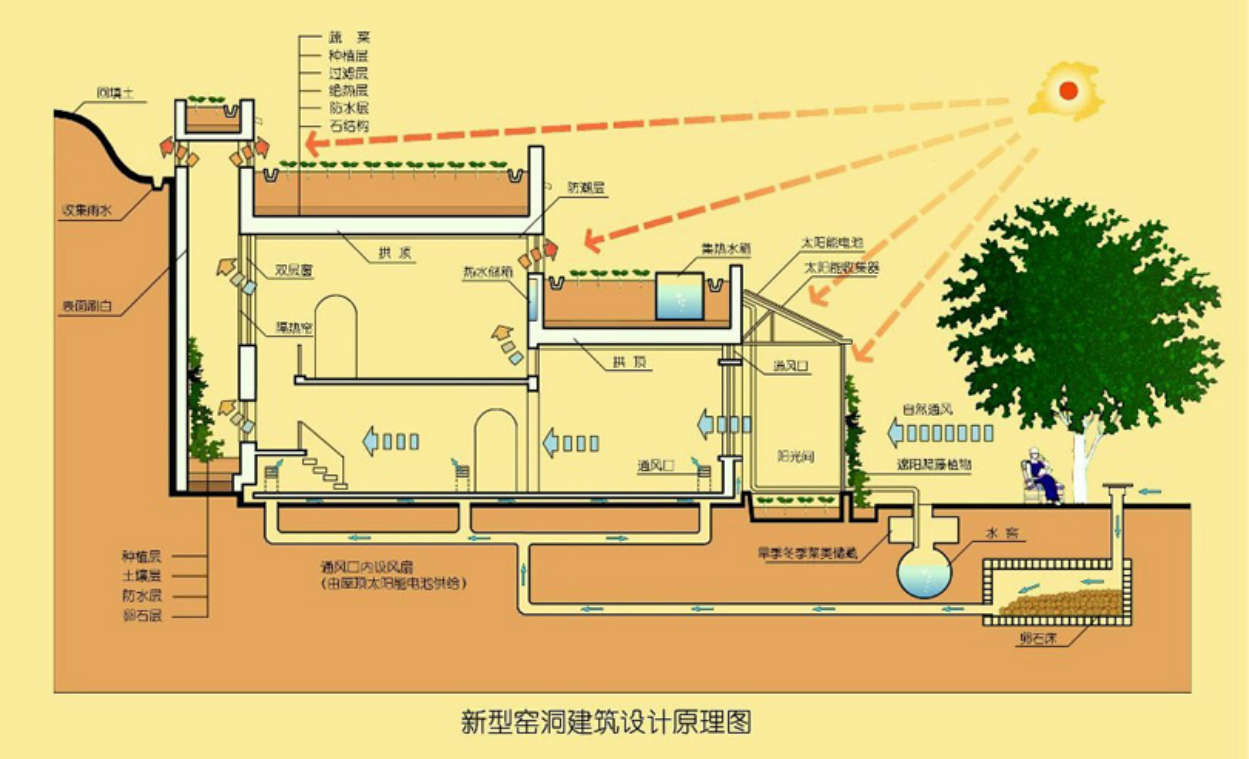

Figure 3. Modern Yao Dong section. Source: https://www.world-habitat.org/world-habitat-awards/winners-and-finalists/the-new-generation-of-yaodong-cave-dwellings-loess-plateau/#award-content

Unlike the necessity of the ancient green roofs, the contemporary buildings with green roofs aim to bring sustainability to the designs.

In the early 1980s, scholars started working on solutions on how to build without destroying the land. Earth Day in the late 1960s and the Energy Crisis of late 1973 and 1974 both led to increased thinking among architects about how buildings could be more energy efficient and environmentally appropriate. Ian McHarg's *Design with Nature* from the 1960s was an early architectural book focusing on site planning and building placement being appropriate to preserving the existing environments. Malcolm Wells was an architect who was regarded as “the father of modern earth-sheltered architecture” (Higginson, 2006). He believed that the earth’s surface should be “made for living plants, not industrial plants” So he advocated the “underground architecture”. He also made environmental ethics a fundamental part of his design process. His checklist of whether a building enhances or destroys the surrounding environment was an early, explicit, environmentally ethical approach to design. It led him to view vegetated roofs as the only environmentally appropriate way to build. In 1981, Malcolm Wells wrote his book *Gentle Architecture* to advocate his initial idea of contemporary earth-covered architecture. In his follow-up book, *The Earth-sheltered House: An Architect's Sketchbook,* published eighteen years later, Wells illustrated his ideal “Gentle Architecture” to describe the concept of contemporary earth-covered buildings with his own sketching. Gentle Architecture is a style of earth-covered building that minimizes the negative impact on the environment resulting from construction without compromising ecology.

Wells proposed the concept of earth-covered buildings, and believed that instead of launching buildings, architects should train the crews to “sail” them. Architects should be fully involved in their projects throughout the entire process. Wells also argued for the importance for architects to consider the sustainability in an original design. The philosophy of his theory aimed to minimize the negative impact generated by humans. He attempted to educate the public about how nature elements should be part of architecture. His design is always hidden in an idyllic environment. In his projects, he widely applied earth cover and passive solar strategies in residential, commercial, and public facilities. Wells proposed to lower the exterior walls down to semi-underground and use the low heat conductivity soil for insulation. In addition, he used stack ventilation in most of his projects to bring fresh air into the underground earth-covered buildings. The natural ventilation strategy minimizes the use of fans. Wells claimed that the earth-covered buildings can reduce energy use. His argument is founded in his practical experience and observation, and it is a valuable reference for the potential benefits of earth-covered architecture.

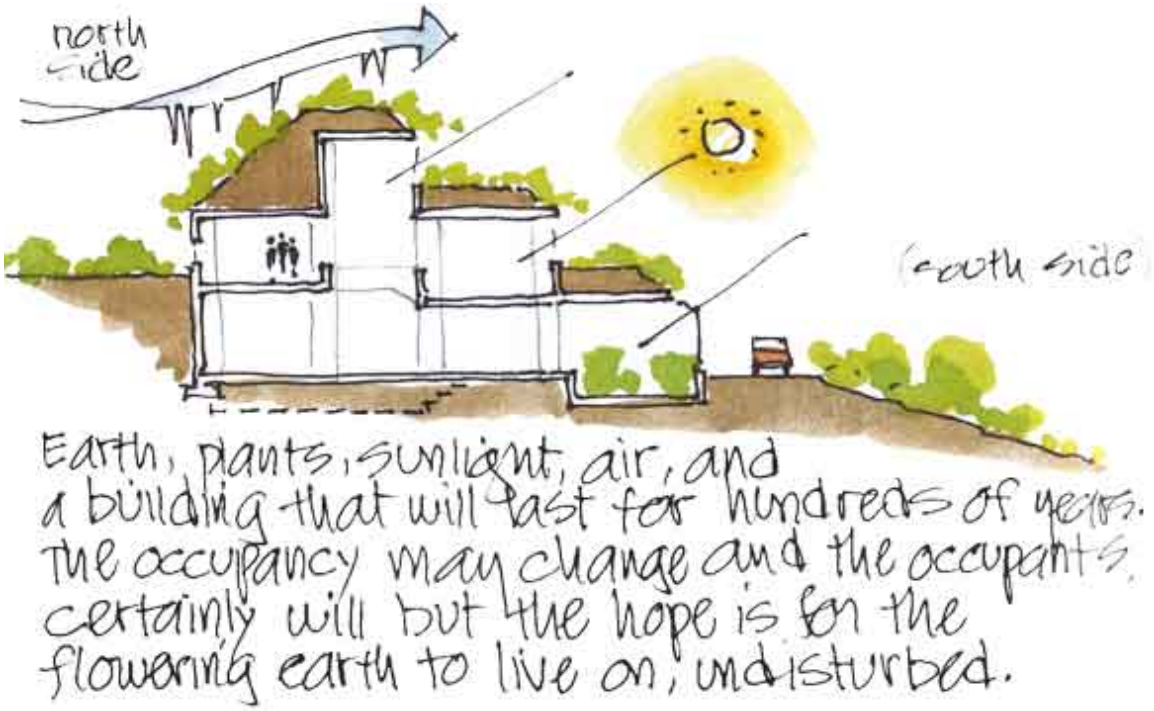

Figure 4. Malcom Wells's sketch of earth-covered house. Source: The Earth-Sheltered House: An Architect's Sketchbook

James Wines, an architect associated with environmental design, emphasizes integrating buildings with their surrounding context. Unlike Malcom Wells, he is not an ecological ethicist, but saw the environment as an opportunity for a designer to explore the dichotomies between nature and the built environment. This difference between ethical imperative of green design and nature as a design element continues to exist today in architectural practice.

Emilio Ambasz is another early proponent of 'green' architecture. Similar to James Wines, Ambasz sees nature as a design opportunity and is not as environmentally strident as Malcolm Wells (nor as openly ethical). Within his works, nature must interact with the structure in a way he calls "Green over the gray". In many of his projects, this idea manifests itself through green roofs and gardens built into the

projects. Ambasz believes that architects should minimize the impact of buildings on environment. Architecture could be both environmentally friendly and aesthetically pleasing. His work, Casa de Retiro Espiritual, is a retreat center built underground. The only components above ground are two tall white walls standing against each other. Emilio Ambasz brought natural elements into the design of Casa de Retiro Espiritual (Alassio & Buchanan,2005). Besides the poetic and idyllic mood built by Ambasz, this building achieves the sustainable design principles. He dug deep into the earth and took advantage of natural cooling and insulation. Even though it was built below ground, Ambasz still maximized natural light with the fluid shapes of the openings (Pham, 2012). However, as shown in Figure 4, the landscapes around this building is greener than its surrounding. The choice of the plants is not adaptive to this location and requires irrigation, which is not a water sustainability strategy.

Figure 5. Casa de Retiro Espiritual. Source: Emilio Ambasz: Casa de Retiro Espiritual

Modern green roofs have their "roots" in earth-covered buildings, but advanced technologies and feasibility make green roofs efficient and acceptable to most residents and designers. Modern green roofs are built with reliable technologies, such as sophisticated irrigation and protection against from water leakage. Later on, the use of green roof became tightly connected with sustainability due to its ecological benefits, including reducing energy consumption for heating and cooling, storm water retention, and heat island mitigation. Green roofs have additional benefits, such as habitat restoration, filtration of acid rain and air pollutants, noise pollution reduction, and the therapeutic effects found from being in the presence of nature.

The green roof on the Delft University of Technology (DUT) Library is one of the largest green roofs in Netherland. Mecanoo Architecten designed the library and claimed it as “a building that does not really want to be a building, but a landscape.” (Mecanoo, 1998) The green roof maintains the existing green spaces. As shown in Figure 4, the library has a sloped plane extending the grass from the ground to the very edge of the roof, allowing people to walk to the top. At the top of the library, the roof has a steel cone, giving the structure its unique, identifying shape. The opening around the cone introduces daylight for the study space, as shown in Figure 6. In the winter, the green roof is converted into a sledding hill, so people can utilize the green roof throughout the year. Figure 7 illustrates the details of the roof. The component numbered 91 is the soil layer, which is a six inch (15 cm) lightweight deep substrate. A roof with a substrate 5cm thick can retain 40% rainwater, and one thicker than 50cm can take 90% water (Liesecke, 1999). Based on the estimated water absorption ratio, the green roof at DUT can retain approximately more than 50% rainwater.

Figure 6. University Library in Delft. Source: http://www.mecanoo.nl/

Figure 7. Cone holding study space. Credit to: Mike Utzinger

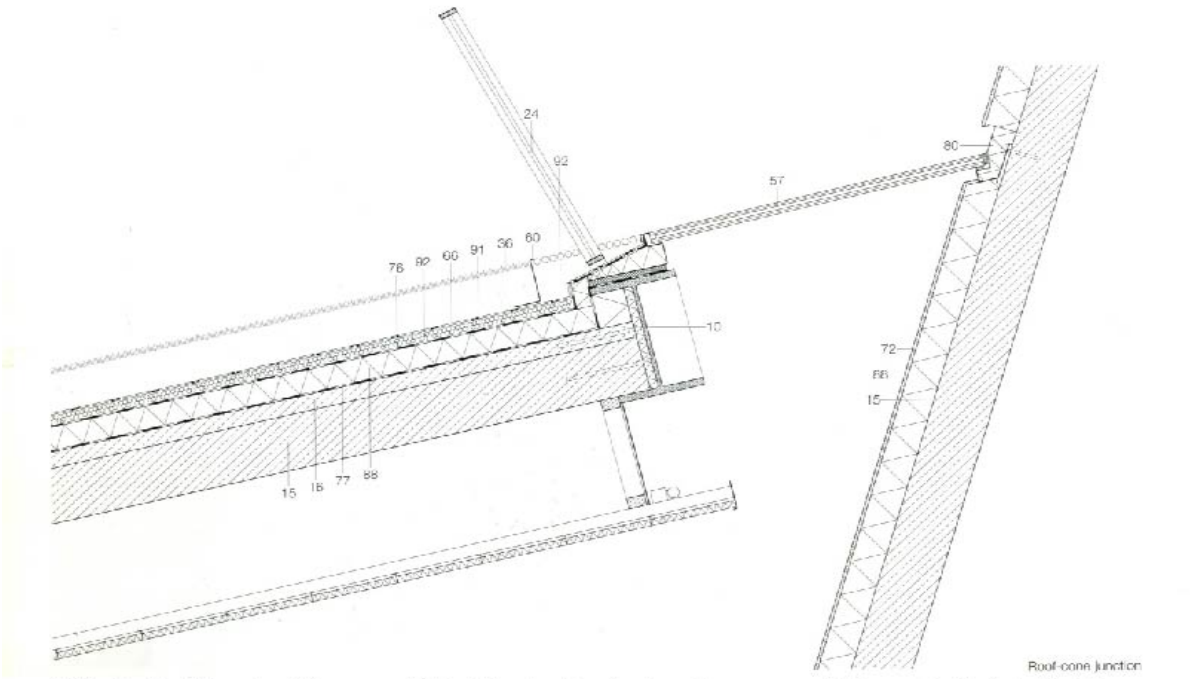

10 Steel I-section 460mm deep (IPE)
15 220mm reinforced concrete
16 60mm concrete column
17 Reinforced concrete column
20 Steel I-section 260mm deep (HEB)
24 Railing
36 Extensive turfing
57 Insulating glass: 12mm toughened glass +2 panes of 8mm laminated glass
58 70 mm trapezoidal sheet
59 3 mm aluminium sheet
60 90 x 180 x 20mm Cor-Ten steel angle, cover sheet
66 Filter mat
72 Rendering
76 6 mm root-resistant sheeting, 1.2 mm EPDM coal
77 0.2 mm polyethylene sheet vapour barrier
80 Thermally insulated rooflight support
88 90 mm foam glass thermal insulation
91 Substrate
92 40 mm gravel layer, drainage chippings
94 Drainage pipe

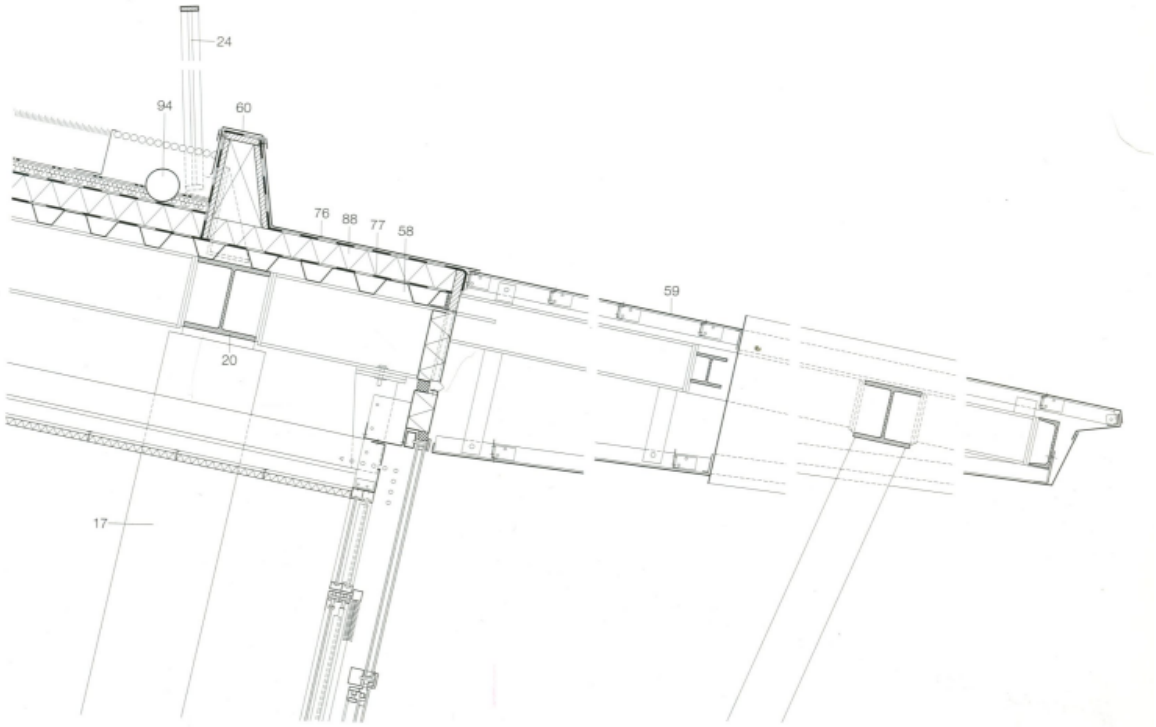

Figure 8 Green roof details of Delft University library. Source: Roof Construction Manual

The green roof of California Academy of Sciences (CAS) building is another example of minimizing the destruction of the existing green spaces. This 2.5 acres green roof consists of two 90-foot domes above the roofline and rolling hills, which trace back the contours of the planetarium and artificial rainforest. The green roof is penetrated with skylights around the building's central piazza. Unlike DUT's selection of grass for the green roof, CAS chose native plants including annual and perennial species that attract wildlife like birds and bees. 90-98% of the building rainfall is absorbed by this green roof (CAS, 2009).

Figure 9. The native plants on California Academy of Sciences green roof. Source: https://www.swagroup.com/projects/california-academy-of-sciences/

Figure 10. The skylight of California Academy of Sciences. Source:

https://www.swagroup.com/projects/california-academy-of-sciences/

2.2 Mathematical Model of Green Roofs

Mathematical models can help build simulation programs and explore the performance of green roofs in energy saving and water retention. There have been studies proposing predictive models of energy and water performance with green roof energy balance and mass balance.

2.2.1 Energy Balance of Green Roofs

For roofs, the major heat transfers going through surfaces are radiation, conduction, and convection (Lienhard, 2013). In summer conditions, the majority of the energy added to the surface of a building is from solar radiation absorption including absorbed solar radiation, infrared radiation exchange, and convective heat gain or loss on an exterior surface to maintain an energy balance (Kuehn, Ramsey & Threlkeld,

1998). Organisms like plants on the roof include heat exchanges immersed in air, water and soil driven by convection, conduction, and radiation (Gates, 2012). Compared to conventional roofs, water plays a more significant role in thermal convection and conduction through green roofs (Gates, 2012).

Basically, energy balance of green roofs can clearly present the heat flux through radiation, conduction, and convection. Studying mathematical models of green roofs can find the correlation between energy performance and characteristics of green roofs.

Regarding the level of energy performance, sensitive and latent heat transfer are the two heat flows in foliage and soil layers (Gates, 2012). Therefore, the characteristics that impact energy performance can be sorted out from the heat balance equations in green roof mathematical models.

We see the whole green roof system as a simple layer, without considering the heat exchange between foliage and ground, or latent heat loss through evaporation. The three major heat transfer equations are listed below:

$$\frac{dq_{cond}}{dt} = kA\frac{\Delta T}{d} \tag{2.1}$$

$$\frac{dq_{conv}}{dt} = \overline{h_c}A\Delta T \tag{2.2}$$

$$\frac{dq_{solar}}{dt} = I_{solar}A \tag{2.3}$$

$$\frac{dq_{sky\_rad}}{dt} = \varepsilon\sigma\left(T_{sky}^4 - T_{surface}^4\right)A \tag{2.4}$$

Where

$$\frac{dq_{rad}}{dt} + \frac{dq_{sky\_rad}}{dt} = -\left(\frac{dq_{cond}}{dt} + \frac{dq_{conv}}{dt}\right) \tag{2.5}$$

Currently, the most widely used mathematical model for green roof simulation is the one used by EnergyPlus EcoRoof (Sailor, 2008) and developed by the U.S. Army Corp. Engineer. The average bias of the simulation is 2.9 °C with an RMSE of 4.1°C. Sailor (2008) split the math model into heat radiation, conduction, and convection. In addition, he linearized the heat budget equations in both soil and foliage, and then solved the coefficients in the linearized equation by inverting the Conduction Transfer Functions (CTF) within the EnergyPlus solution scheme.

Sailor (2008) separated the energy balance into two parts: foliage layer and soil layer.

The Energy budget in the foliage layer:

$$F_f = k\left[I^{\downarrow}{}_s\left(1-\alpha_f\right) + \varepsilon_f I_{ir}^{\downarrow} - \varepsilon_f \sigma T_f^4\right] + \frac{k\varepsilon_g\varepsilon_f\sigma}{\varepsilon_1}\left(T_g^4 - T_f^4\right) + H_f + L_f \qquad (2.6)$$

F_f Net heat flux to foliage layer (W/m^2)

α_f Albedo (short-wave reflectivity) of the canopy

I_{ir} Total incoming long-wave radiation (W/m^2)

I_s Total incoming short-wave radiation (W/m^2)

σ Stefan-Boltzmann constant (5.67 x 10^{-8} W/m^{2}K^4)

k Fractional vegetation coverage

ε_g Emissivity of the ground surface

ε_f Emissivity of canopy

ε_1 $\varepsilon_g + \varepsilon_f - \varepsilon_f\varepsilon_g$

T_g Ground surface temperature (Kelvin)

T_f Foliage temperature (Kelvin)

H_f Foliage sensible heat flux (W/m^2)

L_f Foliage latent heat flux (W/m^2)

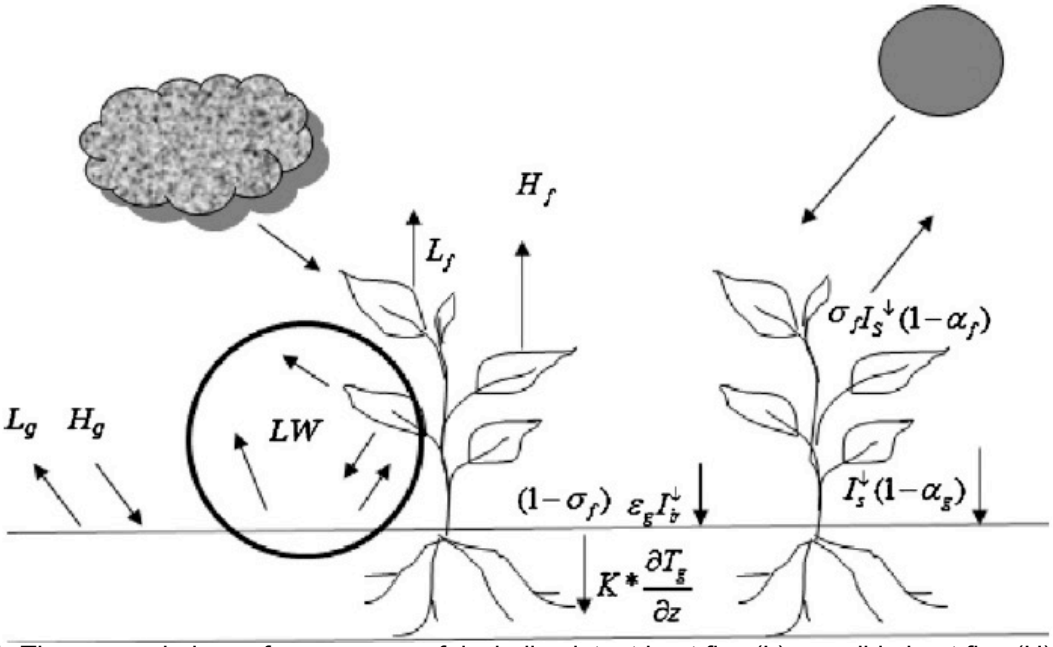

Figure 11. The energy balance for a green roof, including latent heat flux (L), sensible heat flux (H), shortwave radiation (Is) and incoming long-wave radiation (Iir) (Sailor, 2008)

The sensible heat flux in the foliage:

$$H_f = (1.1LAI\rho_{af}C_{p,a}C_fW_{canopy})(T_{af} - T_f) \quad (2.7)$$

LAI Leaf area index (m^2/ m^2)

ρ_{af} Density of air at foliage temperature (kg/m^3)

$C_{p,a}$ Specific heat of air at constant pressure (1005.6 J/kgK)

C_f Bulk heat transfer coefficient

W_{canopy} Wind speed with in the canopy (m/s)

T_{af} Air temperature with in the canopy (Kelvin)

T_f Foliage temperature (Kelvin)

Average of the air density near the foliage:

$$\rho_{af} = 0.5(\rho_a + \rho_f) \tag{2.8}$$

ρ_a Density of air at instrument height (kg/m^3)

ρ_f Density of air at foliage temperature (kg/m^3)

The air temperature within the foliage is estimated by:

$$T_{af} = \left(1 - \sigma_f\right)(T_a) + \sigma_f(0.3T_a + 0.6T_f + 0.1\,T_g) \tag{2.9}$$

T_a Air temperature at the instrument height (Kelvin)

T_f Foliage temperature (Kelvin)

T_g Ground surface temperature (Kelvin)

σ_f Fractional vegetation coverage

The wind speed within the foliage is:

$$\mathrm{W_{canopy}} = 0.83\sigma_\mathrm{f}\mathrm{W}\sqrt{\mathrm{C_{hnf}}} + (1 - \sigma_\mathrm{f})\mathrm{W} \tag{2.10}$$

W The actual wind speed above the canopy

C_{hnf} The transfer coefficient at near neutral atmospheric stability condition

$$\mathrm{C_{hnf}} = \mathrm{K_v^2}\left(\ln\left(\frac{\mathrm{Z_a - Z_d}}{\mathrm{Z_{o,f}}}\right)\right)^{-2} \tag{2.11}$$

K_v Von Karmen's constant (0.4)

Z_a The instrument height (m)

Z_d The zero displacement height (m)

$Z_{o,f}$ The foliage roughness length scale (m) Check the the work of Balick

So

$$\mathrm{Z_d} = 0.701\mathrm{Z_f^{0.979}} \tag{2.12}$$

$$\mathrm{Z_o} = 0.131\mathrm{Z_f^{0.997}} \tag{2.13}$$

Bulk heat transfer coefficient:

$$C_f = 0.01 \times \left(1 + \frac{0.3(m/s)}{W_{canopy}(m/s)}\right) \tag{2.14}$$

Latent heat flux in the foliage layer:

The latent heat transfer is achieved through transpiration, which is the process of water loss from plants.

Actual stomatal resistance $\mathrm{r_s} = \frac{\mathrm{r_{s,min}}}{\mathrm{LAI}} \mathrm{f_1 f_2 f_3}$

$$\frac{1}{f_1} = min\left[1, \frac{0.004I_s^{\downarrow}+0.005}{0.81\times(0.004I_s^{\downarrow}+1)}\right] \tag{2.15}$$

$$\frac{1}{f_2} = \begin{cases} 0 \ \ When\ \theta_r > \bar{\theta} \\ \frac{\bar{\theta}-\theta_r}{\theta_{max}-\theta_r} \ when\ \theta_r \le \bar{\theta} \le \theta_{max} \end{cases} \tag{2.16}$$

$$\frac{1}{f_3} = exp\left[-g_d\left(e_{f,sat} - e_a\right)\right] \tag{2.17}$$

f_1 Multiplying factor for radiation effect on stomatal resistance

f_2 Multiplying factor for moisture effect on stomatal resistance

f_3 Additional multiplying factor for stomatal resistance

θ_r The residual moisture content (around 0.01 m3/m3)

θ_{max} The maximum moisture content (0.3-0.6 m3/ m3)

$\bar{\theta}$ The average soil moisture in the root zone

g_d Plant specific characteristic

$e_{f,sat}$ The saturated vapor pressure at the foliage temperature

e_a Air vapor pressure

$$r_a = \frac{1}{c_f W_{canopy}} \tag{2.18}$$

r_a Aerodynamic resistance to transpiration

c_f Bulk heat transfer coefficient

W_{canopy} Wind speed with in the canopy (m/s)

The combined effect of aerodynamic and stomatal resistances to vapor diffusion:

$$r^{"} = \frac{r_a}{r_a + r_s} \tag{2.19}$$

$$L_f = l_f LAI \rho_{af} C_f W_{canopy} r^{"} \left(q_{af} - q_{f,sat}\right) \tag{2.20}$$

l_f The latent heat of vaporization (J/kg)

$q_{f,sat}$ The saturation mixing ratio at the foliage surface temperature

q_{af} The mixing ratio within the canopy

$$q_{af} = \frac{\left[(1-\sigma_f) q_a + \sigma_f \left(0.3 q_a + 0.6 q_{f,sat} r^{"} + 0.1 q_{f,sat} M_g\right)\right]}{1 - \sigma_f \left[0.6\left(1 - r^{"}\right) + 0.1\left(1 - M_g\right)\right]} \tag{2.21}$$

M_g The ratio of volumetric moisture content to the porosity of the soil. Range 0~1

The latent heat of vaporization can be also estimated by Henderson-Seller (1984) as below:

$$l_f = 1.91846 \times 10^6 \left[\frac{T_f}{T_f - 33.91}\right]^2 \tag{2.22}$$

The heat transfer processes in the foliage layer is the most complex part of the mathematical model. It is affected by the height of the plants, the leaf area index (LAI), coverage fraction, albedo, and the stomatal resistance. The characteristics of the soil of green roofs influencing energy performance are fractional vegetation coverage σ_f, albedo of ground surface α_g, emissivity of the ground surface ε_g, emissivity of canopy ε_f, soil thermal conductivity at the surface K, soil layer depth z, instrument height Z_a, displacement height Z_d, ground roughness lengths $Z_{o,g}$, and foliage roughness lengths $Z_{o,f}$, as shown in Equation 2.6-2.22 (Sailor, 2008). In contrast, the heat transfer of the soil is more straightforward. The Energy budget in the soil layer as below:

$$F_g = \left(1-\sigma_f\right)\left[I_s^{\downarrow}\left(1-\alpha_g\right)+\varepsilon_g I_{ir}^{\downarrow}-\varepsilon_g T_g^4\right]-\frac{\sigma_f\varepsilon_g\varepsilon_f\sigma}{\varepsilon_1}\left(T_g^4-T_f^4\right)+H_g+L_g+K\times\frac{\partial T_g}{\partial z} \quad (2.23)$$

F_g Net heat flux to foliage layer (W/m^2)

σ Stefan-Boltzmann constant (5.67 x 10^{-8} W/m^{2}K^4)

σ_f Fractional vegetation coverage

I_s Total incoming short-wave radiation (W/m^2)

I_{ir} Total incoming long-wave radiation (W/m^2)

α_g Albedo (short-wave reflectivity) of ground surface

ε_g Emissivity of the ground surface

ε_f Emissivity of canopy

ε_1 $\varepsilon_g+\varepsilon_f-\varepsilon_f\varepsilon_g$

T_g Ground surface temperature (Kelvin)

T_f Foliage temperature (Kelvin)

H_g Ground sensible heat flux (W/m^2)

L_g Ground latent heat flux (W/m^2)

K Soil thermal conductivity at the surface (W/mK)

z Soil layer depth

The sensible heat flux in the soil layer:

$$H_g = \rho_{ag} C_{p,a} C_{hg} W_{canopy} \left(T_{af} - T_g\right) \quad (2.24)$$

$$\rho_{ag} = \frac{\rho_a + \rho_g}{2} \quad (2.25)$$

C_{hg} The bulk transfer coefficient

$C_{p,a}$ Specific heat of air at constant pressure (1005.6 J/kgK)

ρ_{ag} The density of air near the soil surface (kg/m3)

ρ_g The density of air at the ground surface temperature

T_{af} Air temperature with in the canopy (Kelvin)

T_g Ground surface temperature (Kelvin)

W_{canopy} Wind speed with in the canopy (m/s)

$$C_{hg} = \Gamma_h \left[\left(1 - \sigma_f\right) C_{hng} + \sigma_f C_{hnf}\right] \quad (2.26)$$

C_{hnf} The bulk transfer coefficients near foliage

C_{hng} The bulk transfer coefficients near ground

Γ_h Stability factor

$$C_{hng} = r_{ch}^{-1} \left[\frac{K_v}{ln\left(Z_a / Z_{o,g}\right)}\right]^2 \quad (2.27)$$

$$C_{hnf} = \left[\frac{K_v}{\ln\left(Z_a - {}^{Z_d}/_{Z_{o,f}}\right)}\right]^2 \tag{2.28}$$

r_{ch} Turbulent Schmidt number (0.63)

K_v Von Karman constant (0.4)

Z_a Instrument height (m)

Z_d Displacement height (m)

$Z_{o,g}$ Ground roughness lengths (m)

$Z_{o,f}$ Foliage roughness lengths (m)

The atmospheric stability factor (Γ_h) is based on the sign of the bulk Richardson number:

$$\Gamma_h \begin{cases} \frac{1.0}{(1.0-16.0R_{ib})^{0.5}} & for\ R_{ib} < 0 \\ \frac{1.0}{(1.0-5.0R_{ib})} & for\ R_{ib} > 0 \end{cases} \tag{2.29}$$

Where R_{ib} is calculated from:

$$R_{ib} = \frac{2gZ_a(T_{af}-T_g)}{(T_{af}+T_g)W_{canopy}^2} \tag{2.30}$$

The latent heat flux in the soil layer:

The water vapor removal is driven by the difference between the mixing ratio of the soil surface and the air, as well as the wind speed within the canopy. The resulting latent heat flux is given by:

$$L_g = C_{e,g}l_g W_{canopy}\rho_{ag}(q_{af} - q_g) \tag{2.31}$$

$C_{e,g}$ The bulk transfer coefficient

ρ_{ag} The density of air near the soil surface (kg/m^3)

q_{af} The mixing ratio at the foliage-atmosphere interface

q_g The mixing ratio at the ground surface

$$q_g = M_g q_{g,sat} + (1 - M_g) q_{af} \quad (2.32)$$

$$C_{e,g} = \Gamma_e \left[(1 - \sigma_f) C_{eng} + \sigma_f C_{hnf} \right] \quad (2.33)$$

$C_{e,g}$ The near ground bulk transfer coefficient for latent heat flux

Γ_e The latent heat exchange stability correction factor (assumed to be the same as Γ_h)

σ_f Fractional vegetation coverage

M_g $0 \leq M_g \leq 1$, moisture saturation factor. If it is raining,$M_g = 1$, otherwise, it is equal to the surface soil moisture content.

$q_{g,sat}$ Saturation mixing ratio at ground temperature

$q_{f,sat}$ Saturation mixing ratio at foliage temperature

Sailor (2008) linearized the heat budget equations in both soil and foliage listed above, and then solved the coefficients in the linearized equation by inverting the Conduction Transfer Functions (CTF) within the EnergyPlus solution scheme.

Another numerical model of green roofs, which was developed in TRNSYS (a building simulation software), utilizes finite difference methods to divide the soil into three layers (Lazzarin, Castellotti & Busato, 2005). Each layer has a node, and each node represents the heat and mass balance of its own layer. These nodes are

numbered as I, II and III. The three other nodes, d, w and c, represent the drainage layer, waterproofing sheet, and structural concrete roof. The finite differences model of the physical system is shown in Figure 8. For instance, for node I, its balance in terms of specific fluxes is:

$$R_n + A_o + ET_{II} = G_{I,II} + ET_I + C_I \quad (2.34)$$

R_n Solar radiation flux coming into the system

A_o Adduction flux condensing outside convective and radiative thermal fluxes

ET_{II} Evapotranspiration flux of node II

ET_I Evapotranspiration flux of node I

$G_{I,II}$ Conduction flux between node I and II

C_I Thermal accumulation of node I

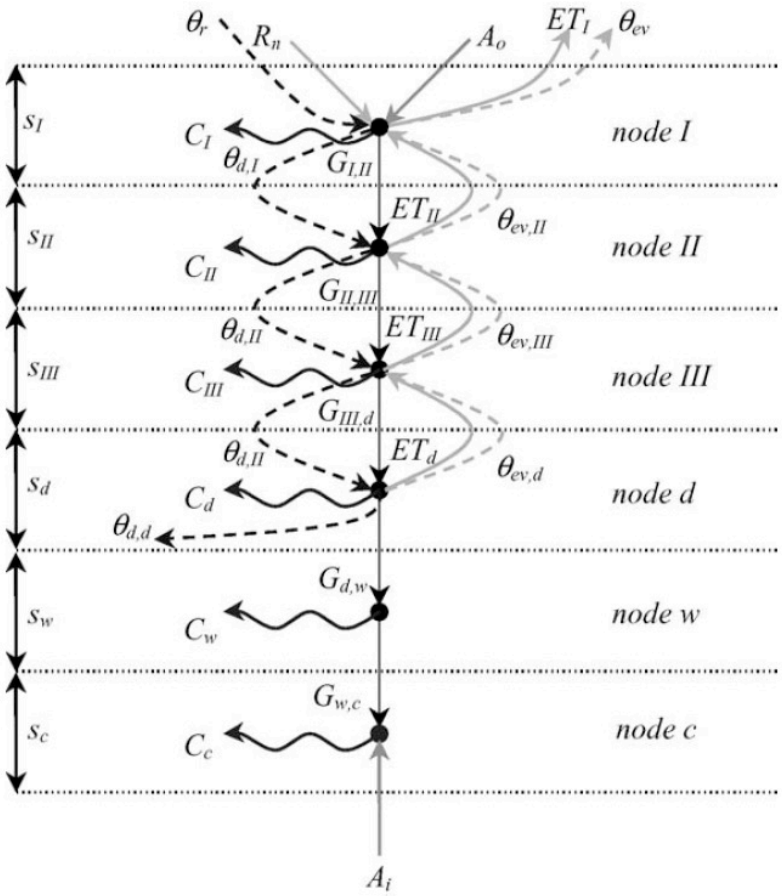

Figure 12. The finite differences model of physical system (Lazzarin, Castellotti & Busato, 2005).

This paper validated its numerical model by comparing the calculated and measured evaporative flux (ET in the numerical model). The authors calculated the evaporative flux with the proposed energy balance model, and then used the measured green roof surface temperature to calculate the evaporate flux on the surface. The comparison between the measured and calculated ET is shown in Figure 13. Instead of calculating the accuracy or standard errors, the authors made a correlational comparison between measured and modeled data. The diagram shows that the validation in 2002 is stronger than 2003 and 2004.

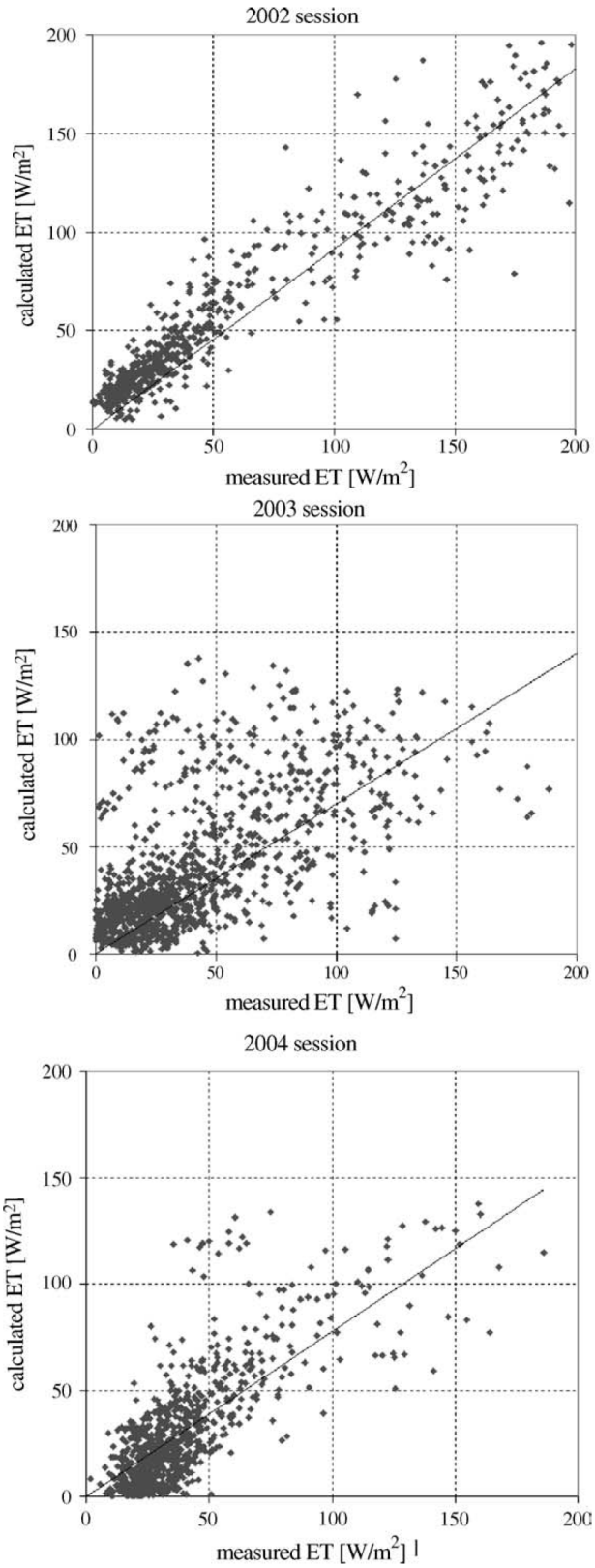

Figure 13. Correlation between measured and calculated values of evapotranspiration for the three measurement sessions (Lazzarin, Castellotti & Busato, 2005).

The time-dependent energy budgets for plants studied in Biophysical Ecology solve the equations to get the leaf temperatures (Gates, 2012):

$$Q_a - P + W - \epsilon\sigma(T_l + 273)^4 - k_1\left(\frac{V}{D}\right)^{0.5}(T_l - T_a) - \lambda(T_l)E - C\frac{dT_l}{dt} = 0 \qquad (2.35)$$

Q_a The amount of absorbed radiation

P The energy consumed in photosynthesis

W The energy released by respiration

ϵ The leaf emissivity

σ The Stefan-Boltzmann constant (5.673×10^{-8} Wm^{-2} K^{-4})

T_l Leaf temperature

k_1 Constant

V Wind speed, m/s

D Characteristics dimension, m

T_a Air temperature

$\lambda(T_l)$ Latent heat of vaporization as a function of leaf temperature

E The rate of transpiration

C Heat capacity of the plant part

t Time

Radiation term can be linearized by expanding it about a mean surface temperature $\overline{T_l}$ as following manner:

$$(T_l + 273)^4 = 4(T_l + 273)(\overline{T_l} + 273)^3 - 3(\overline{T_l} + 273)^4 \qquad (2.36)$$

If $\mathcal{R} = 4\epsilon\sigma(\overline{T_l} + 273)^3$, $H = k_1\left(\frac{V}{D}\right)^{0.5}$, and $Q_n = Q_a + 3(\overline{T_l} + 273)^4 - 273\mathcal{R}$

Then equation 2.36 becomes

$$\frac{C}{\mathcal{R}+H}\frac{dT_l}{dt} + T_l - \frac{Q_n+HT_a}{\mathcal{R}+H} - \frac{W-P-\lambda E}{\mathcal{R}+H} = 0 \tag{2.37}$$

$$\frac{C}{\mathcal{R}+H}\frac{dT_l}{dt} + T_l - T_e - T_\Delta = 0 \tag{2.38}$$

$T_e = \frac{Q_n+HT_a}{\mathcal{R}+H}$ is the operative environmental temperature.

$T_\Delta = \frac{W-P-\lambda E}{\mathcal{R}+H}$ is physiological offset temperature.

Then equation 2.38 can be written

$$\frac{dT_l}{dt} + \frac{T_l}{\tau} = \frac{T_e+T_\Delta}{\tau} \tag{2.39}$$

Where the time constant τ is $C/(\mathcal{R}+H)$. The solution to this equation has the form

$$T_l = T_\infty + (T_o - T_\infty)e^{-t/\tau} \tag{2.40}$$

T_o The initial temperature

T_∞ The final temperature approached asymptotically with time

The time constant for small and intermediate-sized plant leaves is generally between 5-20 seconds. This model studies the heat flux on the leaves' surface including solar radiation absorption, radiation between leaves and atmosphere, convection on the surface, evaporation, and heat capacity of plants.

Some mathematical models do not study a comprehensive energy balance of green roofs, but only the heat conduction of within the soil. Many studies have proved

that the model combining the gradient method and calorimetry is the most reliable to estimate ground soil heat flux G_0 . The heat storage of two vertical surfaces is equal to the heat flux reduction between them (Evett et al. 2012, Heitman et al. 2010, Liebethal et al. 2005, Venegas et al. 2013).

$$G_0 = G_z + \Delta S \tag{2.41}$$

G_0 Ground surface soil heat flux

G_z Heat flux at a certain depth z

ΔS Heat storage between the depth z and the surface

G_z and ΔS can be estimated as:

$$G_z = -c_v \cdot \kappa \cdot \frac{\partial T}{\partial z}\Big|_z = -c_v \cdot \kappa \cdot \frac{T_1 - T_2}{z_1 - z_2}\Big|_z \tag{2.42}$$

$$\Delta S = \int_z^0 c_v \cdot \frac{\partial T}{\partial T} dz = \Delta z \cdot c_v \cdot \frac{T_i - T_{i-1}}{\Delta t}\Big|_{0\sim z} \tag{2.43}$$

T_1 Soil temperature measured at depth z_1, K

T_2 Soil temperature measured at depth z_2, K

Δz The difference of z_1 and z_2

T_i The soil temperature at time t_i

i i th observation

In addition to the model derived by the gradient method and calorimetry, there are other models that were proposed in some previous studies. Force-restore, conduction-convection, harmonic, and plate calorimetric are four popular models used to estimate the ground soil heat flux.

Force-restore model:

$$G_0 = \Delta z \cdot c_v \cdot \frac{\partial T}{\partial t}\Big|_{0\sim z} + \sqrt{\frac{\omega \cdot \kappa \cdot c_v}{2}} \left[\frac{1}{\omega} \cdot \frac{\partial T}{\partial t} + T(z,t) - T\right]\Big|_z \quad (2.44)$$

Conduction-convection:

$$G_0 = c_v \cdot \kappa \cdot \frac{\Delta T}{\Delta t}\Big|_{0\sim z} + c_v \cdot W \cdot \Delta T_{0.05m} + G_{pl} \quad (2.45)$$

Harmonic:

$$G_0 = \Delta z \cdot c_v \cdot \frac{\partial T}{\partial t}\Big|_{0\sim z} + \kappa \cdot c_v \frac{\Delta T}{\Delta z}\Big|_z + \kappa \cdot c_v \cdot \sum_{p=1}^{n} A_p \sqrt{2} B_p \cdot exp\left(-B_p \cdot \Delta z\right) \sin\left(p\omega t + \varphi_p + \frac{\pi}{4} - B_p \cdot \Delta z\right)\Big|_z \quad (2.46)$$

Plate calorimetric:

$$G_0 = \Delta z \cdot c_v \cdot \frac{\partial T}{\partial t}\Big|_{0\sim z} + G_{pl} \quad (2.47)$$

These four energy balance models were validated and compared in An and Wang's research (2016). They simulated these four models under different weather conditions and compared the results with the gradient method and calorimetry combination model. They found that Harmonic model worked well on clear days but generated a number of errors on overcast or rainy days when soil temperature in an unsteady sine wave. Conduction-convection is only suitable for conditions without any rainfalls. Conduction-convection models perform poorly during rainfall events. However, force-restore models do not work well on rain-free days. It could be an alternative model to estimate G_0, when the soil temperature is the only known variable. The plate calorimetric model was estimated to be the most accurate G_0 among all four models under all clear, overcast, or rainy weather conditions. But the accuracy of the plate calorimetric model depended on the depth of the measurement equipment.

2.2.2 Mass Balance of Green Roofs

Rainwater is generally stored in the substrate, absorbed by plants, or released to the atmosphere by evapotranspiration. Green roofs' water retention capabilities and runoff dynamics depend on their characteristics: the number of layers and type of materials, soil thickness, soil type, vegetation cover, type of vegetation, and roof geometry (Berndtsson, 2010; VanWoert, Rowe,Andresen, Rugh, Fernandez & Xiao,2005). In general, the component terms of the water balance equation of a soil column are shown in Figure 14 and equation 2.48 to 2.51 (Oke, 2002; Yu, Loureiro, Cheng, Jones, Wang, Chia & Faillace,1993).

The water balance in soil layers:

$$p = E + \Delta r + \Delta S \tag{2.48}$$

p Precipitation

E Evaporation

Δr Net runoff

ΔS Soil moisture change

$$S = \theta \times V_t \times \rho_s \tag{2.49}$$

S Soil water content in mass

θ Volumetric water content

V_t Total volume of the soil sample

ρ_s Density of soil

$$\theta = p_t \times R_s \tag{2.50}$$

p_t Total porosity

R_s Saturation ratio

Precipitation p can be measured by gathering rainfalls in standard rain gauges, and net runoff Δr can be measured by hydrologic steam gauging at the boundaries of the system (Oke, 2002). Soil moisture change ΔS is measurable with soil moisture content sensors (Oke, 2002). Evaporation E can be estimated by the bulk aerodynamic equation, as shown in eq. 2.51:

$$E = -\rho C_{(z)} \bar{u}_{(z)} \Delta \bar{q} \tag{2.51}$$

ρ Air density

$C_{(z)}$ Dalton number, approximately 1.5×10^{-3}

$\bar{u}_{(z)}$ Mean wind speed

$\Delta \bar{q}$ The difference of humidity between the surface and the air

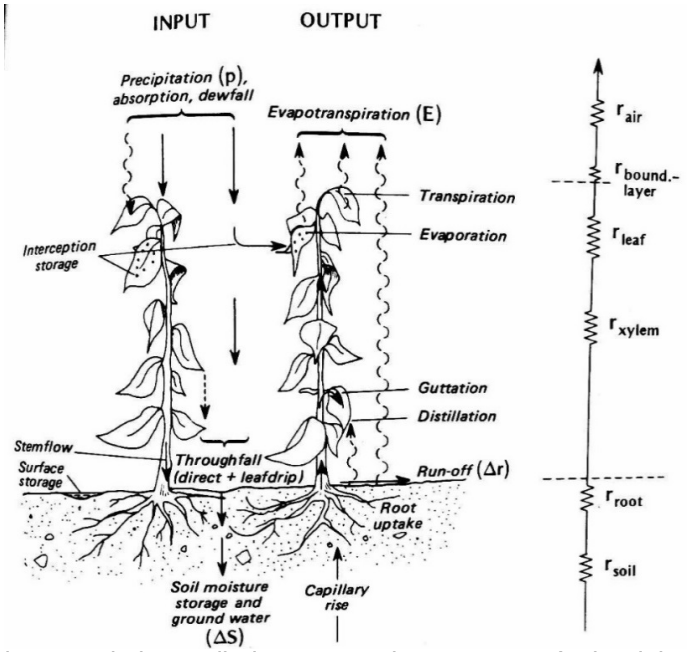

Figure 14. The hydrologic cascade in a soil-plant-atmosphere system. At the right is an analogue of the flow of water from the soil moisture store to the atmosphere sink via the plant system. (Oke, 2002)

Rain, snow, fog, dew, and frost from the atmosphere are the primary water inputs if there is no irrigation (Oke, 2002). Rain and snow are intercepted by the foliage or fall to the ground. Therefore, without considering the nature and amount of the precipitation, the efficiency of precipitation interception depends upon the vegetation characteristics such as the stand architecture, density, and the area of foliage (Oke, 2002).

In the numerical model of Lazzarin, Castellott and Busato (2005)'s paper, they divide the soil layer into three layers as I , II and III. As shown in Figure 12, the water fluxes take place simultaneously as energetic fluxes. For each layer, the amount of water drained to the lower layer varied under three conditions:

$$\theta_{d,I} =$$

$$\frac{1}{\Delta\tau}\begin{cases} \psi_I + (\theta_r - \theta_{ev,I} + \theta_{ev,II})\Delta\tau - \psi_{sat}, & if\ \psi_I + (\theta_r - \theta_{ev,I} + \theta_{ev,II})\Delta\tau > \psi_{sat} \\ \psi_I + (\theta_r - \theta_{ev,I} + \theta_{ev,II})\Delta\tau, & if\ \psi_I + (\theta_r - \theta_{ev,I} + \theta_{ev,II})\Delta\tau < 0 \\ 0, & if\ 0 \le \psi_I + (\theta_r - \theta_{ev,I} + \theta_{ev,II})\Delta\tau \le \psi_{sat} \end{cases} \quad (2.52)$$

$\theta_{d,I}$ The drainage flux towards the node II

$\Delta\tau$ Time interval (s)

ψ_I Soil water content at node I (kg/m^2)

θ_r Rainfall flux

$\theta_{ev,I}$ Evaporative flux at node I

$\theta_{ev,II}$ Evaporative flux at node II

ψ_{sat} Saturated water content

When the upper node reaches saturation, then the excess water drains down to the lower one. To the contrary, if a node gets completely dry, it will absorb water from

the same node. The mass model in this paper was adopted in its energy model to calculate evaporative flux.

Evaporation and transpiration drive the water movement going through foliage to the environment. Evaporation also happens at the boundary of the surface of moist soil and air (Gates, 2005).

Evaporation drives latent heat flux within plants and soil (Gates, 2005). In Sailor's green roof model, as shown in equation 15, the latent heat flux within foliage is determined by the mixing ratio of vapor within foliage. When it is higher than saturation, L_f is positive and the foliage layer absorbs heat. To the contrary, when the mixing ratio within foliage is lower than saturation, the foliage loses heat. Therefore, the energy balance and mass balance are not separate. They are connected with each other through latent heat transfer. Based on the literature review, the characteristics of green roofs that can affect storm water retention are soil porosity p_t, saturation ratio R_s, and density of soil ρ_s.

2.3 Green Roof Performance

2.3.1 Temperature Adjustment

During daytime, leaf temperatures are commonly 6°C to 10°C higher than the simultaneous air temperature. During overcast days, leaf temperatures can drop to 2°C above the air temperature. At night, leaf temperatures are mostly 2°C to 4°C lower than the air temperature in clear days. However, on overcast days, leaf temperatures are generally only 1°C to 2°C lower than the air temperature (Gates, 2012). In addition, the size of a leaf will affect its surface temperature. A small leaf's surface temperature is

usually close to the air temperature. On the other hand, a large leaf will be influenced by solar radiation. The surface temperature of a large leaf is higher than the air temperature at a high radiation and lower than the air temperature at a low radiation (Gates, 1971).

Soil moisture content plays a critical role in energy balance during wintertime. On the other hand, the foliage has only a minor impact on green roof energy performance as compared to the summertime (Del Barrio, 1998). For an area in a climate zone north of the frozen line, green roofs can be considered as just a soil layer in winter.

The climatic factors that significantly influence green roofs are radiation, air temperature, wind, relative humidity, and vapor pressure (Gates, 2005). As climatic factors are not changeable by green roof designers, improving the characteristics of green roofs is the only approach to optimize their performance. Referring to the energy balance equations in the literature review, some characteristics of both foliage and soil determine the energy flux of green roofs.

The heat transfer processes in the foliage layer are the most complex part of the mathematical model. They are affected by the height of the plants, leaf area index (LAI), coverage fraction, albedo, emissivity of canopy, foliage roughness lengths, and stomatal resistance of the vegetation. The characteristics of the soil of green roofs influencing energy performance are fractional vegetation coverage, albedo of ground surface, emissivity of the ground surface, soil thermal conductivity at the surface, soil thickness, instrument height, displacement height, and ground roughness lengths, as shown in Equation 2.6-2.33 (Sailor, 2008).

In the absence of insulation, green roofs with thicker soil substrates better reduce heat gain or loss of the building. Soil with smaller density and higher porosity is a better insulator. The intensity of evapotranspiration is driven by the soil moisture content, and the more intense the evapotranspiration is, the larger the heat loss. Also, the higher the moisture content, the higher the conductivity. So, dryer soil is a better thermal insulator (Castleton, Stovin, Beck & Davison, 2010). Therefore, the soil with greater porosity can contain more water, which can increase heat loss, but reduce insulation.

Lundholm (2010) studied the correlation of plant species and green roof performance and found that in summer the conventional roofs had the highest roof surface temperature. The growing-medium-only roof was 10°C cooler than a conventional one; the roofs with plants are an extra 2°C cooler than the growing-medium-only roofs. Every 1.5°C reduction of the roof surface corresponded to a 7.14 ± 0.38 W/m^2 heat flux reduction into the building.

2.3.2 Storm water Runoff Reduction

Storm water runoff can be reduced by storage, infiltration, and retention (Bass, et al., 2003). Green roofs have a much lower runoff than non-vegetated or gravel roofs, and intensive green roofs with thick substrates can reduce runoff more than extensive green roofs (Mentens et al., 2006). It is also shown that green roofs can postpone the peak flow of runoff compared to conventional roofs (Moran et al., 2003). The amount of storm water reduction depends on many variables. Minke and Witter (1992) found that a 20-40 cm substrate can hold 10-15 cm of water, which is 25% below the normal runoff levels. In general, conventional roofs with gravel have the lowest capacity to retain

rainfall. The vegetated and the growing-media-only roof platform showed larger retention ability than gravel roof platforms for the rain event with rainfall depth over 2mm. Vegetation over and above the growing medium had minimal effect on water capture (VanWoert at el. 2005).

3 Methodology

Quantitative research methods are the primary methodology for this research which includes experiments and simulations. The experiments include monitoring the green roofs and measuring the ambient conditions and soil properties, which all occur in a natural setting. The simulations are based on proposed mathematical green roof models and validated by the data collected in the experiments.

3.1 Experiments and Data Collection

The experiment of the green roof performance is conducted on the green roofs of Golda Meir library in Milwaukee. The green roof is shown in Figure 15.

Figure 15. Golda Meir Library Green Roofs. Photo credit: University of Wisconsin - Milwaukee

The Golda Meir green roof consists of growing mediums, water retention fabrics, drainage composite, water proofing membranes, separation layers, grounding screens, insulation layers, and vapor retarders. The irrigation system was operating on the green roofs in the summer of 2012 and 2013, however, it has not been functioning since the winter of 2013. The green roofs are laid on the existing concrete decks. In 2014, we measured the inside surface temperature of the concrete deck. The temperature is constantly kept around 22 °C to 24 °C throughout the year. The U-value of the layers underneath the growing medium is 2.89 $W/m^2 \cdot K$, which is estimated by eQuest (as shown in Appendix A).

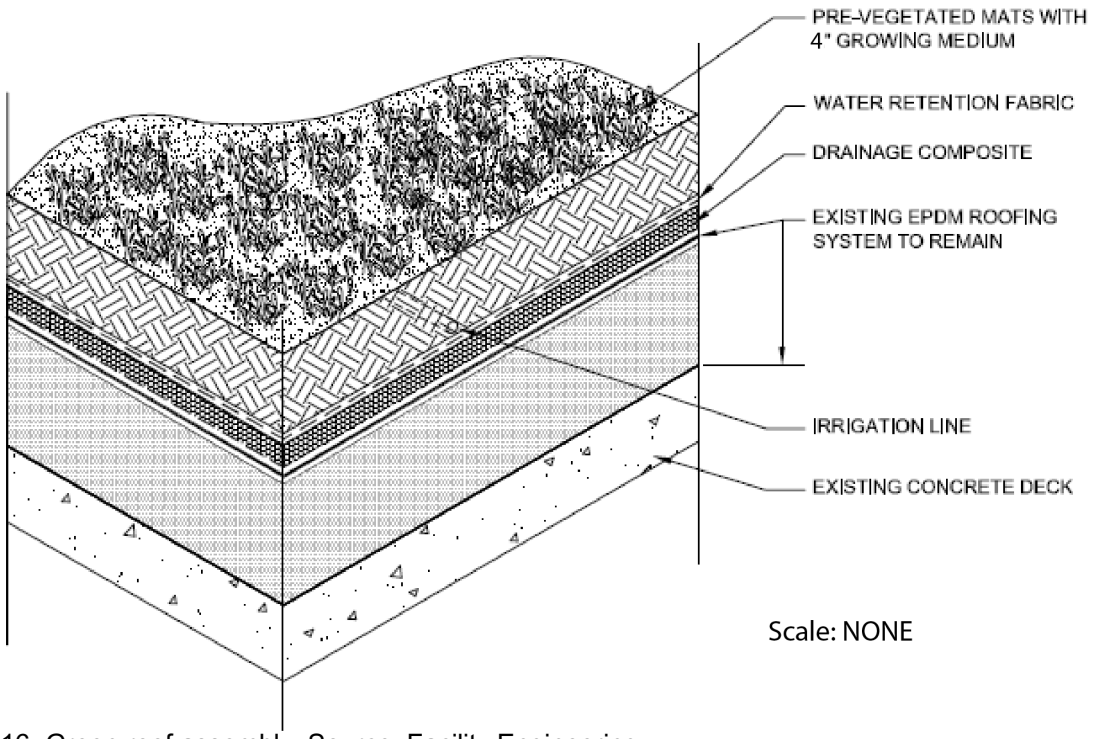

Figure 16. Green roof assembly. Source: Facility Engineering.

The experimental equipment was provided by Onset Computer Corporation. The equipment consists of two weather stations, including two HOBO U30 NRC data loggers, solar panels, and temperature/RH smart sensors with a solar radiation shield, a

wind speed smart sensor, a wind direction smart sensor, a full cross arm for wind speed/direction sensors, pyranometers, photosynthetic light (PAR) smart sensors, soil moisture sensors, soil temperature sensors, and one rain gauge.

The measurement ranges of temperature/RH smart sensor is -40°C to 75°C (-40°F to 167°F) for temperature, and 0-100% RH for humidity. The temperature accuracy is ±0.21 °C for 0°C to 50°C (0.38°F from 32° to 122°F). The accuracy for humidity is ±2.5% from 10% to 90% RH (typical), and accuracy for below 10% and above 90% is ±5% (typical).

The pyranometers measure total radiation including beam and diffuse radiation. Its measurement range cover from 0 to 1280 $W/m^{2.}$, and accuracy is ±5%.

The PAR smart sensor is designed to detect photons between 400-700 nm in wavelength. Ideally the sensor would count photons with equal efficiency between 400-700 nm and no photons would be counted outside this range. However, in reality, this sensor undercounts photons between 400-550 nm and between 670-700 nm, and it over-counts photons between 550-670 nm. In most applications, where the sensor is used in natural sunlight, the error is not significant. Its accuracy is ±5%.

The temperature smart sensor is designed to work with HOBO stations, and can be used to measure liquid or solid temperature between -40°C to 100°C. Its accuracy is ±0.2 °C.

The soil moisture smart sensors are used for measuring the soil water content. Its measurement range is between 0 and 0.550 m^3/m^3, and accuracy is ±0.031.

Before installing the weather stations, I measured the soil density and saturation water content, and calibrated the soil moisture sensors in a lab with Golda Meir green roof samples. The measurement and calibration procedure are presented in Appendix B. With the measurement of soil properties, we know that the dry soil density is 690 kg/m^3.

After calibration, the weather stations were ready to be installed on the roof, as shown in Figures 17 and 18.

Figure 17. Weather Station on the east green roof.

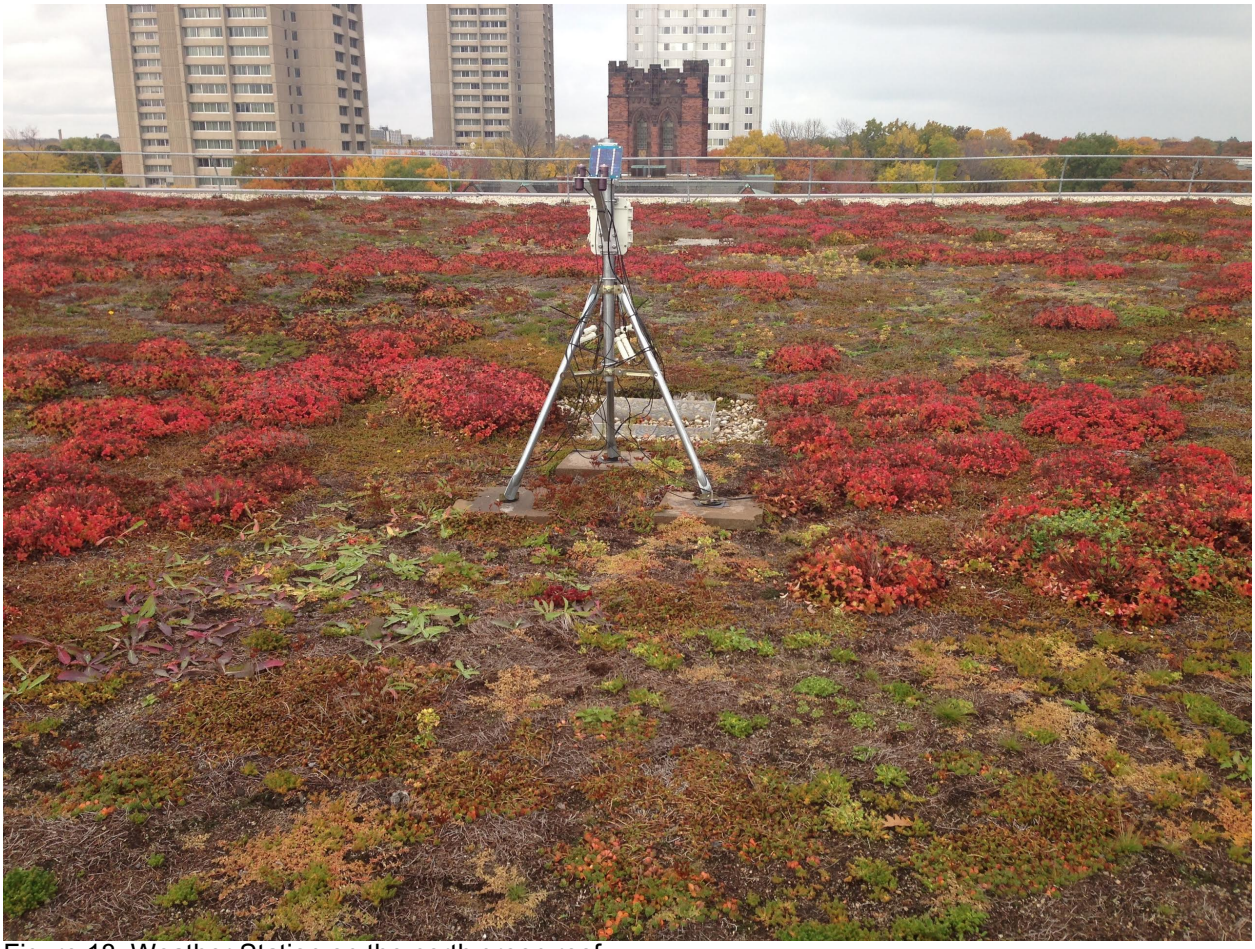

Figure 18. Weather Station on the north green roof.

Figure 19. The panorama of the north green roof.

Figure 20 shows the inside of data logger connected with sensors.

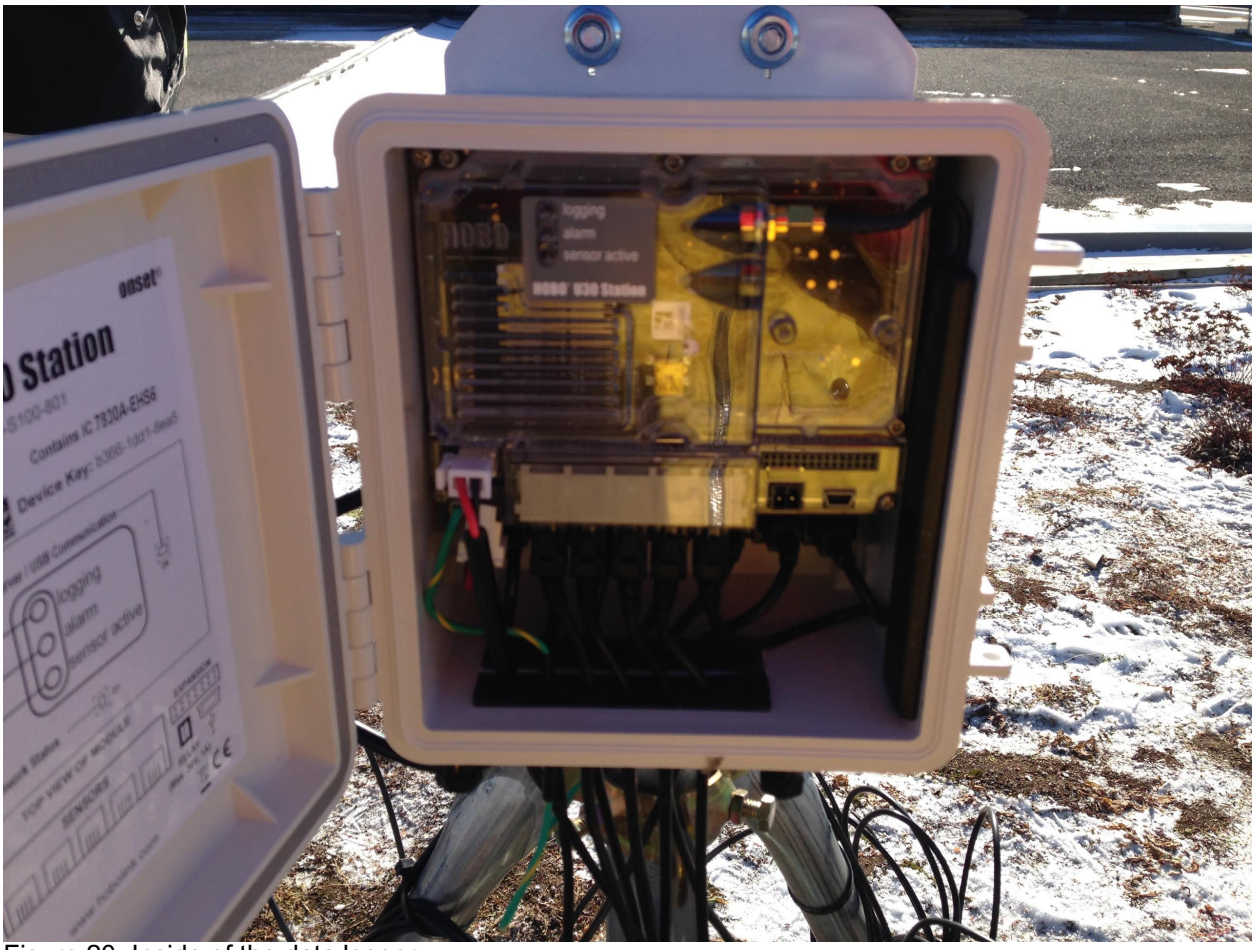

Figure 20. Inside of the data logger.

The locations of soil moisture and temperature sensors are shown in Figures 21 and 22.

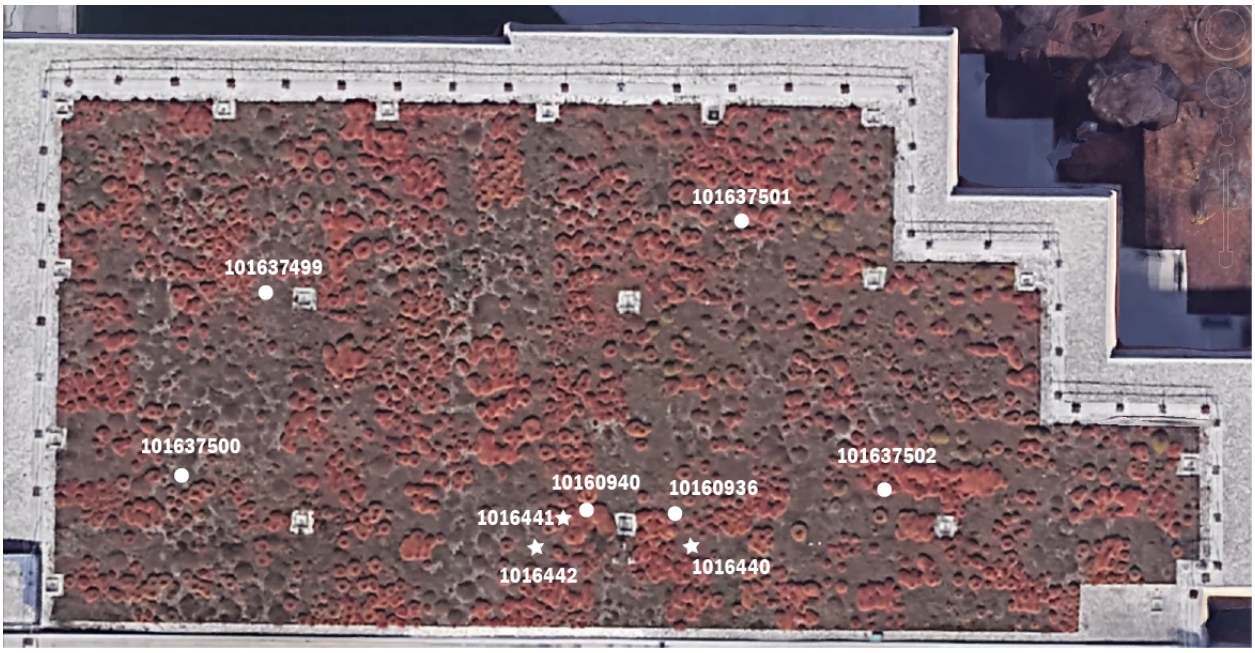

Figure 21. The soil moisture and temperature sensors location on north green roof: The symbol ● is soil moisture sensor. The symbol ★ is soil temperature sensor. Source: Google Earth Pro, August 31st, 2017

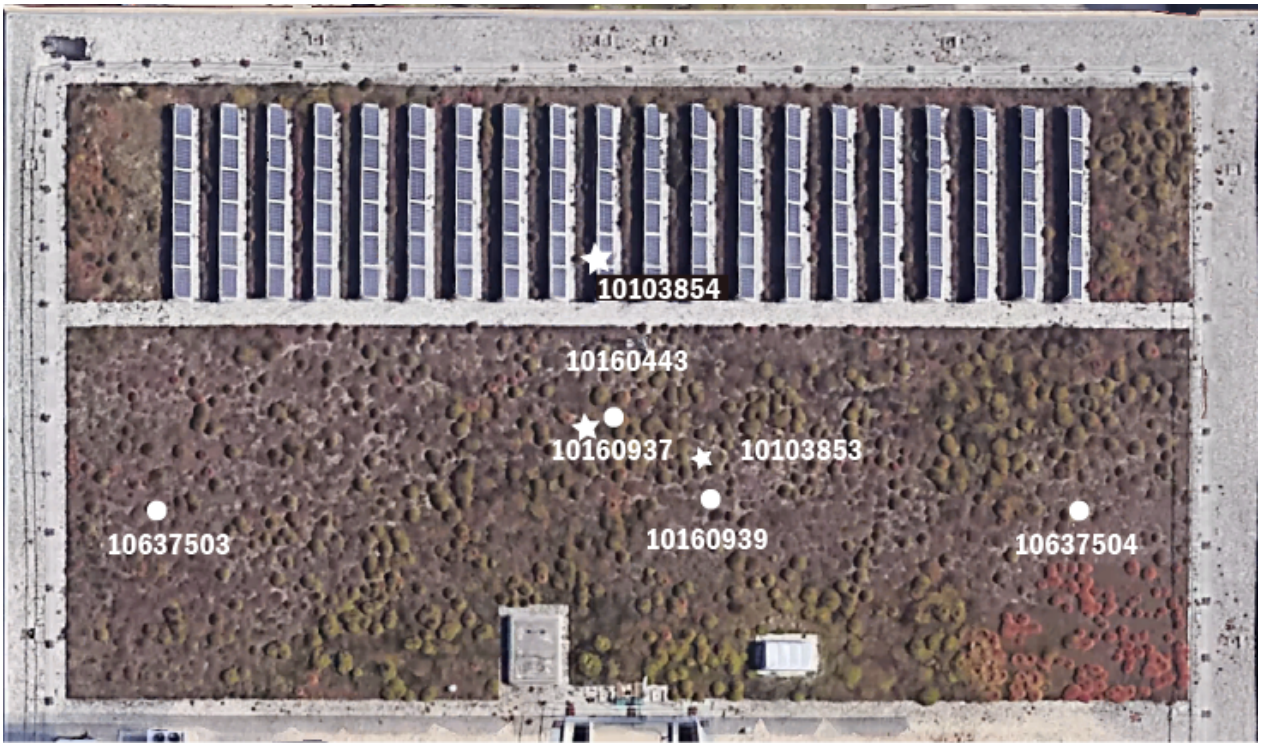

Figure 22. The soil moisture and temperature sensors location on east green roof: The symbol ● is soil moisture sensor. The symbol ★ is soil temperature sensor. Source: Google Earth Pro, August 31st, 2017

The data logger installed on the north portion of the roof includes six soil moisture sensors, three soil temperature sensors, two pyranometers and two photosynthetic sensors. The one installed on the east roof includes four soil moisture sensors, three soil temperature sensors, one ambient temperature sensor, one relative humidity sensor, one wind monitor sensor and one rain barrel (monitoring precipitation). Figure 17 shows the looks of the ambient temperature sensor, relative humidity sensor, wind monitor sensor and rain barrel.

On the north portion of the green roof, the soil temperature sensor 1016442 is in the soil without vegetation coverage, as shown in Figure 23. The soil temperature sensor 1016441 is in the soil with vegetation cover, as shown in Figure 24. The soil temperature sensor 1016440 was in the soil without vegetation cover, but was later relocated underneath gravel surface in November 2014.

Figure 23. Soil temperature sensor 1016442 in bare soil

Figure 24. Soil temperature sensor 1016442 in soil covered by vegetation.

On the east portion of the green roof, the soil temperature sensor 10160443 was embedded in the soil with vegetation coverage. The soil temperature sensor 10103853 was embedded the soil without vegetation coverage. The soil temperature sensor 10103854 was placed underneath the solar panels.

The data was collected by the HOBO data loggers at 15-minutes intervals from October 2013 to October 2014, and then at 5-minute intervals from November 2014 until the present.

To monitor the surface temperature of bare soil and vegetation, an infrared thermometer was used, as shown in Figure 25. The thermometer has a measuring range from -18 to 400°C (0 to 750°F). Its accuracy is ±2°C (±3.5°F) for -1 to 275°C, and ±3°C (±5°F) for -18 to -1°C (0 to 30°F). The surface temperatures were measured in 2017, but the weather data used for the simulation was gathered in 2014. Therefore, the measured temperature from 2017 can be used as a reference for the modeled surface temperature, but it was not used for validation in this research.

Figure 25. Measuring surface temperature with an infrared thermometer

The surface temperatures were measured on a clear day and an overcast day, as shown in Figures 26 and 27.

Figure 26. Golda Meir green roof on a clear day. September 15th, 2017

Table 1. Surface temperature measurement on a clear day.

Clear Day Surface Temperature Monitoring (September 15th, 2017)				
Sensor	Surface	10:00 A.M.	1:00 P.M.	4:00 P.M.
10160441	Soil	34°C	46°C	36°C
10160442	Plant	27°C	32°C	27°C
Difference		7°C	14°C	9°C
Ambient Temp.		23°C	22°C	22°C

As shown in Table 1, on a clear day, the soil surface temperature is 11°C to 24°C higher than the ambient temperature. The plant surface temperature is 4 °C to 10°C

higher than the ambient temperature. The soil surface temperature is 7°C to 14°C higher than the vegetation-covered surface temperature.

Figure 27. Green roof on an overcast day. September 29th, 2017.

Table 2. Surface temperature measurement on an overcast day.

Overcast Day Surface Temperature Monitoring (September 29th, 2017)				
Sensor	Surface	10:00 A.M.	1:00 P.M.	4:00 P.M.
10160441	Soil	23°C	29°C	29°C
10160442	Plant	18°C	17°C	17°C
Difference		5°C	12°C	12°C
Ambient Temp.		17°C	18°C	18°C

As shown in Table 2, on an overcast day, the soil surface temperature is 5°C to 11°C higher than the ambient. The plant surface temperature is close to the ambient

temperature. Moreover, the soil surface is 6°C to 11°C hotter than the vegetation-covered surface.

3.2 Simulation and Validation

To study the performance of a green roof, the proposed water balance and energy balance need to be simulated and then validated before data analysis. The energy and mass balance equations for a system are as follows:

$$Input - Output = Energy\ or\ mass\ storage \tag{3.1}$$

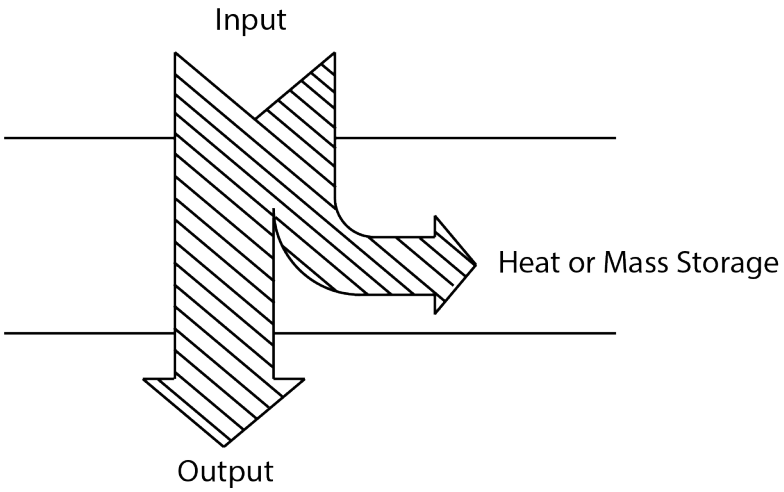

Figure 28. Heat or mass balance flow diagram.

Referring to the mathematical models of green roofs discussed in the literature review, the following water balance and energy balance equations are adopted for this simulation.

3.2.1 Energy Balance

Based on the literature review presented in the previous chapters, the energy balance on a soil surface is:

$$Q_{solar} + Q_{rad} + Q_{conduction} + Q_{convection} - Q_{evaporation} = 0 \tag{3.2}$$

Q_{solar} Solar radiation energy transfer, J/m^2

Q_{rad} Sky radiation energy transfer, J/m^2

$Q_{conduction}$ Conduction energy transfer, J/m^2

$Q_{convection}$ Convection energy transfer, J/m^2

$Q_{evaporation}$ Evaporation energy transfer, J/m^2

In them,

$$Q_{solar} = \bar{I}_{solar}\Delta t \propto_{solar} \quad (3.3)$$

$$Q_{rad} = \varepsilon_{surf}\sigma\Delta t\left(T_{sky}^4 - T_{surf}^4\right) \quad (3.4)$$

$$Q_{cond} = \frac{k_e}{d}\Delta t\left(T_{soil} - T_{surf}\right) \quad (3.5)$$

$$Q_{conv} = h_c\Delta t\left(T_{air} - T_{surf}\right) \quad (3.6)$$

$$Q_{evap} = \lambda \mathrm{E}\Delta t \quad (3.7)$$

Q Energy flux within the time step, J/m^2

$\bar{I}_{solar}$ Average solar radiation within the time step, W/m^2

$\propto_{solar}$ Solar absorptance, %

ε_{surf} Surface emissivity, %

σ Stefan–Boltzmann constant, 5.67 x 10^{-8} W/m^2 ·K^4

k_e Effective conductivity, W/m· K, refer to Eq. for bare soil surface, and Eq. for vegetation-covered surface.

T_{surf} Surface Temperature, K

h_c Convection coefficient, W/m^2·K

d Soil depth at soil temperature measurement, 0.05m.

λ Latent heat of vaporization, approximately 2.43 x 10^6 J/kg

E Evaporation rate, kg/(m^2s)

(A) Bare Soil Energy Balance- Surface Temperature

The energy transfer flow of the bare soil is illustrated in Figure 29. The surface of the bare soil absorbs the solar radiation, absorbs or releases radiation from or to the sky, convects heat with the air on the surface, and then conducts the heat down to the soil and building. There is also some heat restored in the soil during heat conduction.

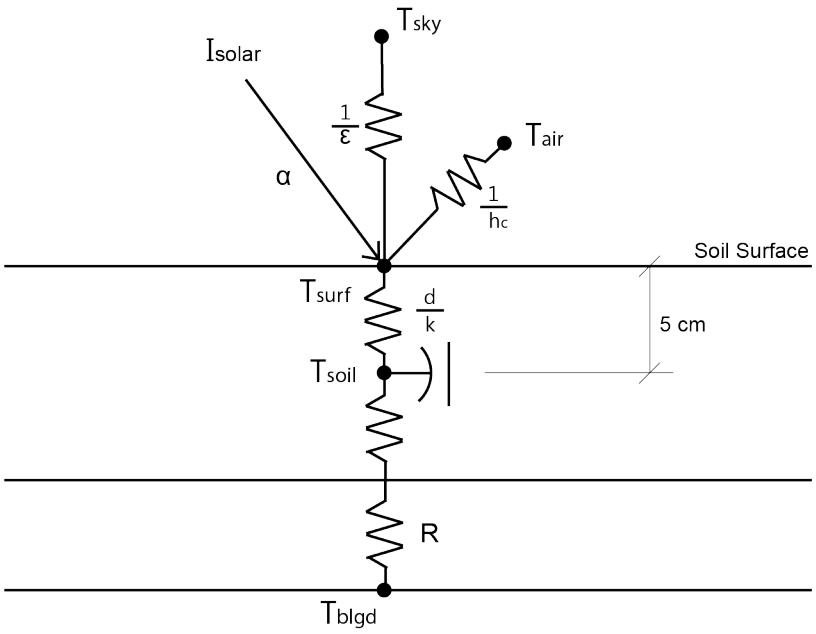

Figure 29. Energy flow for the bare soil.

The energy balance of the heat flux through the bare soil surface is as follows:

$$\bar{I}_{solar} \propto_{solar} + \varepsilon_{soil,surf}\sigma\left(T_{sky}^4 - T_{surf}^4\right) + h_c\left(T_{air} - T_{surf}\right) + \frac{k_e}{d}\left(T_{soil} - T_{surf}\right) - \lambda \mathrm{E} = 0 \quad (3.8)$$

In terms of solar radiation, the average solar radiation can be measured or provided by the weather data, for example, TMY-3. Solar absorption $\propto_{solar}$ is determined by the surface color.

The radiation between the sky and surface is estimated by the function of the emissivity, Stefan–Boltzmann constant, and the difference of the fourth power of the sky and surface temperature.

The emissivity of the moist soil can be estimated by the emissivity of the dry soil and the saturated soil:

$$\varepsilon_{soil,surf} = \varepsilon_{soil,dry} + \left(\varepsilon_{soil,sat} - \varepsilon_{soil,dry}\right)x_s \tag{3.9}$$

$\varepsilon_{soil,surf}$ Emissivity of moist soil

$\varepsilon_{soil,dry}$ Emissivity of dry soil

$\varepsilon_{soil,sat}$ Emissivity of saturated soil

And $\left(T_{sky}^4 - T_{surf}^4\right)$ in Equation 3.8 can be expressed as:

$$\left(T_{sky}^4 - T_{surf}^4\right) = \left(T_{sky}^2 + T_{surf}^2\right)\left(T_{sky}^2 - T_{surf}^2\right) = \left(T_{sky}^2 + T_{surf}^2\right)\left(T_{sky} + T_{surf}\right)\left(T_{sky} - T_{surf}\right) \tag{3.10}$$

For two arbitrary surfaces that have close temperatures, an estimated average temperature $\overline{T}$ can be introduced to simplify the sky radiation heat transfer (Duffie & Beckman, 1980).

$$4\overline{T}^3 = (T_2^2 + T_1^2)(T_2 + T_1) \tag{3.11}$$

Since the surface temperature is close to the air temperature, we can get an approximate $\overline{T}$ using the average of sky temperature and ambient air temperature.

$$\overline{T} = \overline{T_{sky}, T_{air}} \tag{3.12}$$

Then $\left(T_{surf}^4 - T_{soil}^4\right)$ can be expressed as:

$$\left(T_{sky}^4 - T_{surf}^4\right) = 4\overline{T}^3\left(T_{sky} - T_{surf}\right) \quad (3.13)$$

Therefore, the energy balance for a node in the soil can be expressed as:

$$\bar{I}_{solar} \propto_{solar} + 4\varepsilon_{soil,surf}\sigma\overline{T}^3\left(T_{sky} - T_{surf}\right) + h_c\left(T_{air} - T_{surf}\right) + \frac{k_e}{d}\left(T_{soil} - T_{surf}\right) - \lambda \mathrm{E} = 0 \quad (3.14)$$

The method of estimating sky temperature T_{sky} is related to the function of the dew point temperature, dry bulb temperature, and number of hours since midnight t (Berdahl & Martin, 1984).

$$T_{sky} = T_{air}\left[0.711 + 0.0056T_{dp} + 0.000073T_{dp}^2 + 0.013\cos(15t)\right]^{0.25} \quad (3.15)$$

T_{sky} Effective sky temperature, K

T_{air} Dry bulb temperature, K

T_{dp} Dew point temperature, °C

The convection heat transfer happens on the surface boundary, and it can be estimated by the function of convection coefficient and difference between the air temperature and surface temperature. The convection coefficient can be estimated with a given wind speed (Watmuff et al, 1977). And this wind speed is monitored by the weather station.

$$h_c = 2.8 + 3.0V \quad (3.16)$$

V Wind speed, m/s

The effective thermal conductivity k_e can be estimated by the idealized models of heat flow through a unit cube of moist soil (Farouki, 1982).

$$\frac{1}{k_e} = \frac{x_s}{k_s} + \frac{x_f}{k_f} \quad (3.17)$$

k_e Effective thermal of conductivity of moist soil, W/m· K

k_f Thermal of conductivity of fluid in soil, W/m· K

k_s Thermal of conductivity of dry soil solid, W/m· K

x_s Volume fraction of solids in unit soil volume

x_f Volume fraction of fluid in unit soil volume

x_f and x_s are monitored by the weather station. k_s and k_f can be estimated by tests or referred to the engineering property charts.

For the water retained in the topsoil, the evaporation can be estimated by Equation 3.18 (Oke, 2002):

$$E = \rho_{air} C V \Delta\bar{q} \quad (3.18)$$

E Evaporation rate, kg/(m^{2}s)

ρ_{air} Air density, kg/m^3

C Dalton number, assume 1.5 × 10^{-3}

V Mean wind speed on the surface, m/s

$\Delta\bar{q}$ The difference of humidity between the surface and the air, kg/kg

The air density was calculated using the built-in function of the Energy Equation Solver (EES) with a known dry bulb temperature, dew point temperature and air pressure, as provided by the weather stations.

The humidity can also be calculated with a known temperature and pressure (Gates, 2012):

$$q = \frac{0.622e}{P-0.379e} \cong \frac{0.622e}{P} \quad (3.19)$$

e Water vapor pressure Pa

P Total atmospheric pressure Pa

Tetens' formula for temperatures above 0 °C define the water vapor pressure as indicated below (Monteith & Unsworth, 2007):

$$e = 0.61078\exp\left(\frac{17.27T}{T+237.3}\right) \quad (3.20)$$

T Air temperature, °C

e Water vapor pressure kPa

Therefore, the evaporation rate can be estimated by the soil temperature and ambient air temperature:

$$E = \rho_{air} CV \frac{0.622}{P} 0.61078\left(\exp\left(\frac{17.27T_{soil}}{T_{soil}+237.3}\right) - \exp\left(\frac{17.27T_{air}}{T_{air}+237.3}\right)\right) \quad (3.21)$$

To solve the equation above, the surface temperature T_{surf} can be estimated as below:

$$T_{surf,soil} = \frac{\bar{I}_{solar}\propto_{solar}+4\varepsilon_{soil,surf}\sigma(\bar{T})^3 T_{sky}+h_c T_{air}+\frac{k_e}{d}T_{soil}-\lambda E}{h_c+4\varepsilon_{soil,surf}\sigma(\bar{T})^3+\frac{k_e}{d}} \quad (3.22)$$

(B) Bare Soil Energy Balance- Soil Temperature

Equation 3.22 can be used to predict the surface temperature on the bare soil of a green roof with the known soil temperature. If the soil temperature is unknown, it can be derived by the function of the heat conduction between the soil surface and building surface, and heat storage in the soil. The heat flow is shown in Figure 29:

$$\Delta G = \frac{k_e}{d}\left(T^i_{surf,soil} - T^i_{soil}\right) + \left(\frac{1}{\frac{d}{k_e}+\frac{1}{U_{bldg}}}\right)\left(T_{bldg} - T^i_{soil}\right) \quad (3.23)$$

ΔG Soil heat storage, J/m^2

U_{bldg} Existing roof U-value, W/m^{2}K

T_{bldg} Building surface temperature, K

The heat capacity of the soil will store heat. The heat storage between any two points of the soil is

$$\Delta G = \int_z^0 C_v \cdot \frac{\partial T}{\partial T} dz = \Delta z \cdot C_v \cdot \left.\frac{T^{i+1}_{soil} - T^i_{soil}}{\Delta t}\right|_{0\sim z} \quad (3.24)$$

ΔG Soil heat storage, J/m^2

C_v Volumetric thermal capacity of soil, J/m^3·K

Δz Distance between two points

T^{i+1}_{soil} The soil temperature at the end of the time step, K

T^i_{soil} The soil temperature at the beginning of the time step, K

$$C_v = \rho_d(c_d + wc_w) \quad (3.25)$$

C_v Volumetric heat capacity of moist soil, J/m^3·K

ρ_d Dry bulk density, kg/m^3

c_d Specific heat capacity of dry soil, J/kg·K

c_w Specific heat capacity of water, J/kg·K

w Water content, kg/kg

Combine Equation 3.23, 3.24 and 3.25, the energy balance of the soil temperature is as below:

$$\frac{2dC_v\left(T_{soil}^{i+1}-T_{soil}^{i}\right)}{\Delta t}=\frac{k_e}{d}\left(T_{surf,soil}^{i}-T_{soil}^{i}\right)+\left(\frac{1}{\frac{d}{k_e}+\frac{1}{U_{bldg}}}\right)(T_{bldg}-T_{soil}^{i})$$

(3.26)

The soil temperature T_{soil}^{i+1} can be expressed as:

$$T_{soil}^{i+1}=T_{soil}^{i}+\frac{\Delta t}{2C_v d}\left[\frac{k_e}{d}\left(T_{surf,soil}^{i}-T_{soil}^{i}\right)+\left(\frac{1}{\frac{d}{k_e}+\frac{1}{U_{bldg}}}\right)(T_{bldg}-T_{soil}^{i})\right]$$

(3.27)

The T_{surf}^{i} in Equation 3.27 was replaced with the surface temperature Equation 3.22, achieving the following soil temperature equation:

$$T_{soil}^{i+1}=\frac{\frac{\Delta t k_e}{2C_v d^2}\left(I_{solar}\propto_{solar}+4\varepsilon_{soil,surf}\sigma(\bar{T})^3T_{sky}+h_cT_{air}-\lambda E\right)}{h_c+4\varepsilon_{soil,surf}\sigma(\bar{T})^3+\frac{k_e}{d}}+\frac{\frac{\Delta t}{2C_v d}T_{bldg}}{\frac{d}{k_e}+\frac{1}{U_{bldg}}}$$

$$-\left[\frac{\Delta t k_e}{2C_v d^2}+\frac{\frac{\Delta t}{2C_v d}}{\frac{d}{k_e}+\frac{1}{U_{bldg}}}-\left(\frac{\Delta t {k_e}^2}{2C_v d^3\left(h_c+4\varepsilon_{soil,surf}\sigma(\bar{T})^3+\frac{k_e}{d}\right)}\right)-1\right]T_{soil}^{i}$$

(3.28)

$$\lambda E=\lambda\rho_{air}CV\frac{0.622e}{P}0.61078(\exp\left(\frac{17.27T_{soil}^{i}}{T_{soil}^{i}+237.3}\right)-\exp\left(\frac{17.27T_{air}}{T_{air}+237.3}\right)$$

(3.29)

Note: The T_{soil}^{i} in Equation 3.28 is in Kelvin units, but the T_{soil}^{i} in Equation 3.29 is in Celsius units.

As mentioned at the beginning of Chapter 3, the soil temperature was measured by the weather stations on the Golda Meir Library. Therefore, the soil temperature calculated in Equation 3.28 can be validated by the measured soil temperature beneath the bare soil. If the validation proves the reliability of the equations, then both surface and soil temperature of the bare soil can be estimated by the proposed mathematical models.

(C) Vegetation-covered Soil Energy Balance – Surface Temperature

The energy transfer flow of the vegetation-covered surface is illustrated in Figure 30. The surface of the vegetation absorbs the solar radiation, absorbs or releases radiation from or to the sky, convects heat with the air on the surface, and then conduct the heat down to the air between vegetation and soil surface, the soil, and the building. There is some heat restored in the soil during heat conduction.

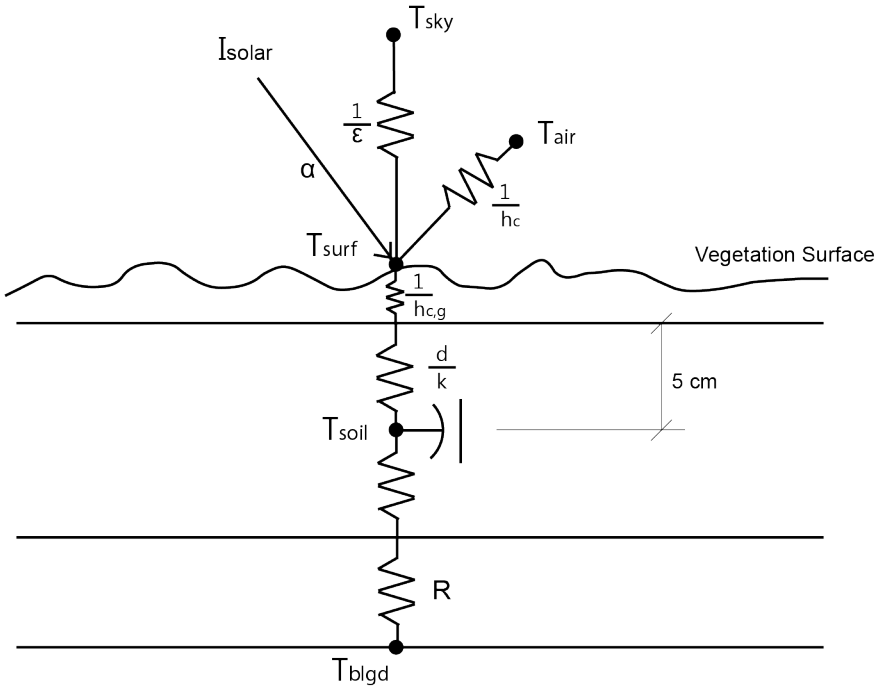

Figure 30. Energy flow for the vegetation-covered soil.

For vegetation-covered surfaces, the energy balance includes the transpiration of the plants. The heat flux though the vegetation surface is:

$$\bar{I}_{solar} \propto_{solar} + 4\varepsilon_{veg,surf}\sigma\overline{T}^{3}\left(T_{sky} - T_{surf,veg}\right) + h_c\left(T_{air} - T_{surf,veg}\right) + \frac{1}{\frac{d}{k_e} + \frac{1}{h_{c,g}}}\left(T_{soil} - T_{surf,veg}\right) - \lambda E = 0 \quad (3.30)$$

$h_{c,g}$ Thermal resistance of air space between canopy and ground, 4 ~ 5.67 w/m$^{2\circ}$ C

E The rate of transpiration, kg/(m^{2}s)

The methods for estimating solar radiation, sky radiation and convection of the vegetation-covered soil surface are the same as those for the bare soil surface. For the heat conduction, the conductivity between the surface and soil integrates the soil's effective conductivity and the thermal conductivity of the air space between canopy and

ground. Additionally, the plants' transpiration becomes the primary approach of evaporation.

The rate of water vapor escaping from a leaf is (Gates. 2012):

$$E = \frac{d_l - h d_a}{r_l - r_a} \tag{3.31}$$

E Water vapor escape rate, kg/m^{2}s^{-1}

d_l The saturation density of water vapor in the leaf intercellular air spaces as a function of leaf temperature, kg/m^3

d_a The saturation density of water vapor in the air as a function of air temperature, kg/m^3

h Relative humidity of the air, %

r_l Internal leaf resistance, 100~2000 s/m

r_a Surface boundary-layer resistance

Under similar atmospheric conditions and temperatures, the humidity ratio of dry air is also similar. Compared to the relatively large solar radiation, convection and conduction, the difference between saturation densities of water vapor in the leaf and air are not significant. Therefore, we assume $d_l \approx d_a$ in the equation.

$$d_l \approx d_a = \omega_a \rho_a \tag{3.32}$$

ω_a Humidity ratio, kg/kg

ρ_a Dry air density, kg/m^3

The humidity ratio can be estimated as below (Oyj, 2013):

$$\omega_a = \frac{BP_w}{(P_{total} - P_w)} \tag{3.33}$$

B 0.622 for air, kg/kg

P_w Water vapor pressure, mbar

P_{total} Ambient total pressure, mbar

If low accuracy is allowed, a simpler formula of P_{ws} can be estimated as:

$$P_w = P_{ws} \cdot \frac{RH}{100} = A \cdot 10^{\frac{mT}{T+T_n}} \cdot \frac{RH}{100} \tag{3.34}$$

A 6.116441 for water between -20°C ~ 50°C

m 7.591386 for water between -20°C ~ 50°C

T_n 240.7263 for water between -20°C ~ 50°C

T Ambient temperature, °C

RH Relative humidity

P_w Saturated water vapor pressure, mbar

$$r_a = k_2 \frac{W^{0.2} D^{0.3}}{V^{0.5}} \tag{3.35}$$

W The dimension at right angles to the width of a leaf, m

D Width of a leaf in the direction of the air flow, m

V Wind speed, m/s

k_2 200 $s^{1/2}/m$

The dimension of a leaf of the sedum plant is about 0.01m x 0.01 m, so

$$r_a = 200 \times \frac{0.01^{0.2} \times 0.01^{0.3}}{V^{0.5}} = \frac{20}{V^{0.5}} \tag{3.36}$$

Solving Equation 3.29 with Equation 3.31 to 3.36 , the surface temperature of vegetation is

$$T_{surf,veg} = \frac{\bar{I}_{solar} \propto_{solar} + 4\varepsilon_{veg,surf}\sigma(\bar{T})^3 T_{sky} + h_c T_{air} + \frac{1}{\frac{d}{k_e} + \frac{1}{h_{c,g}}} T_{soil} - \lambda \left[\frac{(1-h)d_a}{r_l - \frac{20}{V^{0.5}}} \right]}{h_c + 4\varepsilon_{canopy}\sigma(\bar{T})^3 + \frac{1}{\frac{d}{k_e} + \frac{1}{h_{c,g}}}}$$

(3.37)

(D) Vegetation-covered Soil Energy Balance – Soil Temperature

Equation 3.37 can be used to predict the surface temperature on the vegetation of a green roof with the known soil temperature. Following the same derivation method of the bare soil temperature, we can achieve an energy balance with the function of the heat conduction between the vegetation surface and building surface, and heat storage in the soil:

$$\frac{2dC_v\left(T_{soil}^{i+1} - T_{soil}^{i}\right)}{\Delta t} = \frac{1}{\frac{d}{k_e} + \frac{1}{h_{c,g}}}\left(T_{surf,veg}^{i} - T_{soil}^{i}\right) + \left(\frac{1}{\frac{d}{k_e} + \frac{1}{U_{bldg}}}\right)(T_{bldg} - T_{soil}^{i})$$

(3.38)

The $T_{surf,veg}^{i}$ in Equation 3.38 was replaced with the surface temperature Equation 3.37, we can achieve a soil temperature equation:

$$T_{soil,veg}^{i+1} = \frac{\frac{\Delta t}{2C_v d}\left(\frac{1}{\frac{d}{k_e}+\frac{1}{h_c}}\right)\left\{\bar{I}_{solar}\ \propto_{solar} + 4\varepsilon_{veg,surf}\sigma(\bar{T})^3 T_{sky} + h_c T_{air} - \lambda\left[\frac{(1-h)d_a}{r_l - \frac{20}{V^{0.5}}}\right]\right\}}{h_c + 4\varepsilon_{veg,surf}\sigma(\bar{T})^3 + \frac{k_e}{d}}$$

$$+ \frac{\frac{\Delta t}{2C_v d} T_{bldg}}{\frac{d}{k_e}+\frac{1}{U_{bldg}}}$$

$$- \left\{ \frac{\Delta t}{2C_v d}\left(\frac{1}{\frac{d}{k_e}+\frac{1}{h_{c,g}}}\right) + \frac{\frac{\Delta t}{2C_v d}}{\frac{d}{k_e}+\frac{1}{U_{bldg}}} - \left[\frac{\Delta t\left(\frac{1}{\frac{d}{k_e}+\frac{1}{h_{c,g}}}\right)^2}{2C_v d\left(h_c + 4\varepsilon_{veg,surf}\sigma(\bar{T})^3 + \frac{k_e}{d}\right)} \right] \right.$$

$$\left. - 1 \right\} T_{soil,veg}^{i} \qquad (3.39)$$

The soil temperature calculated in Equation 3.39 can be validated by the measured soil temperature beneath the vegetation-covered soil.

If the validation proves the reliability of the equations, then both surface and soil temperature of the vegetation can be estimated by the proposed mathematical models.

3.2.2 Water Balance

In general, the component terms of the water balance equation of soil are shown in the following equation (Oke, 2002):

$$p = \Delta S + E \times \Delta t + \Delta r \tag{3.40}$$

p Precipitation, kg/ m^2

ΔS Soil moisture change, kg/m^2

E Evapotranspiration, kg/(m^2·s)

Δt Time period, s

Δr Net runoff, kg/ m^2

The precipitation p , which is also the amount of rainfall in the summer, is measured by the weather station located on the east roof. Soil moisture change can be calculated by the water content measured by the five moisture sensors which are installed on the green roofs of Golda Meir Library.

$$\Delta S = (w_{i+1} - w_i) \times d \times \frac{1000kg}{1\ m^3} \tag{3.41}$$

ΔS Soil moisture change, kg/ (m^2·s)

w_{i+1} The water content at the end of the time step, m^3/m^3

w_i The water content at the beginning of the time step, m^3/m^3

d Soil depth, m

The precipitation monitored by weather station is the rainfall depth accumulated in 15 minutes. Therefore, instantaneous evaporation rate should be multiplied by the number of time periods.

$$w_{i+1} = \frac{p - E \times \Delta t - \Delta r}{d \times 1000} + w_i$$

(3.42)

The evaporation rate, E, of uncovered soil is different from the soil beneath canopy.

Regarding to the evaporation rate discussed in energy balance, the evaporation rate for the soil without vegetation coverage is:

$$E_{soil} = \rho_{air} C V \Delta \bar{q} \quad (3.43)$$

E_{soil} The rate of evaporation from the soil, kg/(m^{2}s)

ρ_{air} Air density, kg/m^3

C Dalton number, approximately 1.5 × 10^{-3}

V Mean wind speed, m/s

$\Delta \bar{q}$ The difference in humidity between the surface and the air, kg/kg.

For the bare soil,

$$\Delta \bar{q} = \frac{0.622}{P} 0.61078 (\exp\left(\frac{17.27 T_{soil}}{T_{soil} + 237.3}\right) - \exp\left(\frac{17.27 T_{air}}{T_{air} + 237.3}\right)$$

(3.44)

T_{soil} Soil surface temperature, °C

T_{air} Ambient temperature, °C

Therefore,

$$E_{soil} = \rho_{air} CV \cdot \frac{0.622}{P} 0.61078(\exp\left(\frac{17.27T_{soil}}{T_{soil}+237.3}\right) - \exp\left(\frac{17.27T_{air}}{T_{air}+237.3}\right)$$

(3.45)

For the soil underneath the canopy,

$$E_{veg} = \frac{\rho_a \cdot \frac{BP_{w,l}}{(P_{total}-P_{w,l})} - h \cdot \rho_a \cdot \frac{BP_{w,a}}{(P_{total}-P_{w,a})}}{r_l - r_a}$$

(3.46)

ρ_a Dry air density, kg/m^3

B 0.622 for air, kg/kg

$P_{w,l}$ Water vapor pressure on leaf, mbar

$P_{w,a}$ Water vapor pressure of air, mbar

P_{total} Ambient total pressure, mbar

r_l Internal leaf resistance, 100-2000 s/m

r_a A surface boundary-layer resistance

The vegetation coverage of the roof is represented by LAI in the following equation. The comprehensive evaporation rate can be estimated as:

$$E = LAI \cdot \frac{\rho_a \cdot \frac{BP_{w,l}}{(P_{total}-P_{w,l})} - h \cdot \rho_a \cdot \frac{BP_{w,a}}{(P_{total}-P_{w,a})}}{r_l - r_a} + (1 - LAI) \cdot \rho_{air} CV \cdot \frac{0.622}{P} 0.61078(\exp\left(\frac{17.27T_{soil}}{T_{soil}+237.3}\right) - \exp\left(\frac{17.27T_{air}}{T_{air}+237.3}\right)$$

(3.47)

LAI Leaf area index

To estimate the maximum water content of the saturated soil, I did an experiment to study the soil water absorption capacity. In the experiment, 250 ml to 1000 ml water was added into 250 ml soil to see how much water ran out of the soil. The experiment procedures are presented in Appendix C. In the experiment, the average maximum water content of the soil was found to be 0.384 cm^3/cm^3. The calculation is shown in Equation 3.48.

$$WC_{max} = \frac{V_{water,sat} - V_{run-off}}{V_{soil}} \quad (3.48)$$

WC_{max} Maximum water content of the soil sample, ml/ml

$V_{water,sat}$ The water volume of saturated soil sample, ml

$V_{run-off}$ The runoff water volume of saturated soil sample, ml

V_{soil} The soil sample volume, ml

The measured maximum water content reading of the soil moisture sensor was 0.383 cm^3/cm^3. The accuracy of the soil moisture sensor was ±0.031 m^3/m^3. The error between the calculated and the measured was 0.001, which is acceptable. Therefore, when the reading of the soil moisture reaches 0.383, the water ratio in the soil has reached its maximum water content.

However, the experiment of studying the soil water absorption capacity was done in a measuring cup, for a green roof system with drainage composite beneath the growing medium, water running-off occurs before the soil gets saturated due to the gravity and pores in the soil. I conducted another experiment to study the water runoff ratio, of which the procedures are shown in Appendix D. This experiment mimicked a

green roof drainage system with a strainer set underneath the soil. The experiment results revealed that when adding 100ml water into the 250 soil sample. The soil water content became stable and the soil absorbing capacity declined, as shown in Figure 31.

Finding the ratio between the water runoff volume and added-in water volume can estimate the water runoff amount during a rain event. The runoff ratio of the rainfall is shown in Table 3.

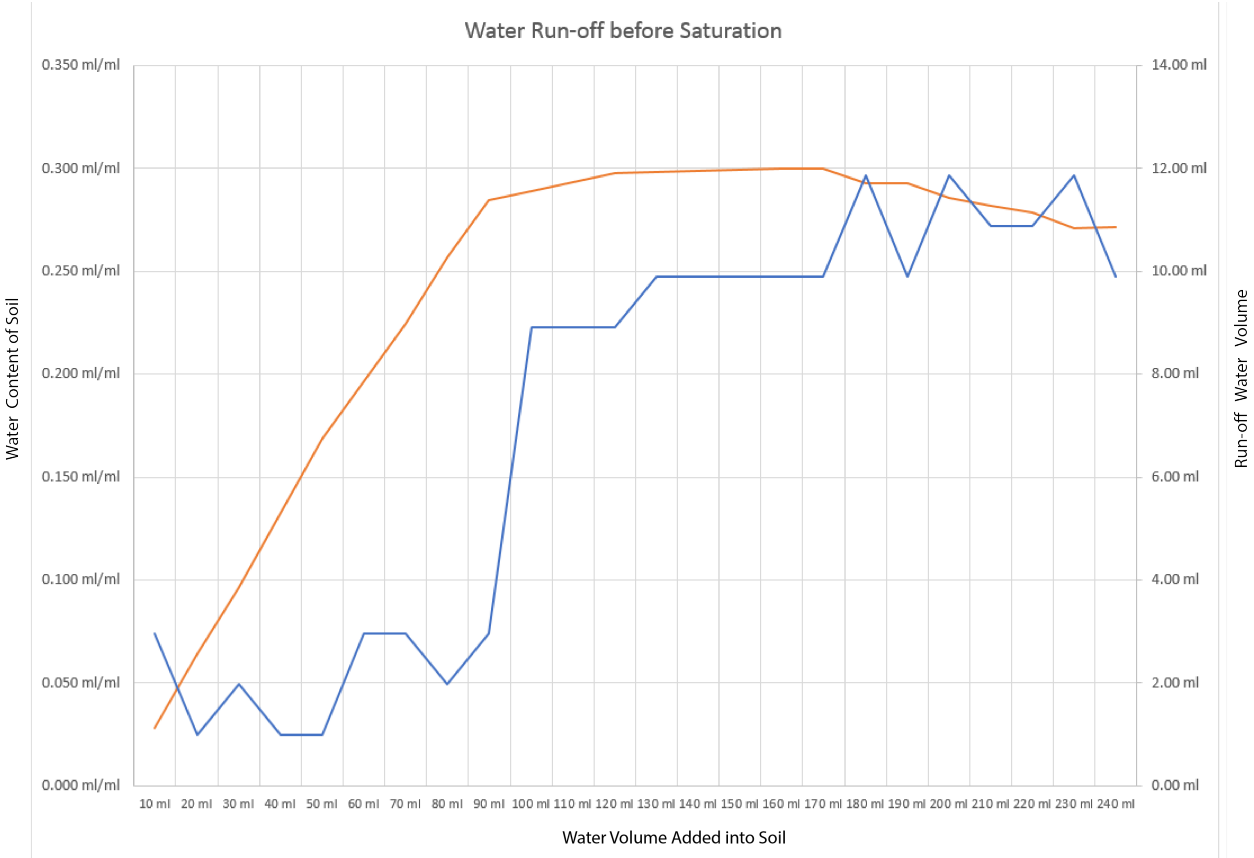

Figure 31. Water runoff ratio.

Table 3. Water runoff ratio estimation.

Added-in Water	Runoff Water	Water Content	Runoff Ratio
10 ml	2.97 ml	0.028 ml/ml	0.30
10 ml	0.99 ml	0.064 ml/ml	0.10
10 ml	1.98 ml	0.096 ml/ml	0.20
10 ml	0.99 ml	0.132 ml/ml	0.10
10 ml	0.99 ml	0.168 ml/ml	0.10

10 ml	2.97 ml	0.196 ml/ml	0.30
10 ml	2.97 ml	0.225 ml/ml	0.30
10 ml	1.98 ml	0.257 ml/ml	0.20
10 ml	2.97 ml	0.285 ml/ml	0.30
10 ml	8.91 ml	0.289 ml/ml	0.89
10 ml	8.91 ml	0.294 ml/ml	0.89
10 ml	8.91 ml	0.298 ml/ml	0.89
10 ml	9.90 ml	0.298 ml/ml	0.99
10 ml	9.90 ml	0.299 ml/ml	0.99
10 ml	9.90 ml	0.299 ml/ml	0.99
10 ml	9.90 ml	0.300 ml/ml	0.99
10 ml	9.90 ml	0.300 ml/ml	0.99
10 ml	11.87 ml	0.293 ml/ml	1.19
10 ml	9.90 ml	0.293 ml/ml	0.99
10 ml	11.87 ml	0.285 ml/ml	1.19
10 ml	10.88 ml	0.282 ml/ml	1.09
10 ml	10.88 ml	0.278 ml/ml	1.09
10 ml	11.87 ml	0.271 ml/ml	1.19
10 ml	9.90 ml	0.271 ml/ml	0.99

Table 3 provides us four information:

1. When the water content is lower than 0.028, there will not be water runoff. When the first 10ml water was added into the 250 ml soil, there was only 2.97 ml water ran off the soil. That meant 7.03ml water was completely absorbed by the soil. So, when the water content is lower than $\frac{7.03}{250} = 0.028$ ml/ml. This means that there is no water runoff.
2. When the water content is lower than 0.196, the water runoff ratio is about 0.1 of the added-in water.
3. When the water content is greater than 0.196, but lower than 0.285, the water runoff ratio is about 0.3 of the added-in water.

4. When the water content is larger than 0.289, but lower than the maximum water content of the soil, the water runoff ratio is about 0.89 of the added-in water.

Cooperate the information harvested in the Experiment A and B to estimate the Δr_i :

$$\Delta r_i = \begin{cases} 0, & p_i = 0 \\ 0, & w_{i-1} < 0.028 \\ p_{i+1}, & \sum_{i=1}^{n} p_i \geq (0.383 - w_{i-1})\, d \\ 0.89 p_i, & \sum_{i=1}^{n} p_i \geq (0.30 - w_{i-1})\, d \\ 0.3 p_i, & \sum_{i=1}^{n} p_i \geq (0.20 - w_{i-1})\, d \\ 0.1 p_i, & \sum_{i=1}^{n} p_i < (0.20 - w_{i-1})\, d \end{cases}$$

(3.49)

w Instantaneous water content, m^3/m^3

d Soil depth, mm

p Precipitation, mm

n The number of time step of the accumulated rainfall

The number of time step of the accumulated rainfall n is determined by the time the saturated soil can be completely dry. By observing the water content variation in the dry season and solving Equation 3.42 to get w_{i+1} with different n. I found that six days of accumulated rain was the best estimation of n. Figure 32 shows how the modeled water content fits the measured water content with different n settings.

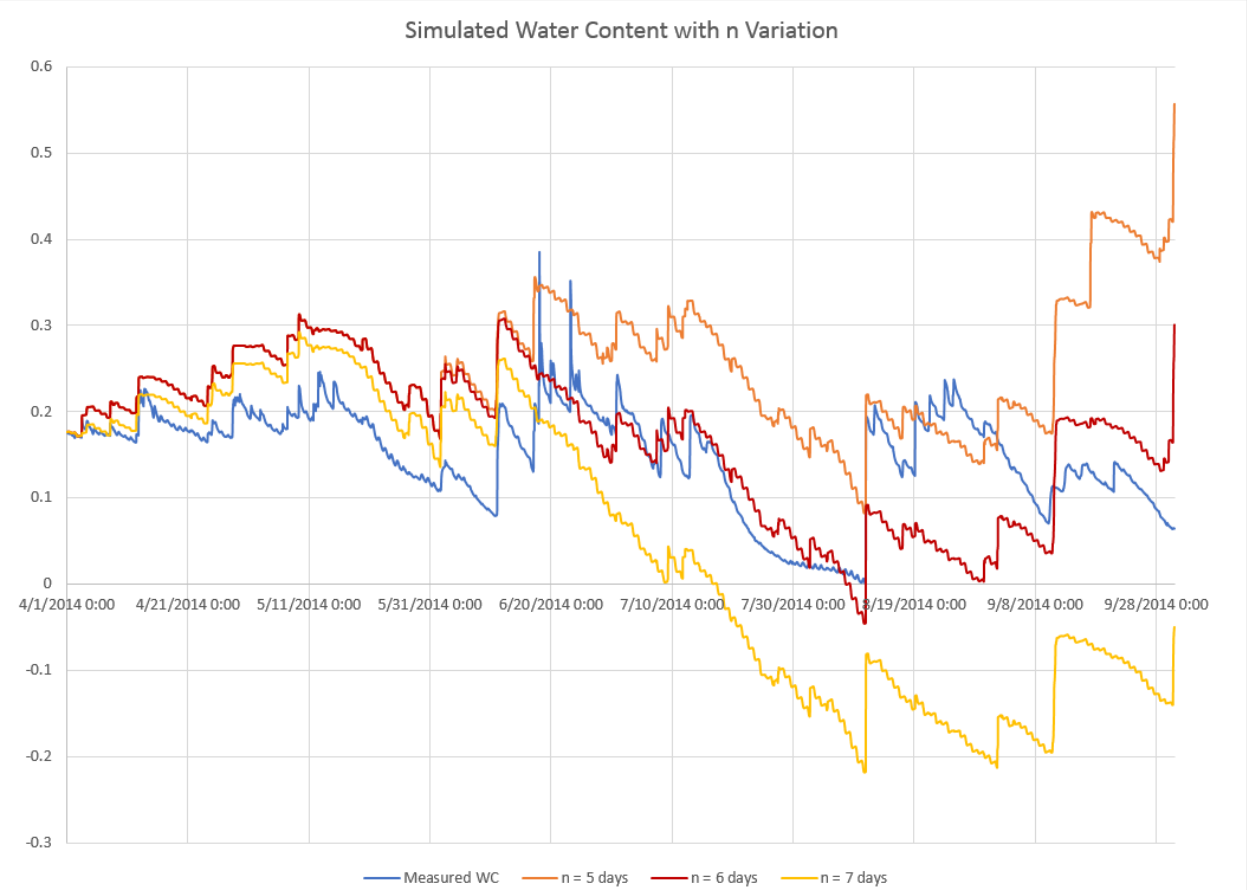

Figure 32. Testing variable n with 5, 6 and 7 days.

3.2.3 The Coefficients in the Equations

To simulate the heat and mass transfer models in MatLab, some coefficients were defined by different sources. Some are based on experiments, some are estimation, and some are from reliable reference.

The color of the dry soil is dark grey, which has a solar absorption of about 0.4-0.5. The absorption of a light green sedum plant is about 0.5-0.7. After rain, the soil turns dark brown, which makes the absorption go up to 0.8. However, there were some dry brown sedum leaves between the green sedum leaves, which made the comprehensive solar absorption of sedum go up to 0.8. After trying different level of

solar absorption in the simulation, I found that an absorption of 0.6 is the best fit for both soil and vegetation surfaces. The solar radiation received by bare soil and vegetation were the same in the simulation.

Following is the list of coefficients and their sources:

Table 4. The coefficients in the Equations for MatLab simulation.

Symbol	Variable Name	Coefficient (if applicable)	Sources
$\propto_{solar}$	Solar absorptance	0.6	Engineering Toolbox
$\varepsilon_{soil,dry}$	Dry soil surface emissivity	0.93	Engineering Toolbox
$\varepsilon_{soil,sat}$	soil surface emissivity	0.96	Engineering Toolbox
ε_{canopy}	Vegetation surface emissivity	0.97	Engineering Toolbox
k_f	Thermal of conductivity of fluid in soil	0.6 W/m· K	Thermal Properties of Soils (1986)
k_s	Thermal of conductivity of dry soil solid	0.15 W/m· K	Thermal Properties of Soils (1986)
d	Soil depth	100 mm	Measurement
r_l	Internal leaf resistance	360 s/m	Estimation
T_{bldg}	Interior concrete deck temperature	22 °C	Measurement
$h_{c,g}$	Thermal resistance of air space between canopy and ground	5.67 W/m$^{2\circ}$ C	ASHRAE Fundamental
ρ_d	Dry bulk density	690 kg/m^3	Measurement
c_d	Specific heat capacity of dry soil	950 J/kg·K	Engineering Toolbox
c_w	Specific heat capacity of water	4180 J/kg·K	Engineering Toolbox
U_{bldg}	Roof U-value	0.273 W/m$^{2\circ}$ C	Estimation

3.2.4 Validation

Validation is necessary for modeling, and it is a means to prove that a simulation is reliable (Knepell & Arangno, 1993). There are four methods to validate the simulation models: subjective recognition, time-frequency analysis, mathematical statistics and dynamic relation analysis (Zhou et.al, 2009). In this research, mathematical statistics is selected to validate both energy and mass balance.

For the energy balance model, the modeled soil temperature was compared with the measured one. Equations 3.28 and 3.39 were simulated in MatLab to calculate the soil temperature in each time step, and then validated by the measured data in the same time step.

The modeled water contents for the mass balance model were compared with the measured ones. Equation 3.42 was simulated in MatLab to calculate the water content in each time step, and then validated by the measured data in the same time step.

The root-mean-square deviation (RMSD) and the standard error (SE) of the differences was used as the criterion to investigate the errors. I validated the April to October 2014 modeled soil temperature with measured ones. The RMSD and SE calculation is as follows:

Table 5. Measured and modeled soil temperature summary.

No.	Time	Measured	Modeled	$d_i = d_{mod}-d_{msd}$	d_i^2
1	4/1/2014 12:00:00 A.M.	8.12	8.12	0.000	0.000
2	4/1/2014 12:15:00 A.M.	8.045	8.009	-0.036	0.0013
3	4/1/2014 12:30:00 A.M.	7.495	7.880	-0.0647	0.0049
:	:	:	:	:	:
11714	8/1/2014 12:00:00 A.M.	23.088	26.655	3.5668	12.7218
:	:	:	:	:	:
17568	9/30/2014 11:45:00 P.M.	12.509	9.538	-2.971	8.8292
Total				27255.9794	128020.592

The sample mean of the difference is

$$\bar{d} = \frac{1}{n}\sum_{i=1}^{n} d_i = \frac{27255.9794}{17568} = 0.5\ °\text{C} \tag{3.50}$$

The sample variance of the difference is

$$s_d^2 = \frac{\sum_{i=1}^{n} d_i^2 - \left(\sum_{i=1}^{n} d_i\right)^2/n}{n-1} = \frac{128020.592 - 27255.9794^2/17568}{17568-1} = 9.687 \tag{3.51}$$

The root-mean-square deviation is

$$RMSD = \sqrt{\frac{\sum_{i=1}^{n} d_i^2}{n}} = \sqrt{\frac{128020.592}{17568}} = 3.15°\text{C} \tag{3.52}$$

The standard error of the differences is

$$SE(\bar{d}) = \sqrt{\frac{s_d^2}{n}} = \sqrt{\frac{10.670}{17568}} = 0.0235 \tag{3.53}$$

Repeating the same procedures with the modeled soil temperature beneath the canopy, the average difference of the simulation is 1.31 °C, RMSD=2.34 °C and the SE is 0.015.

Figures 33 and 34 compare modeled and measured soil temperature of bare soil and vegetation-covered soil in August 2014. In August, for bare soil, the average

difference of the simulation is -0.19 °C, RMSD=1.97 °C and the SE is 0.036. For vegetation-covered soil, the average difference of the simulation is 0.15 °C, RMSD=1.39 °C and the SE is 0.025.

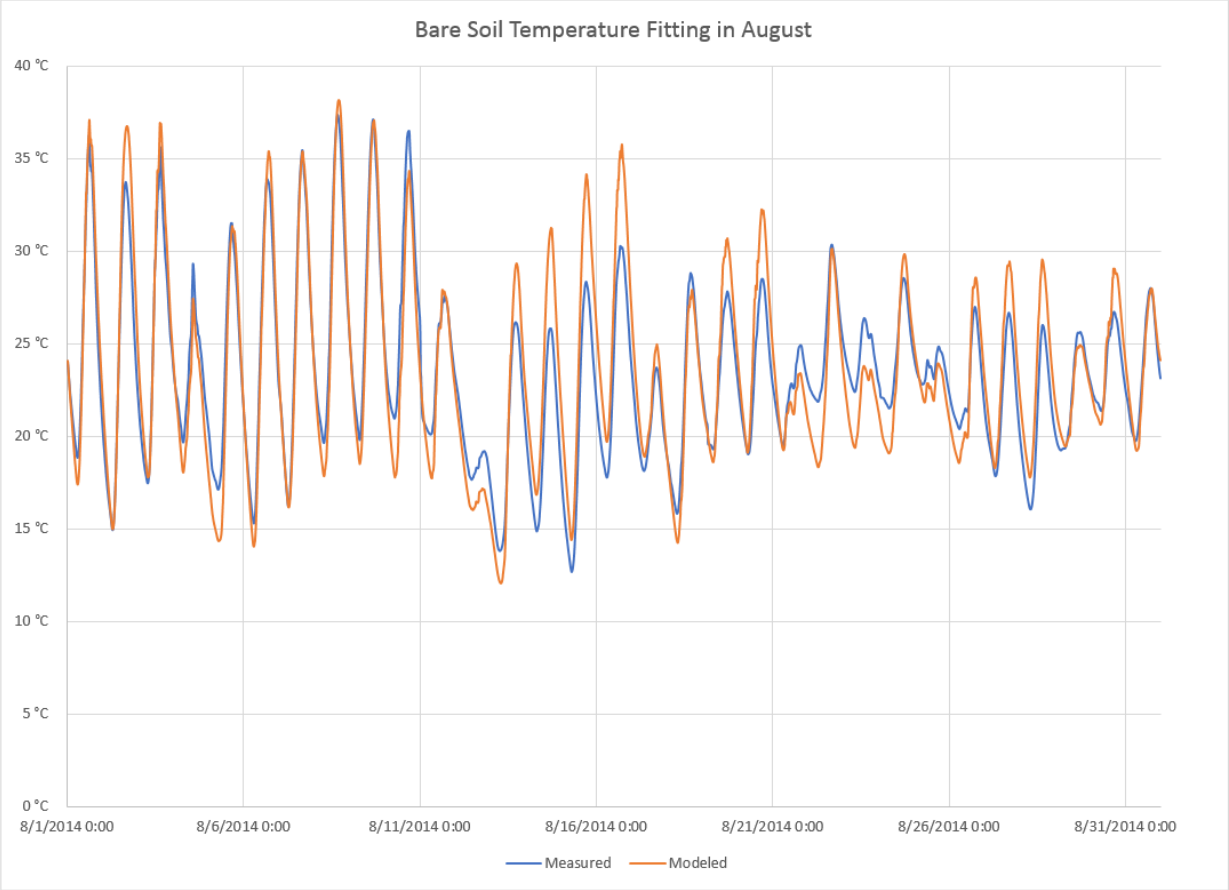

Figure 33. Measured and modeled bare soil temperature comparison in August.

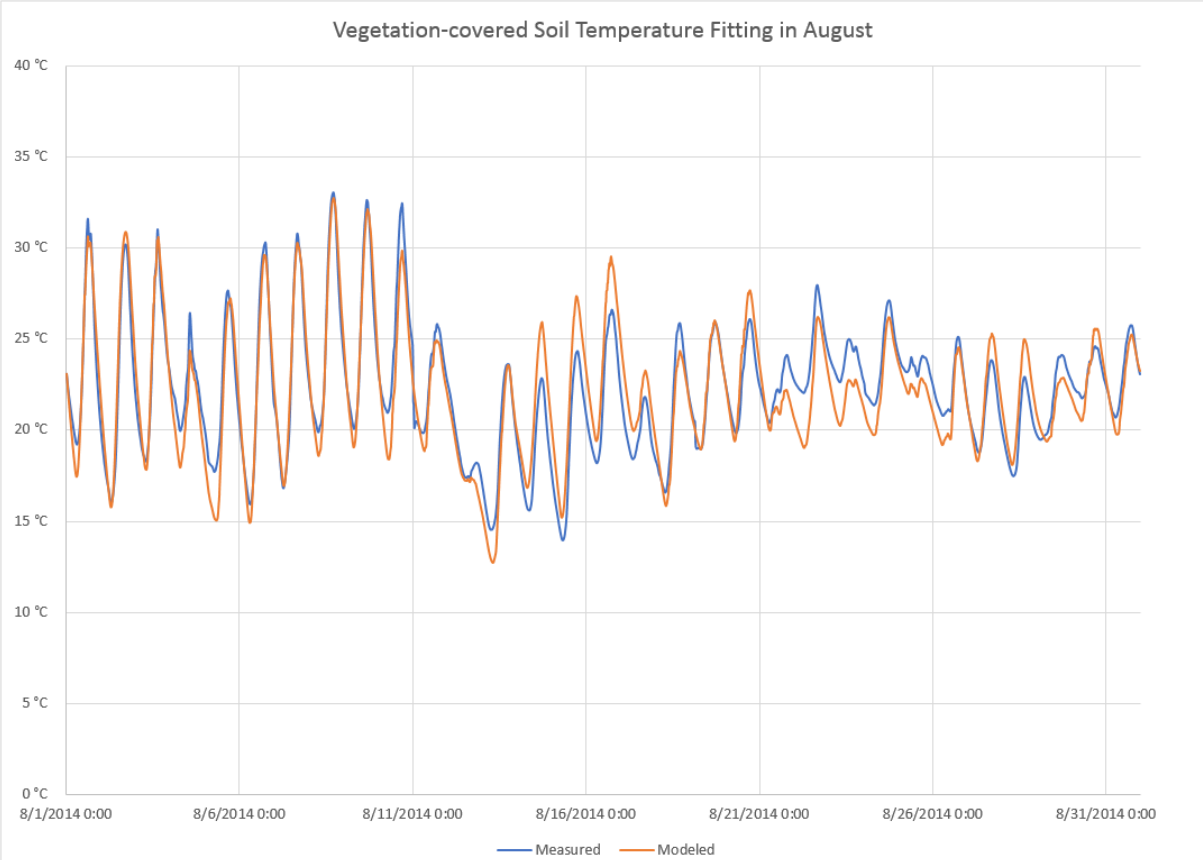

Figure 34. Measured and modeled vegetation-covered soil temperature comparison in August.

The same calculation is applied to the mass balance model. The average difference of the simulation is 0.0197 m^3/m^3. The RMSD is 0.0769 m^3/m^3 and the SE is 0.000561.

The comparison between the measured and modeled water content is shown in Figure 35.

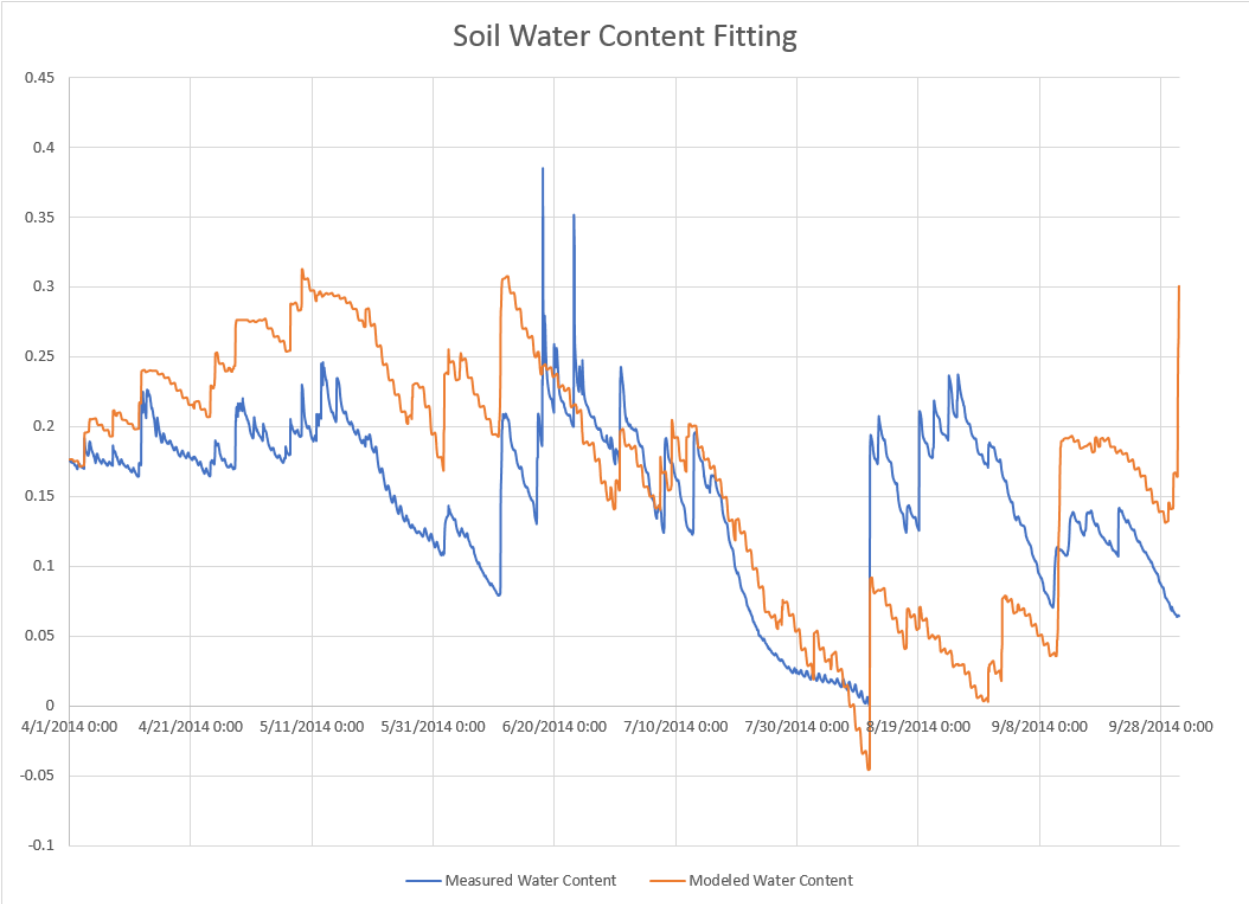

Figure 35. Measured and modeled soil water content comparison from April to September.

4 Results

In this chapter the results of the simulation are described:

4.1 Parametric Analysis of the Green Roof Energy Balance

4.1.1 Energy Flux Density

To make the energy balance easy to read the in the diagram, the energy balance model is revised in Equation 4.1, which is different from Equation 3.2. In Equation 3.2, the $Q_{evaporation}$, energy flux though evaporation, is assumed to lose heat when it is negative. On the other hand, when $Q_{evaporation}$ is positive, the surface is absorbing heat.

$$Q_{solar} + Q_{rad} + Q_{conduction} + Q_{convection} + Q_{evaporation} = 0 \quad (4.1)$$

Figures 36 and 37 show the average hourly energy flux density in August 2014 for bare soil and vegetation-covered surfaces.

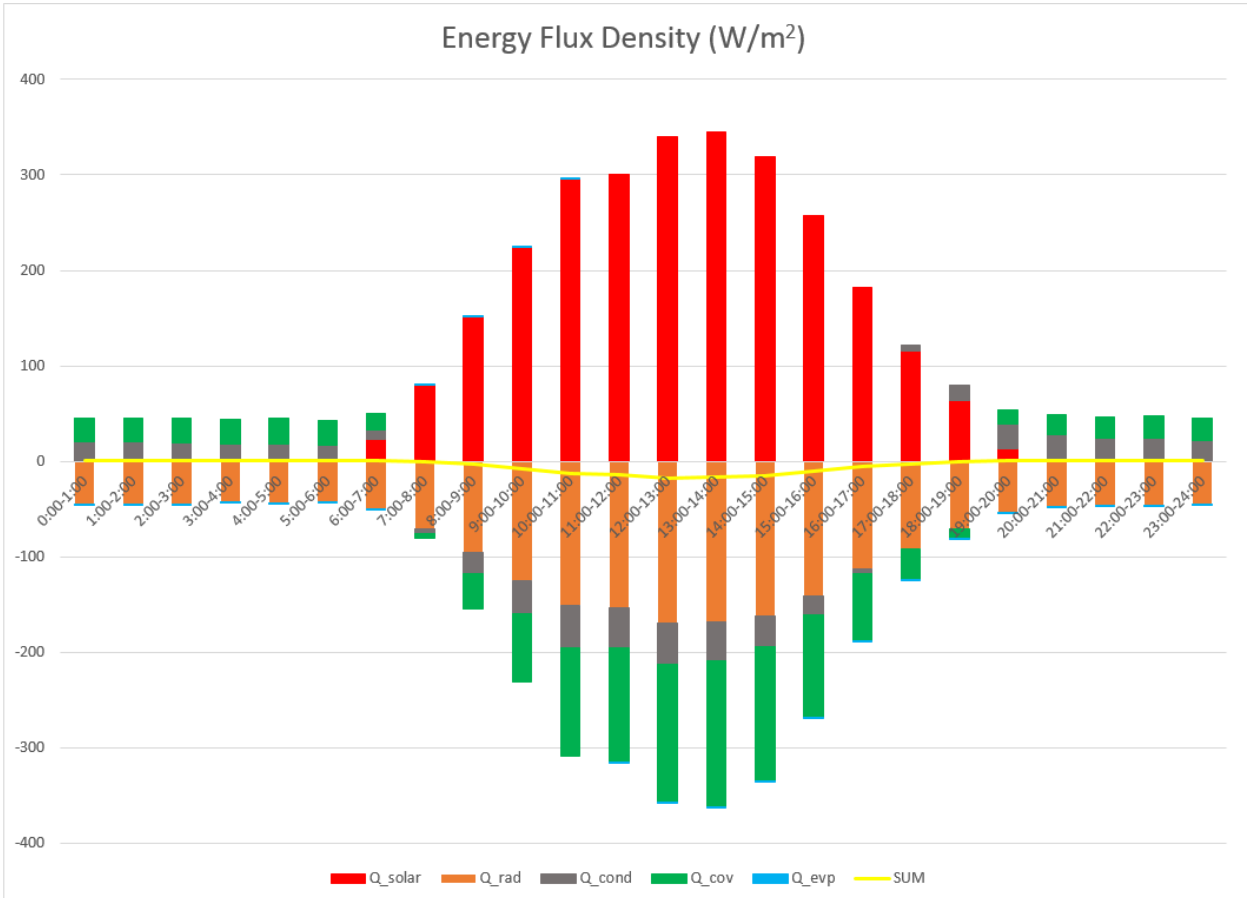

Figure 36. The average energy flux density for bare soil surface in August, 2014.

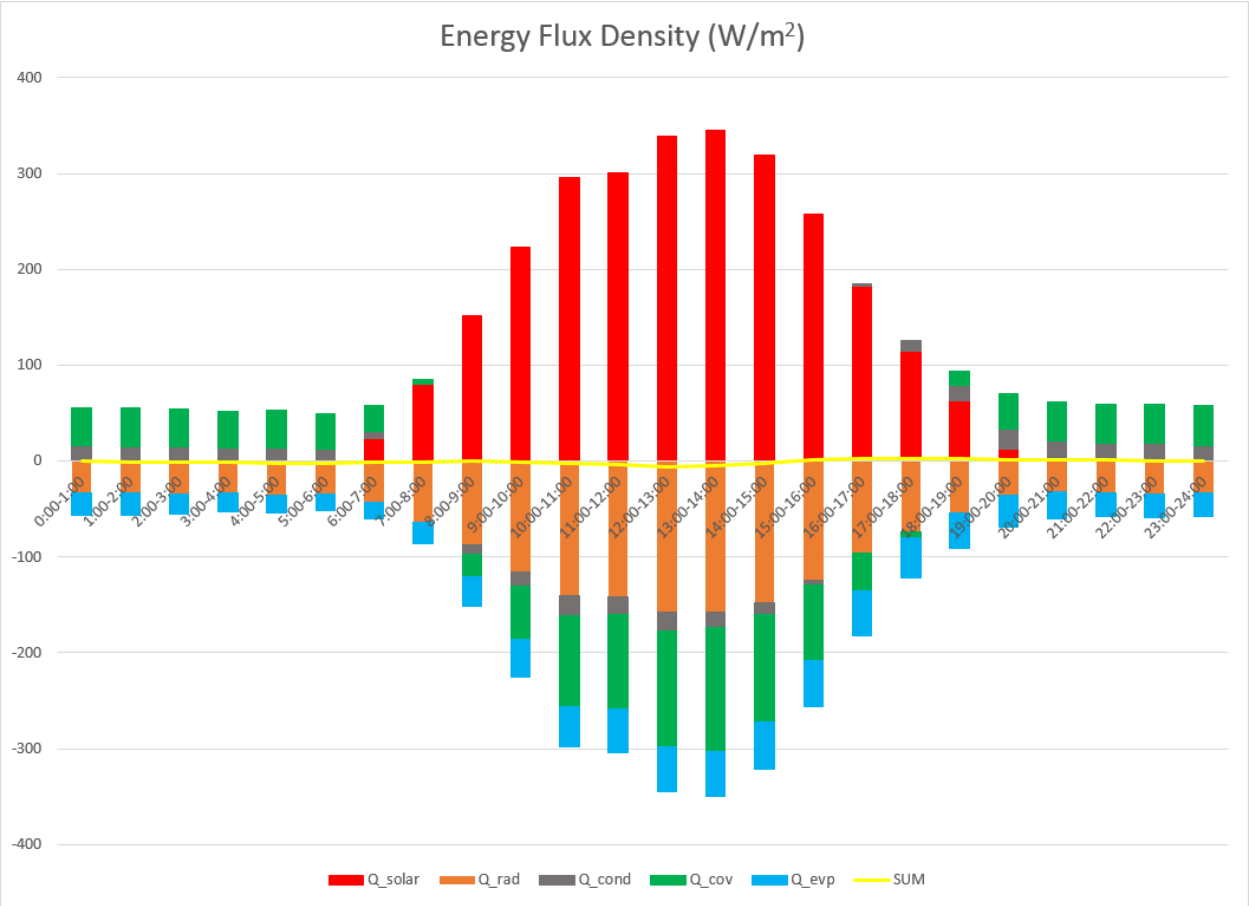

Figure 37. The average energy flux density for vegetation-covered soil surface in August, 2014.

The solar radiation, Q_{solar}, is the major heat source for both bare soil and vegetation-covered surface. In August, solar radiation appears from 6 in the morning, increases to a peak in the afternoon from 13:00 to 14:00 (1 p.m. to 2 p.m.), and then decreases gradually toward sunset at around 18:00 to 19:00 (6 p.m. to 7 p.m.). In the simulation, I assumed the same absorption for both bare soil and vegetation-covered surface.

The diffusive radiation from the atmosphere, Q_{rad} is negative throughout the day. That means the surface temperature is always higher than the sky temperature, which makes sense during summer.

The heat conduction, Q_{cond}, is negative during the day and positive during the night. That means, whether or not there is vegetation coverage, the soil is absorbing heat during the daytime and losing heat during the night. It also demonstrates that the heat is conducted down to the building through the soil during the day and released from the building through the soil at night.

Figure 38 shows the relationship between wind speed, temperature differences between surface and air, and heat convection during a day. The heat convection, Q_{conv}, depends on the wind speed and temperature difference between the surface and the air. The larger the wind speed, the larger the convection. The larger the difference between the surface and the air temperature, the larger the convection. When Q_{conv} is positive, it means the surface is gaining heat through heat convection. On the other hand, if Q_{conv} is negative, the surface is releasing heat to the air through convection. In the stacked columns shown in Figures 36 and 37, the heat convection for a vegetation-covered surface is larger than bare soil during the day. The wind speed above the bare soil and the vegetation-covered surface is the same, so apparently the plant surface temperature is closer to the air temperature than the soil surface temperature. Therefore, both soil and vegetation-covered surfaces have a higher temperature than the ambient air temperature, but the soil surface is hotter than the vegetation surface. Their relationship is as below:

$$T_{soil,surf} > T_{veg,surf} > T_{amb} \tag{4.2}$$

This simulation outcome matches the surface temperature measurement.

However, during the night, the heat convection of the surface is positive, and the convection of the vegetation surface is larger than the bare soil. That means both soil and vegetation surfaces have lower temperatures than the air temperature, but the soil surface temperature is closer to the ambient temperature than the vegetation temperature. Their relationship is as below:

$$T_{amb} > T_{soil,surf} > T_{veg,surf} \tag{4.3}$$

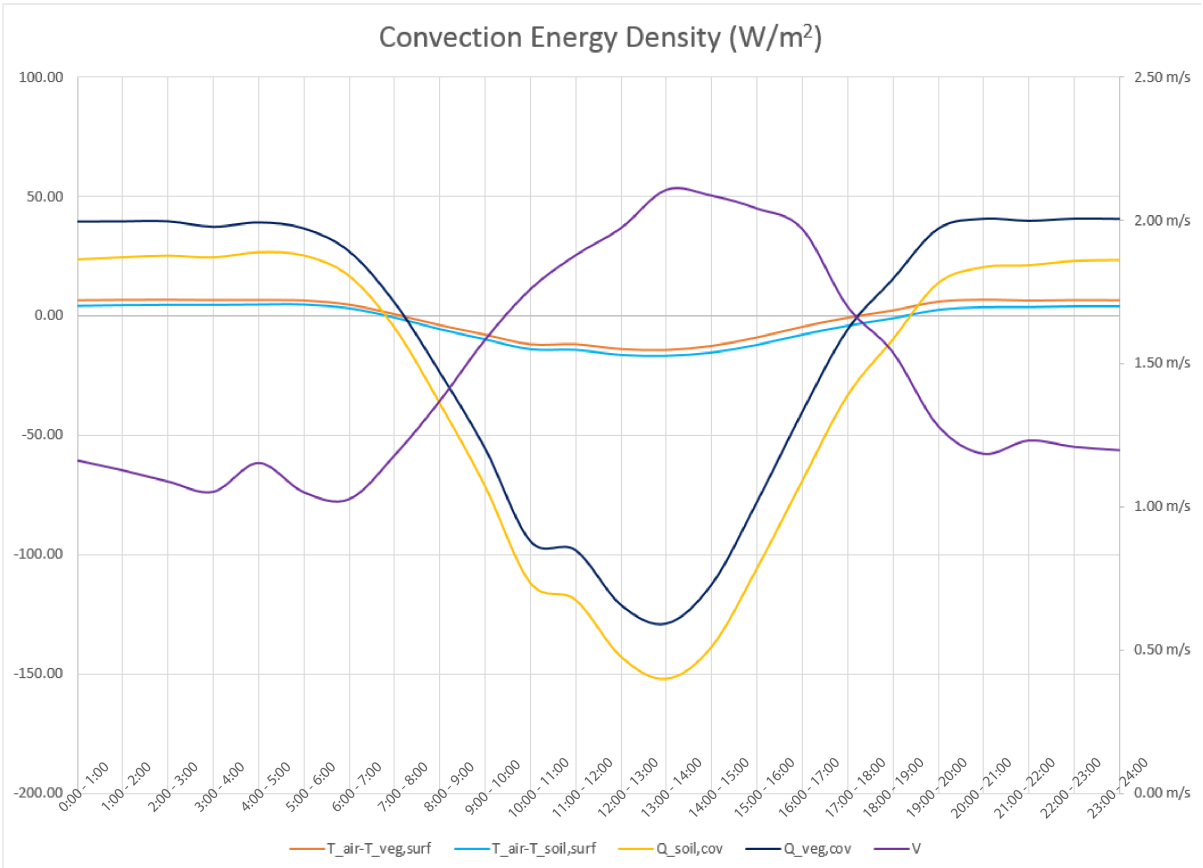

Figure 38. Evaporation energy density for the bare soil surface and the vegetation-covered surface.

The amount of latent heat transferred through evaporation, Q_{evap}, is very little for a bare soil surface. Most of the soil surface evaporation is negative, which means the water vapor on the surface evaporates and releases heat into the air. But in the morning, from 7 a.m. to 11 a.m., Q_{evap} is positive and very low. The surface is absorbing

heat, which means the water vapor on the soil surface is condensed. There should be some dew on the surface in the morning. On the other hand, Q_{evap} is negative throughout the day for vegetation-covered surfaces and much larger than that of the soil surface. Figure 39 shows the temperature difference between the surfaces and the air. Compared to the significant difference of Q_{evap} between soil and vegetation-covered surfaces, the temperature difference between surfaces and air for bare soil and vegetation is very small. Therefore, the major reason for the large heat loss through evaporation must be the plants' own transpiration.

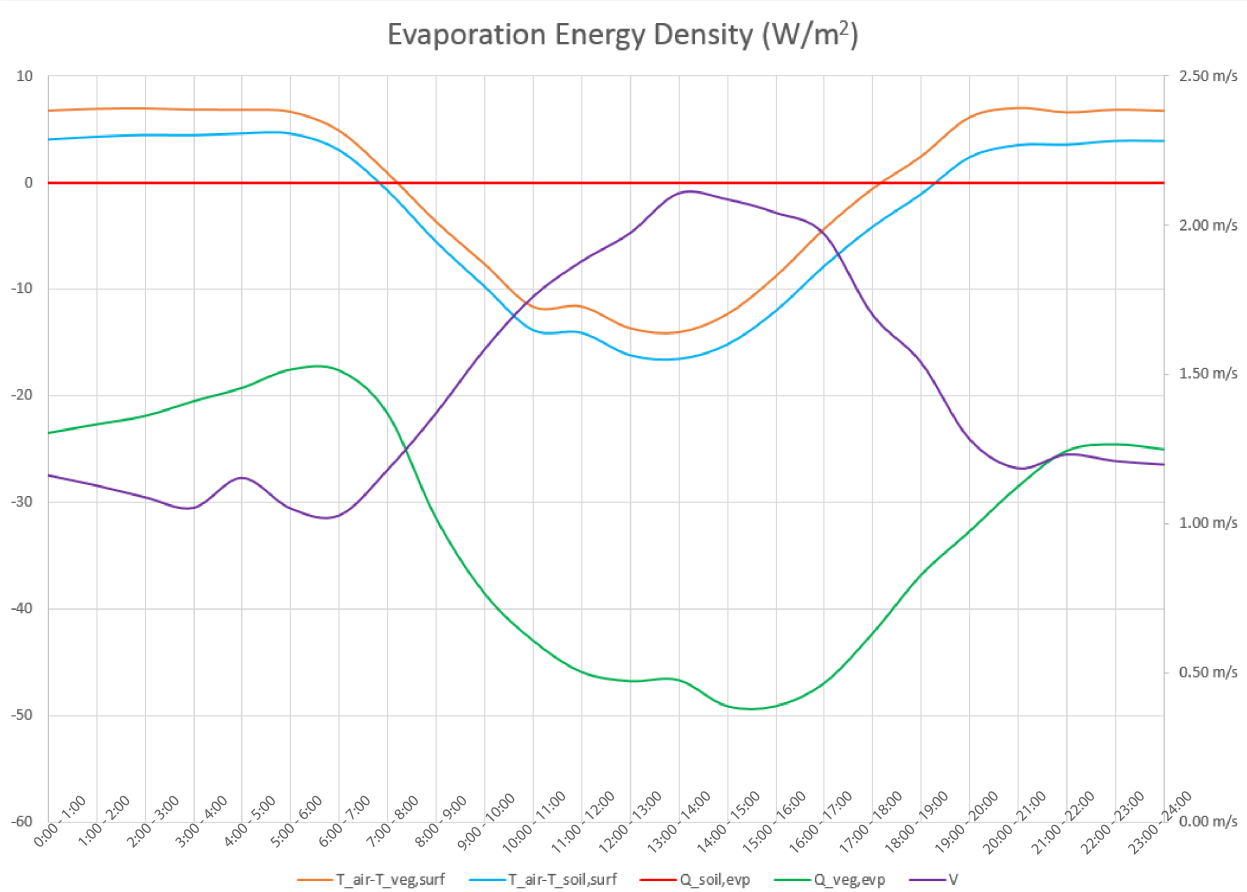

Figure 39. Evaporation energy density for the bare soil surface and the vegetation-covered surface.

4.1.2 Temperature

As shown in Figure 40, on a clear day, the measured soil temperature without vegetation is higher than that beneath sedum plants. The modeled soil temperatures without vegetation coverage are higher than the measured ones. The difference increases with the increase of solar radiation. The vegetation-covered soil temperature does not show too much difference between measurement and simulation. The change in measured and modeled soil temperature shows the same, approximately one-hour delay in the change of solar radiation. It is caused by the heat storage capacity of soil.

However, the surface temperature comparison in Figure 41 shows the opposite. The surface temperature changes reflect the change of solar radiation immediately. In the morning, the surface temperature increases more rapidly. Based on the rate of increase of temperature and solar radiation in the morning, we can see that, the temperature increase is sharper than the solar radiation increase. It means that when the surface receives solar radiation in the morning, it is efficiently heated up. After the peak time of solar radiation, the decrease of solar radiation does not affect the decrease of surface temperature as much as that in the morning. The thermal inertia, which is also the heat capacity of the surface, is the main reason for this phenomenon.

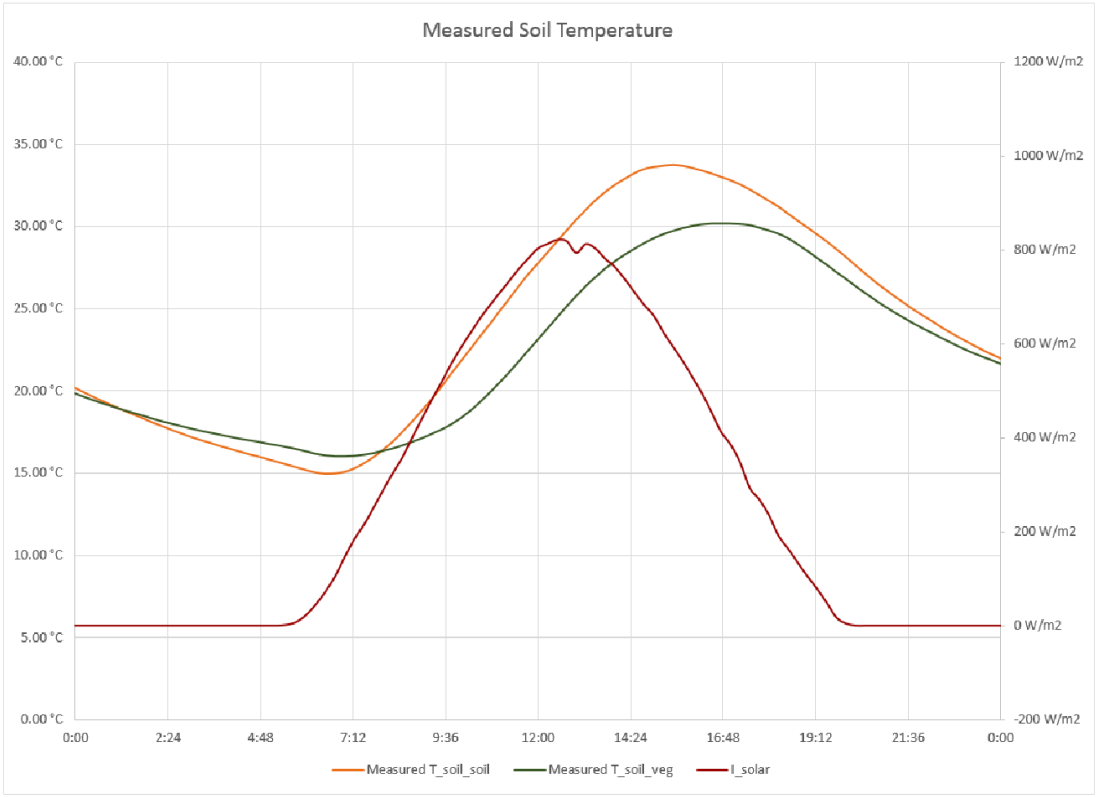

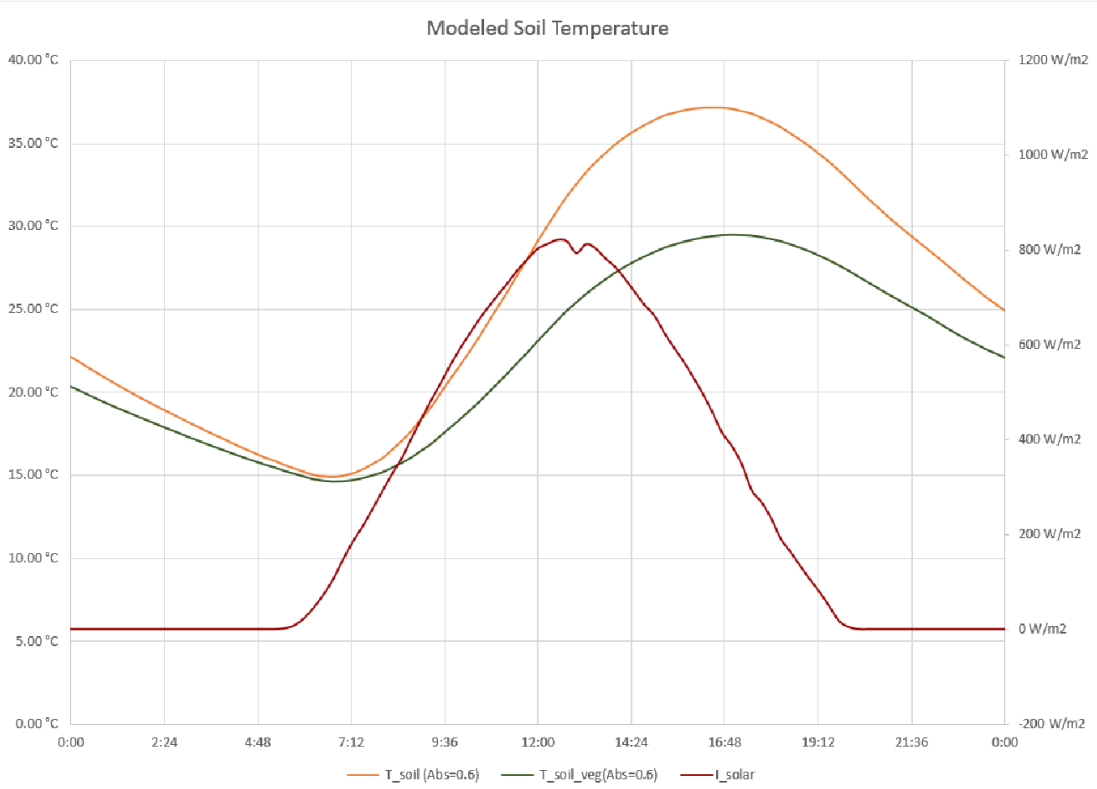

Figure 40. The comparison between measured and modeled soil temperature on a clear day, August 2nd, 2014.

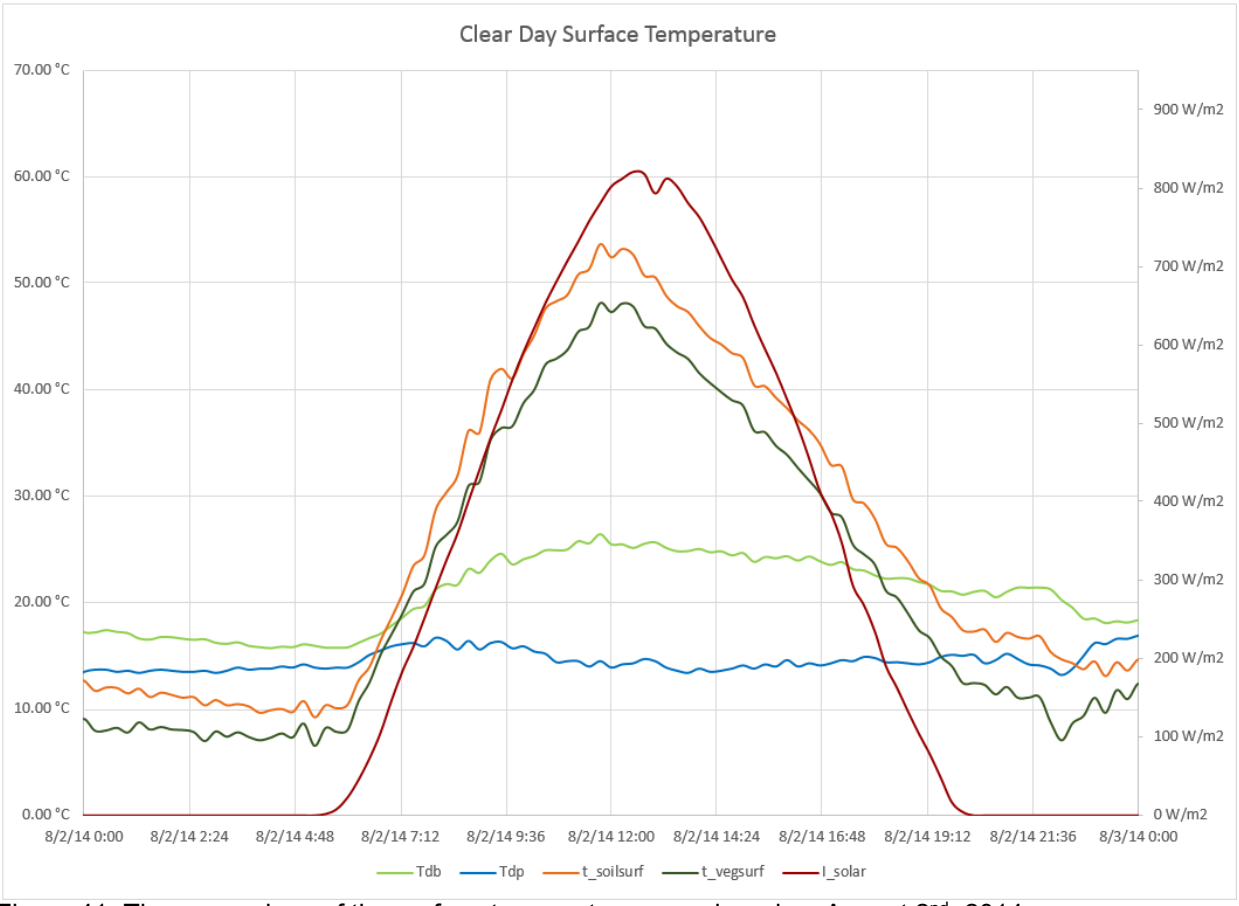

Figure 41. The comparison of the surface temperature on a clear day, August 2nd, 2014.

On an overcast day, the situations are opposite. As shown in Figure 42, the measured and modeled soil temperatures are much more stable than those on a clear day. There are still some minimal increases when the solar radiation significantly increases. However, the temperature increase is far lower than the solar radiation increase. As on the clear days, the increase of soil temperature occurs later than the increase of the solar radiation. Compared to the one-hour delay on a clear day, the delay on a overcast day is only about 15 minutes, which means the soil heat absorption is minimal.

Figure 43 shows the bare and vegetation-covered surface temperature comparison on a overcast day. Just as on a clear day, the daytime surface temperature

still varies closely in step with the change of solar radiation. As on a clear day, the soil surface temperature is still higher than the vegetation-covered surface temperature. Apparently, the temperature difference between these two surfaces on a clear day is much higher than that on a overcast day. This modeled outcome is the same as the surface temperature measurement results.

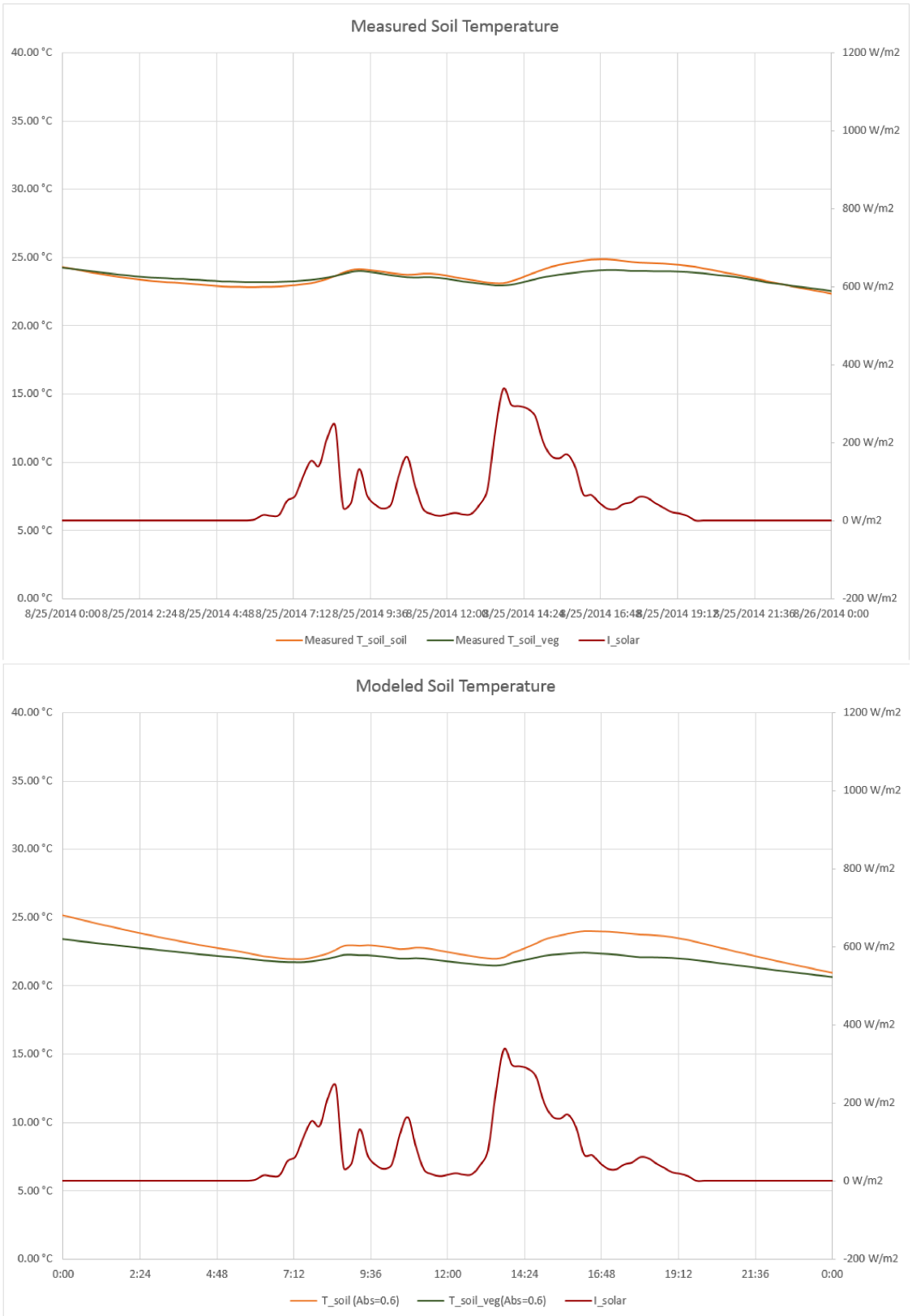

Figure 42. The comparison between measured and modeled soil temperature on a clear day, August 2nd, 2014.

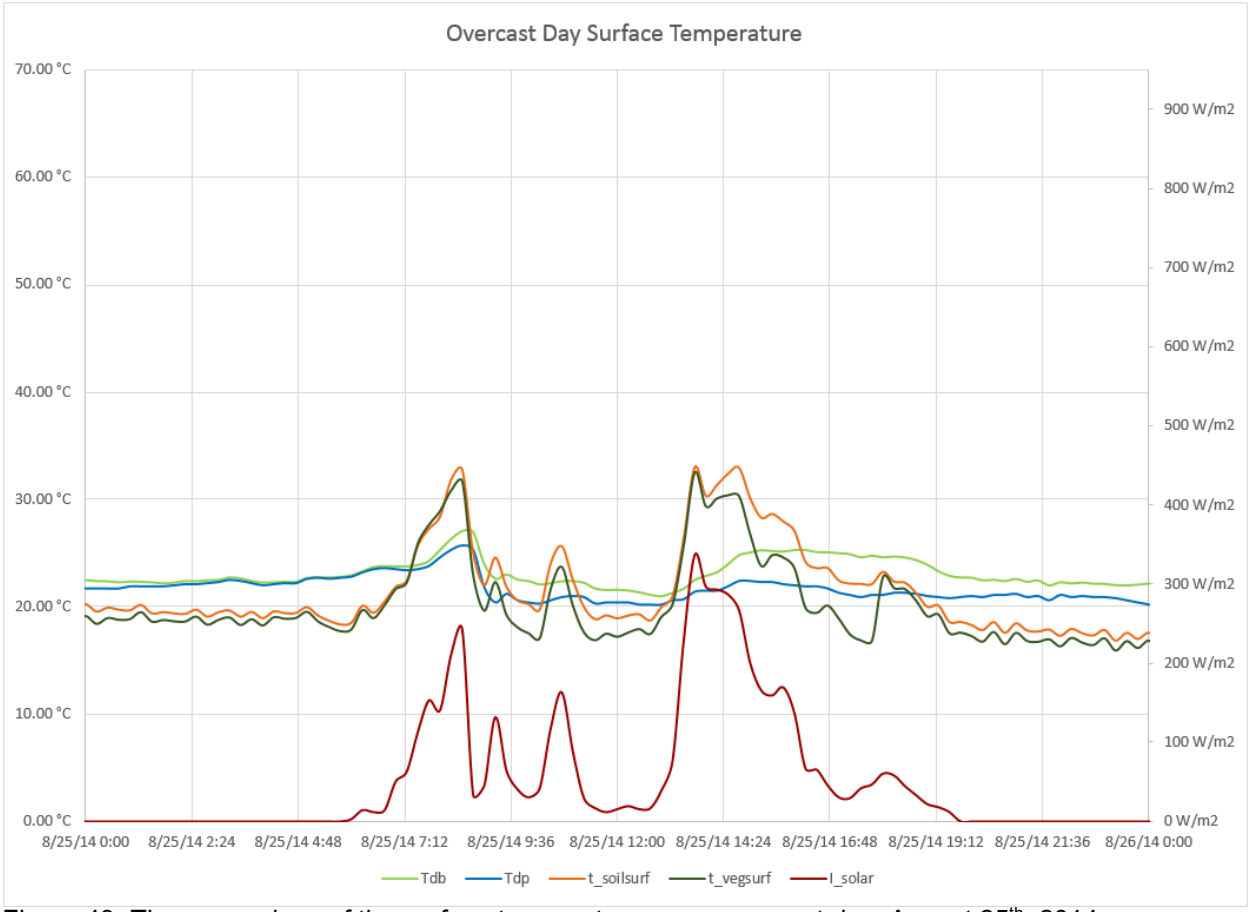

Figure 43. The comparison of the surface temperature on an overcast day, August 25th, 2014.

4.1.3 The Effects of Color, Soil Depth and Plant Type on Surface Temperature

One of the goals that green roofs can achieve is to mitigate the heat island effect. The key to reduce the heat island effect is to reduce the surface temperature.

As stated in the bare soil surface temperature mathematical model, shown in Equation 3.21 and 3.22, I_{solar}, T_{sky}, T_{air} , h_c , V are variables that cannot be controlled. But $\propto_{solar}$, ε_{surf}, d are the variables that can be controlled by green roof designers. $\propto_{solar}$ and ε_{surf} are variables decided by surface color and texture. The soil has similar textures, so the color of the soil is something the designers should be concerned about. Soil depth d is decided by the green roof designers.

$$T_{surf,soil} = \frac{I_{solar} \propto_{solar} + 4\varepsilon_{surf}\sigma(\bar{T})^3 T_{sky} + h_c T_{air} + \frac{k_e}{d} T_{soil} - \lambda \mathrm{E}}{h_c + 4\varepsilon_{surf}\sigma(\bar{T})^3 + \frac{k_e}{d}} \tag{4.4}$$

$$E = \rho C V \frac{0.622}{P} 0.61078 (\exp\left(\frac{17.27 T_{soil}}{T_{soil} + 237.3}\right) - \exp\left(\frac{17.27 T_{air}}{T_{air} + 237.3}\right) \tag{4.5}$$

Because ε_{surf} is proportional to $\propto_{solar}$, and they are both decided by the color of the surface, I used the solar absorption level, $\propto_{solar}$, as the reference to see how the color of the surface affects the surface temperature.

The effect of the surface color and the soil depth on the surface temperature on a clear day and an overcast day is shown in Figures 44 and 45. On a clear day in summer, between sunrise and sunset, the surface temperature of the bare soil is higher than the air temperature. When $\propto_{solar}$ increases by 33%, the soil surface temperature rises about 10 °C during peak solar radiation at noon. However, when d increases by 50%, the surface temperature only rises about 2°C during peak solar radiation at noon. In addition, Figure 44 shows the higher the solar radiation, the more influential $\propto_{solar}$ and d. During the night, the surface temperature is lower than the air temperature and the $\propto_{solar}$ has no impact on surface temperature. Also, the thicker the soil the lower the surface temperature, which is opposite to the activity during the day time.

On an overcast day in summer, similar to a clear day, Figure 45 shows that $\propto_{solar}$ is still the primary element that affects the surface temperature. When $\propto_{solar}$ increases by 33%, the soil surface temperature rises about 5°C at peak solar radiation. On an overcast day, the peak solar radiation does not necessarily happen at noon, but

at the time with less cloudy conditions. When soil depth d increases by 50%, the surface temperature rises less than 1°C. During the night, the effect of $\propto_{solar}$ and d on the bare soil surface on an overcast day is similar to that on a clear day.

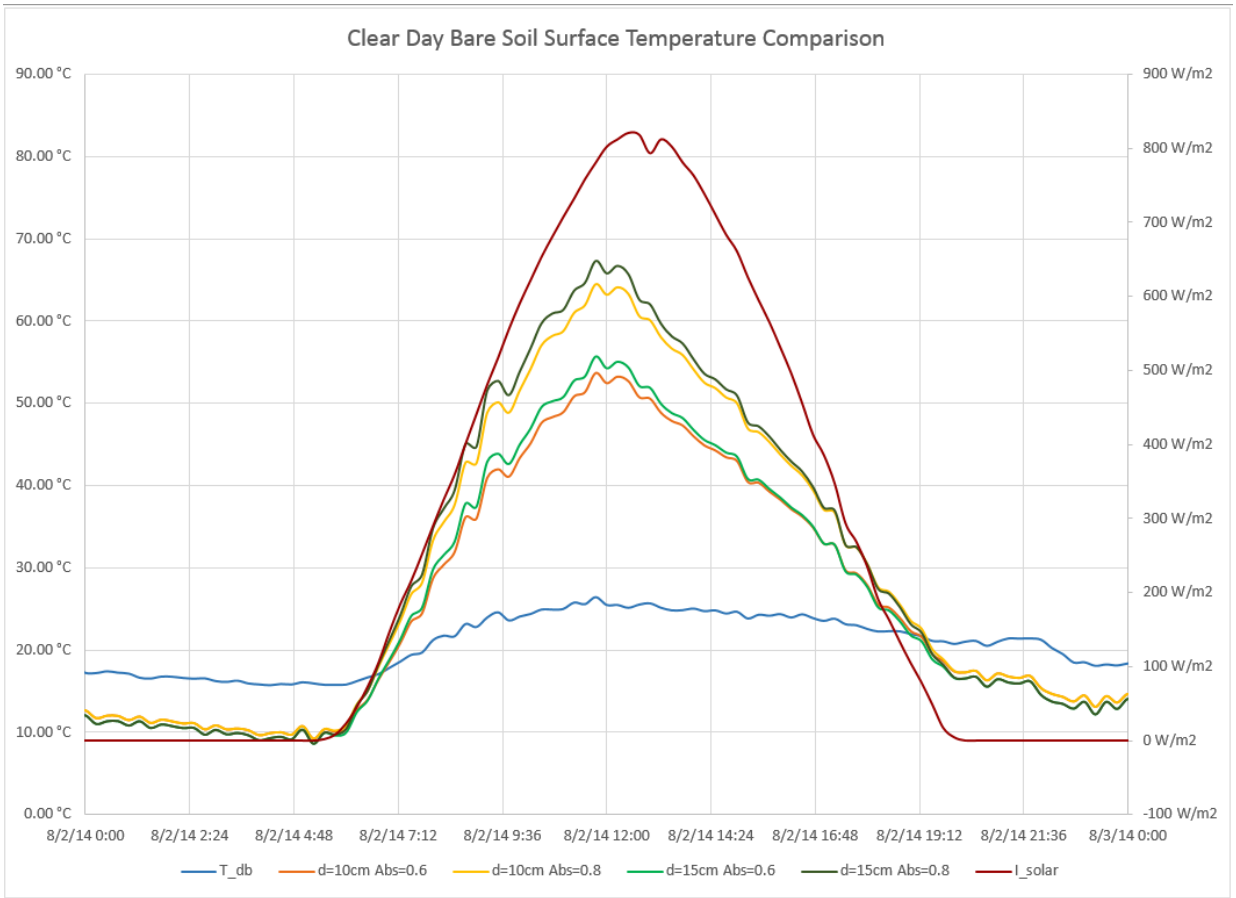

Figure 44. Bare soil surface temperature with soil depth and solar absorption variations on a clear day, August 2nd, 2014.

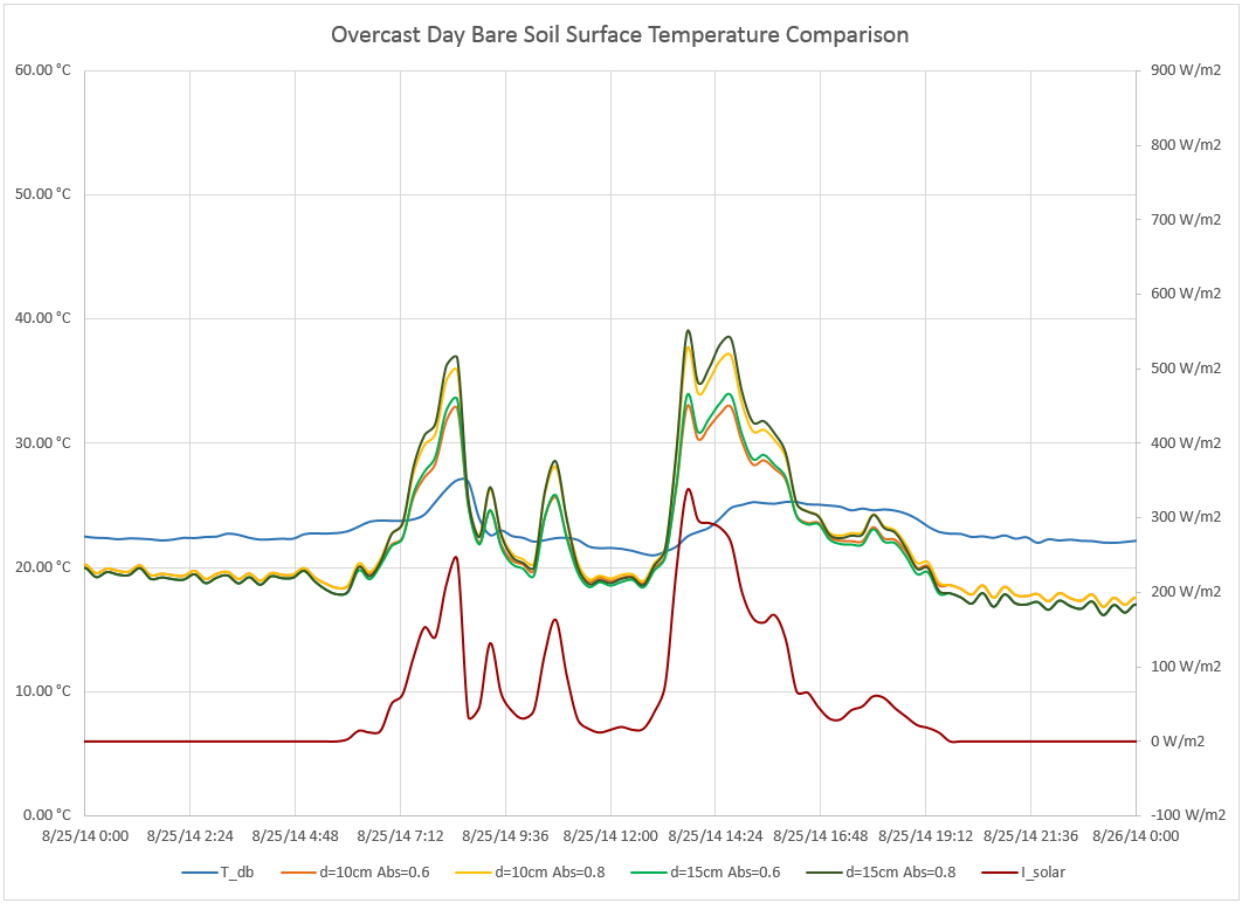

Figure 45. Bare soil surface temperature with soil depth and solar absorption variations on an overcast day, August 25th, 2014

For the vegetation-covered surfaces, as shown in Equation 3.37, I_{solar}, T_{sky}, T_{air}, h_c, V, h are variables that cannot be controlled. But $\propto_{solar}$, ε_{canopy}, d, r_l, W, and D are the variables that can be controlled by green roof designers. The vegetation color and texture determine $\propto_{solar}$ and ε_{canopy}. The leaves have similar textures, so the color of the leaves is what the designers should be concerned about. The green roof designers decide the soil depth d with the needs of the plants in mind. Internal leaf resistance r_l is in a range of 100-2000 s/m. The level of r_l is determined by the type of plant. 200 s/m is the most common internal leaf resistance, but some plants, such as sedum that can live in a relatively arid conditions, have a higher internal leaf resistance. The dimension of a

leaf is $W$and D. Because I already described the effects of the surface color and soil depth in the previous section, here we will focus on testing the plant's parameters. I assumed two other plants on the Gloda Meir Library roof. One is the grass, just like the one planted for Delft University of Technology. Another is a native plant with relatively large leaves in Milwaukee. Grass and the native plants are both adaptive to the summer in Milwaukee and their r_l are both 200 s/m. I assume the effective leaf dimensions of the grass and native plants, which are A_{grass}, for grass and A_{native} for a native plants with relatively large leaves. Measured the size of a grass leaf and a native plant leaf; I got:

$$A_{grass} = W^{0.2}D^{0.3} = (0.005)^{0.2}(0.08)^{0.3} = 0.162 \text{ m}^{1/2} \quad (4.7)$$

$$A_{native} = W^{0.2}D^{0.3} = (0.03)^{0.2}(0.08)^{0.3} = 0.232 \text{ m}^{1/2} \quad (4.8)$$

$$A_{sedum} = W^{0.2}D^{0.3} = (0.01)^{0.2}(0.01)^{0.3} = 0.1 \text{ m}^{1/2} \quad (4.9)$$

$$T_{surf,veg} = \frac{I_{solar} \propto_{solar} + 4\varepsilon_{veg,surf}\sigma(\bar{T})^3 T_{sky} + h_c T_{air} + \frac{1}{\frac{d}{k} + \frac{1}{h_{c,g}}} T_{soil} - \lambda \left[\frac{(1-h)d_a}{r_l - k_2 \frac{W^{0.2}D^{0.3}}{V^{0.5}}} \right]}{h_c + 4\varepsilon_{veg,surf}\sigma(\bar{T})^3 + \frac{1}{\frac{d}{k} + \frac{1}{h_{c,g}}}} \quad (4.10)$$

The surface temperatures of the plants with different internal leaf resistances and sizes on a clear day are shown in Figure 46. The sedum, which requires the least amount of maintenance and survives in harsh conditions, has the highest temperature. A native plant with the same internal leaf resistance as the grass is cooler than the grass because of its larger leaf size. However, on a cloudy day, the difference was

minimal during the day, and there was no difference at night. At the time with low solar radiation, the surface temperature is even lower than the air temperature.

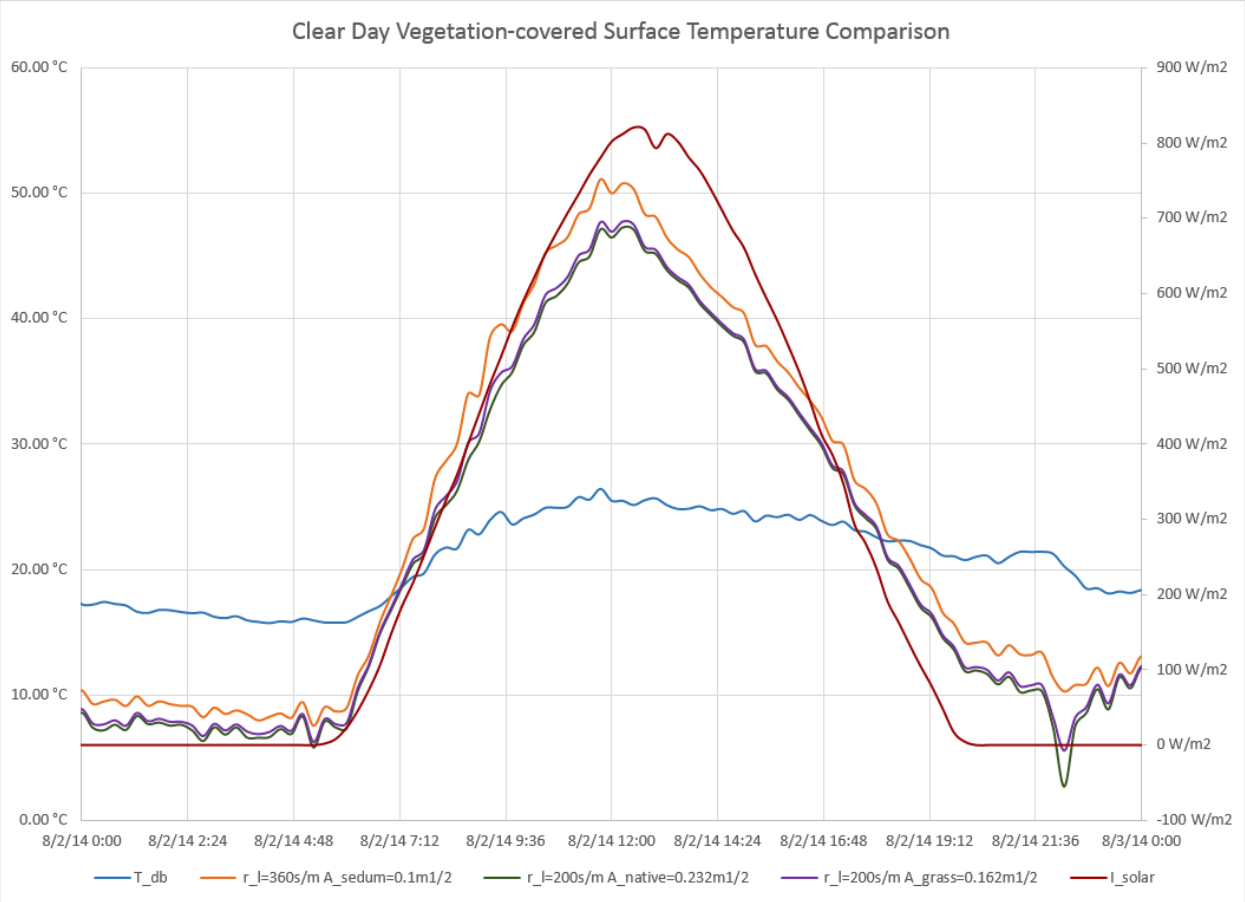

Figure 46. Vegetation-covered surface temperature with internal leaf resistance and leaf size variations on a clear day, August 2nd, 2014.

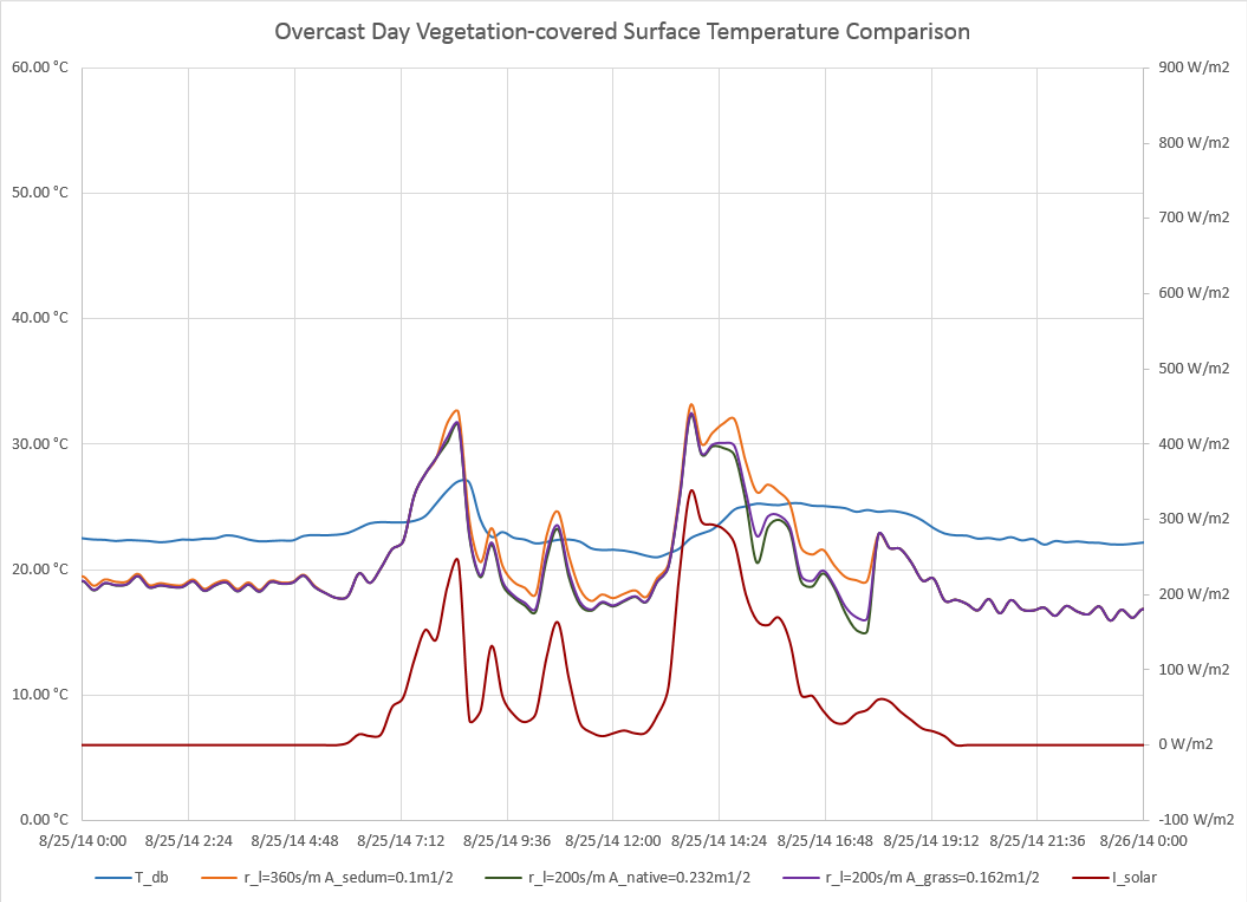

Figure 47. Vegetation-covered surface temperature with internal leaf resistance and leaf size variations on an overcast day, August 25th, 2014.

4.2 Parametric Analysis of the Green Roof Mass Balance

4.2.1 Soil Water Content

As shown in Figure 48, during April to September in 2014, there were six periods of high rainfall. These periods occured between the middle of June and the middle of July were considered big storms. Between June 20th to August 10th there were a dry season with minimal rain. After the dry season, there were a few heavy rainfalls between August 11th and August 25th.

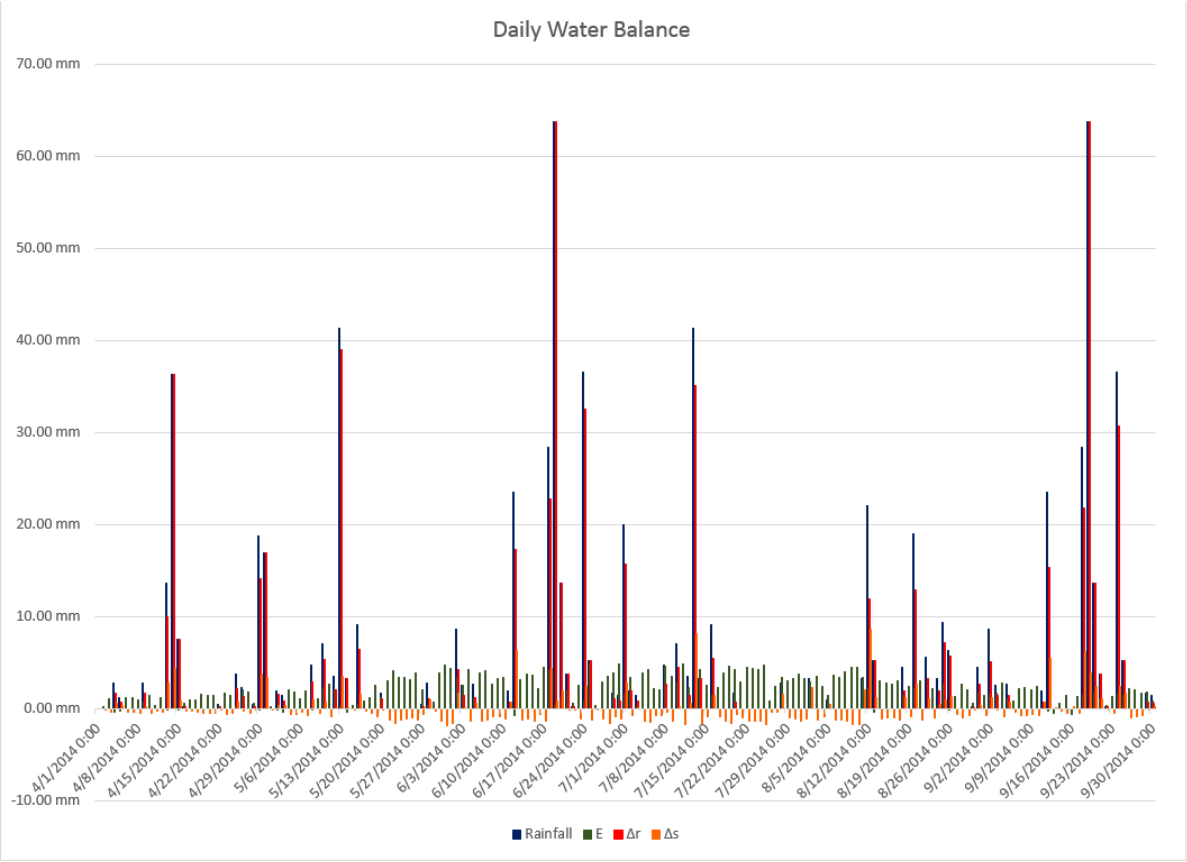

Figure 48. Daily water balance in from April to September, 2014.

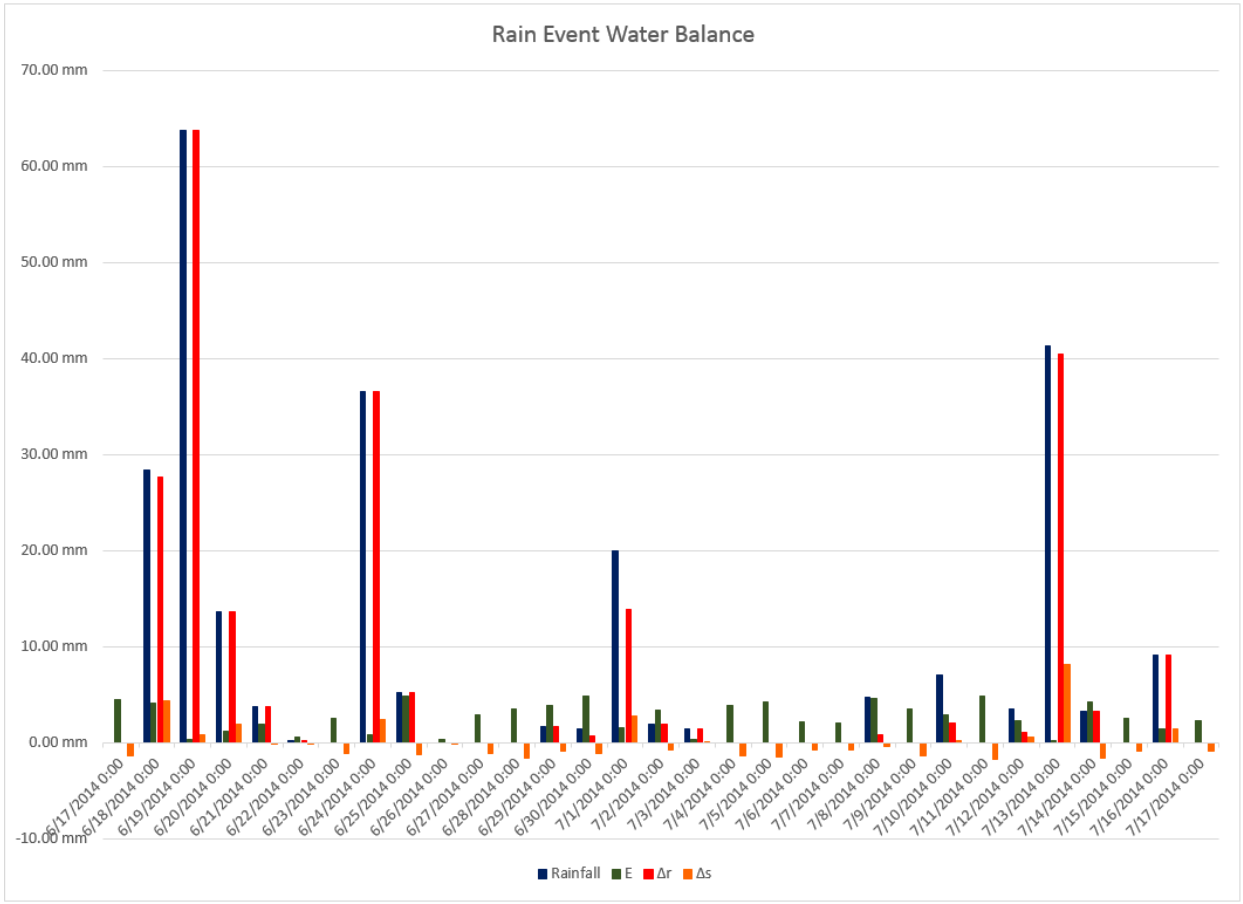

Figure 49. Water balance between June 17th and July 17th, 2014.

Figure 49 shows the big storms between June 18th and June 19th and the rainfall after. On June 17th, the day before the rain came, the soil moisture change ΔS was negative. The soil lost water because of evaporation. On June 18th, when there was a rainfall of 28mm, the runoff was about 23mm, and the water content change was about 10mm. The soil absorbed about 18% of the rain. However, on June 19th, the day there was a storm with about 65mm rainfall, 100% of the rain ran off the roof and the soil absorbed nearly zero water and the plant evaporation was also minimal. On June 20th, there was approximately 14mm rainfall, which was only half of the rainfall of June 18th, but 100% of the rain ran off the roof, and the soil absorbed minimal water. The same

situation occurred on June 21st. Even with 4mm of rainfall, the soil still failed to absorb any water, and 100% of the rainfall left the soil.

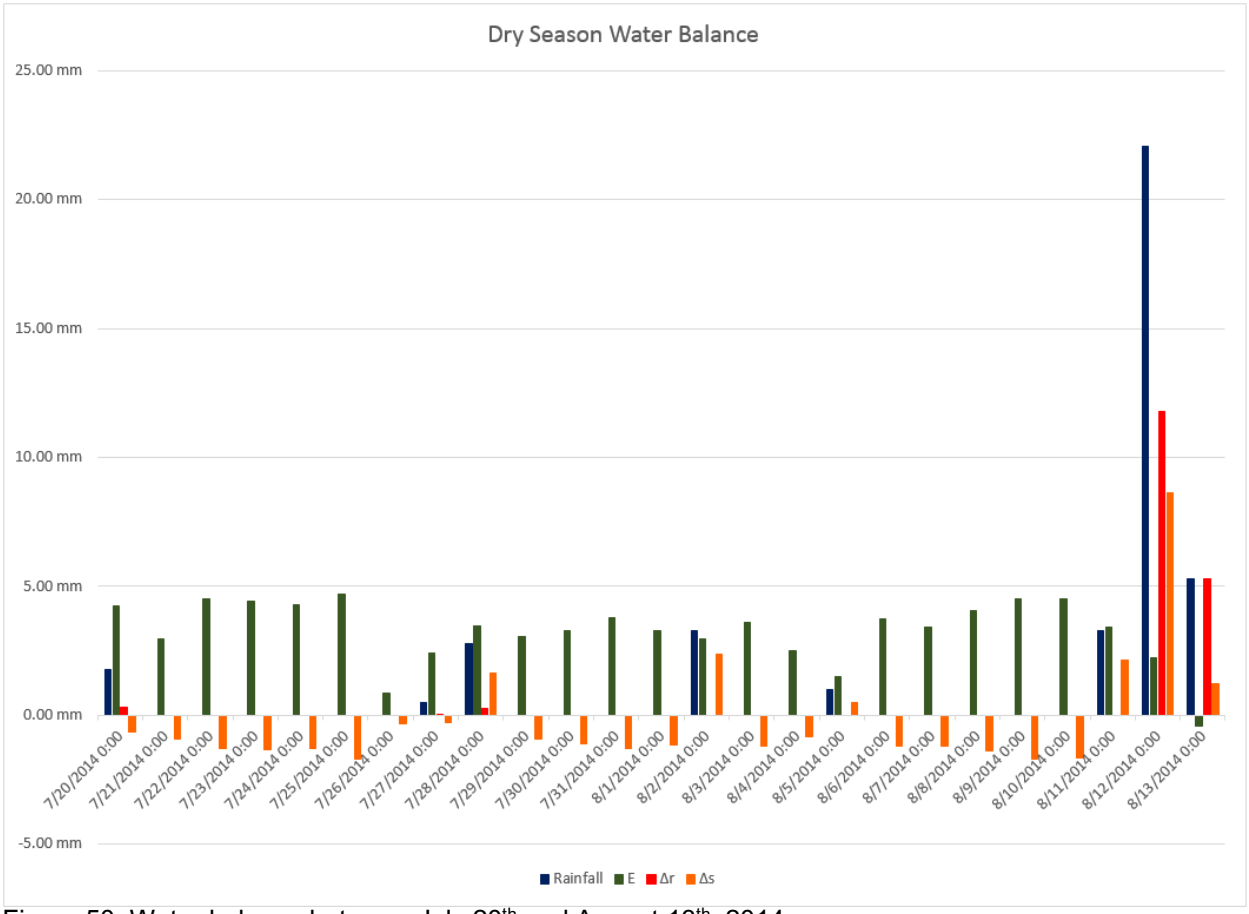

Figure 50. Water balance between July 20th and August 13th, 2014.

As shown in Figure 50, there was a dry period in Milwaukee during July 21st to August 10th in 2014. There were only four days of minimal rain, and the green roof completely absorbed the rain without any runoff. The soil moisture change was negative throughout this period, which means the water either evaporated through the soil or the plants. Since ΔS were getting smaller during this period, I believe the total water amount in the soil was decreasing at this time.

After a 3-week dry period, the soil became porous, which increases its ability to retain water. Therefore, the 3 mm rainfall on August 11th was completely absorbed, and half of the 22.5 mm rainfall on August 12th was absorbed. In those cases, a total of 25.5 mm rain fell on the green roof, but only 11.25 mm ran off the roof. However, on August 13th, when the water content in the soil had reached its maximum water absorption, 100% of the rainfall ran off the roof.

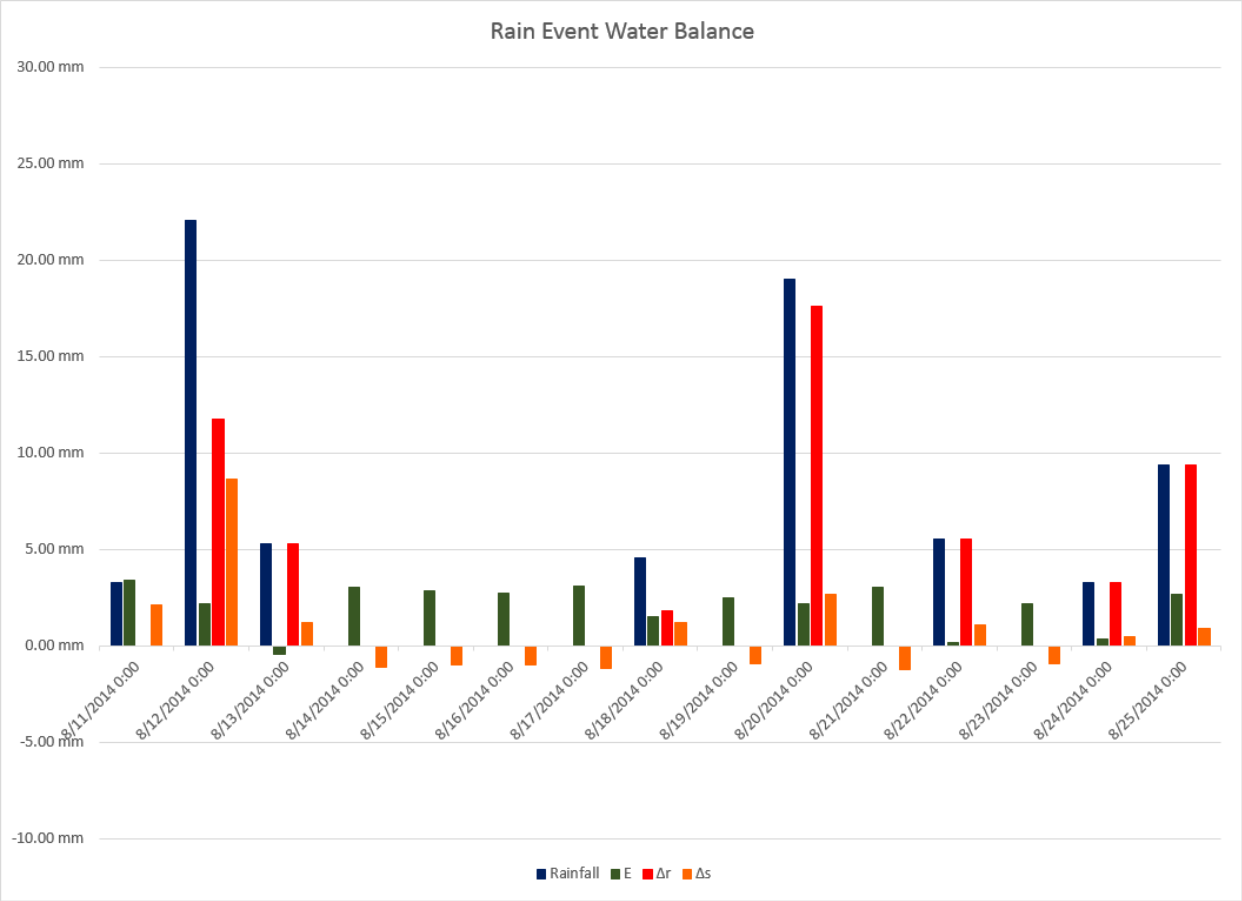

Figure 51. Water balance between August 11th and August 25th, 2014.

As shown in Figure 51, after three days of rain, it did not rain again until August 18th. Unlike the rain on August 11th, it was not completed absorbed by the green roof but had approximately 50% runoff. August 11th and August 18th were both the first day of rain after a dry period, but the green roof reacted to the rain on these two days in

different ways. The main reason was that the soil was dry enough to absorb all the rain on August 18th, which means the water absorbed by the soil between August 11th to August 13th still affected the water absorption on August 18th. This assumption could be proved by the sum of ΔS. The sum of the positive ΔS between August 11th to 13th was larger than the sum of the negative ΔS between August 13th and 17th, which means the water restored between August 11th to 13th was not completely drained or evaporated. The moist soil had lower capacity to absorb incoming rain.

4.2.2 The Effects of Vegetation Coverage, Soil Depth and Plant Type on Storm Water Runoff

The goal of a green roof is to reduce storm water runoff and retain water in the soil. The precipitation p is not controllable. But the vegetation coverege LAI , soil depth d , and plants' internal leaf resistance r_l and leaf dimension $W^{0.2}D^{0.3}$ can be planned in the schematic design phase.

$$p = E \times \Delta t + \Delta r + \Delta S = E \times \Delta t + \Delta r + (w_{i+1} - w_i) \times d \qquad (4.11)$$

Based on Equation 4.11, when the rainfall is a constant, if E is increased, the Δr declines. However, regarding previous analysis, the evaporation rate, E, does not directly reduce the storm water runoff, but it can reduce the water contained in the soil. This will make the soil have more space to retain an upcoming rainfall. Therefore, the larger the evaporation, the higher potential to reduce runoff. Three elements, vegetation coverage, and internal leaf resistance and dimension, have an impact on evaporation. To examine the effects of these three elements on evaporation, I assumed some comparative varibles for them.

The evaporation consists of two parts: evaporation at the soil surface and the evapotranspiration through the plants, as shown in Equation 4.12.

$$E_{total} = E_{veg} + E_{soil}$$

$$= LAI \cdot \frac{\rho_a \cdot \frac{BP_{w,l}}{\left(P_{total} - P_{w,l}\right)} - h \cdot \rho_a \cdot \frac{BP_{w,a}}{\left(P_{total} - P_{w,a}\right)}}{r_l - k_2 \frac{W^{0.2} D^{0.3}}{V^{0.5}}} + (1 - LAI) \cdot \rho_{air} CV$$

$$\cdot \frac{0.622}{P} 0.61078 (\exp\left(\frac{17.27 T_{soil}}{T_{soil} + 237.3}\right) - \exp\left(\frac{17.27 T_{air}}{T_{air} + 237.3}\right)$$

(4.12)

The vegetation coverage LAI is the percentage of the vegetation on the green roof; it determines the total evaporation rate of a green roof. To examine the effect of LAI on E_{total}. I simulated the E_{total} with different LAI settings. Figure 52 shows the evaporation rates with LAI= 0.5, 0.6 and 0.7. The result shows that the evaporation rates increase along with the increasing LAI. The main reason is that the plants have higher evaporation rates than the soil surface. This conclusion was also proved in the Energy Flux Density analysis of Chapter 4.

Figures Y and Z show the effect of vegetation coverage on the evaporation rate during a rainy season and a dry season. Vegetation coverage does not impact the evaporation rate during a rain period as much as during the dry period. That means if a designer increases the vegetation coverage, the evaporation rates during the dry period will be increased. That will shorten the time to dry the soil and retain more water when it rains again.

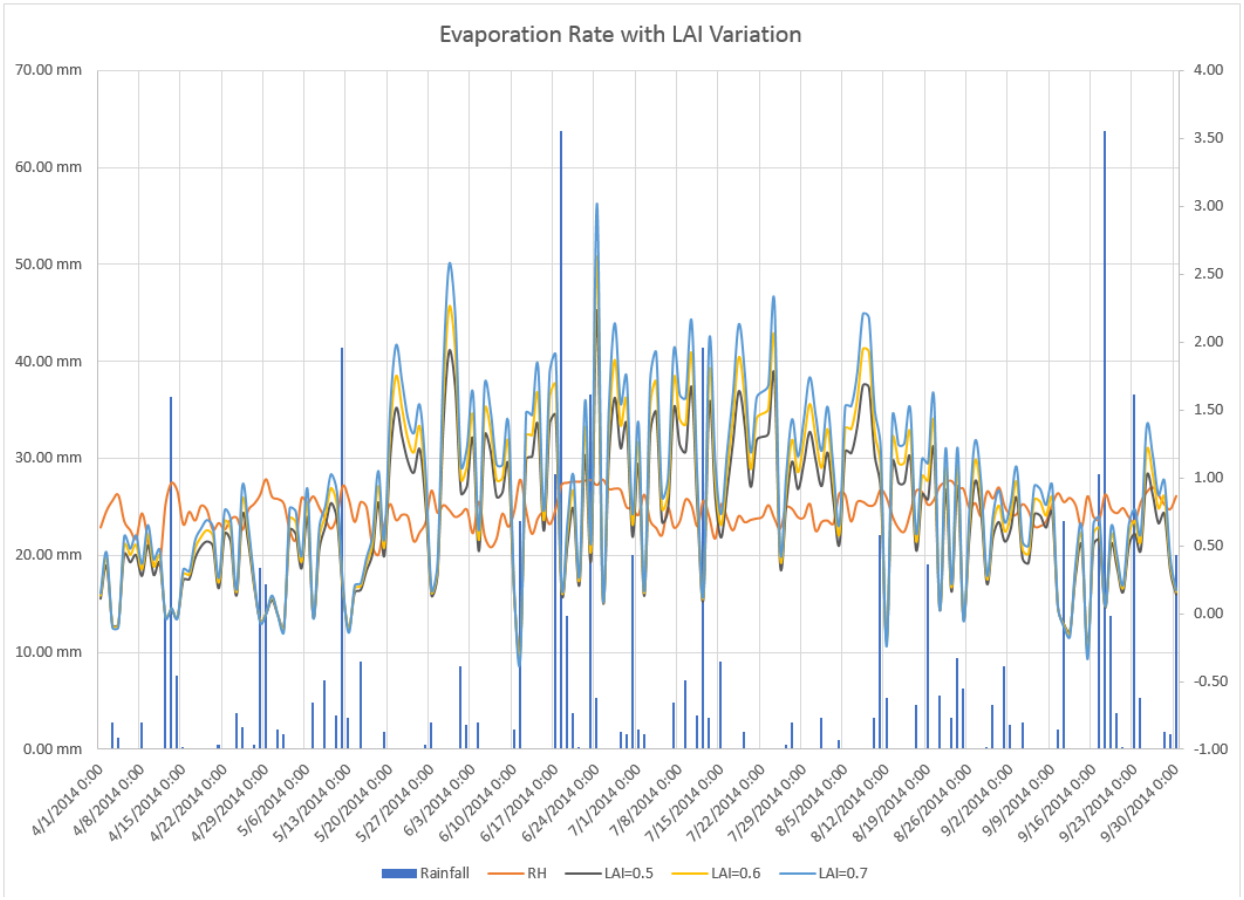

Figure 52. Evaporation rates with LAI= 0.5, 0.6 and 0.7 from April to September, 2014.

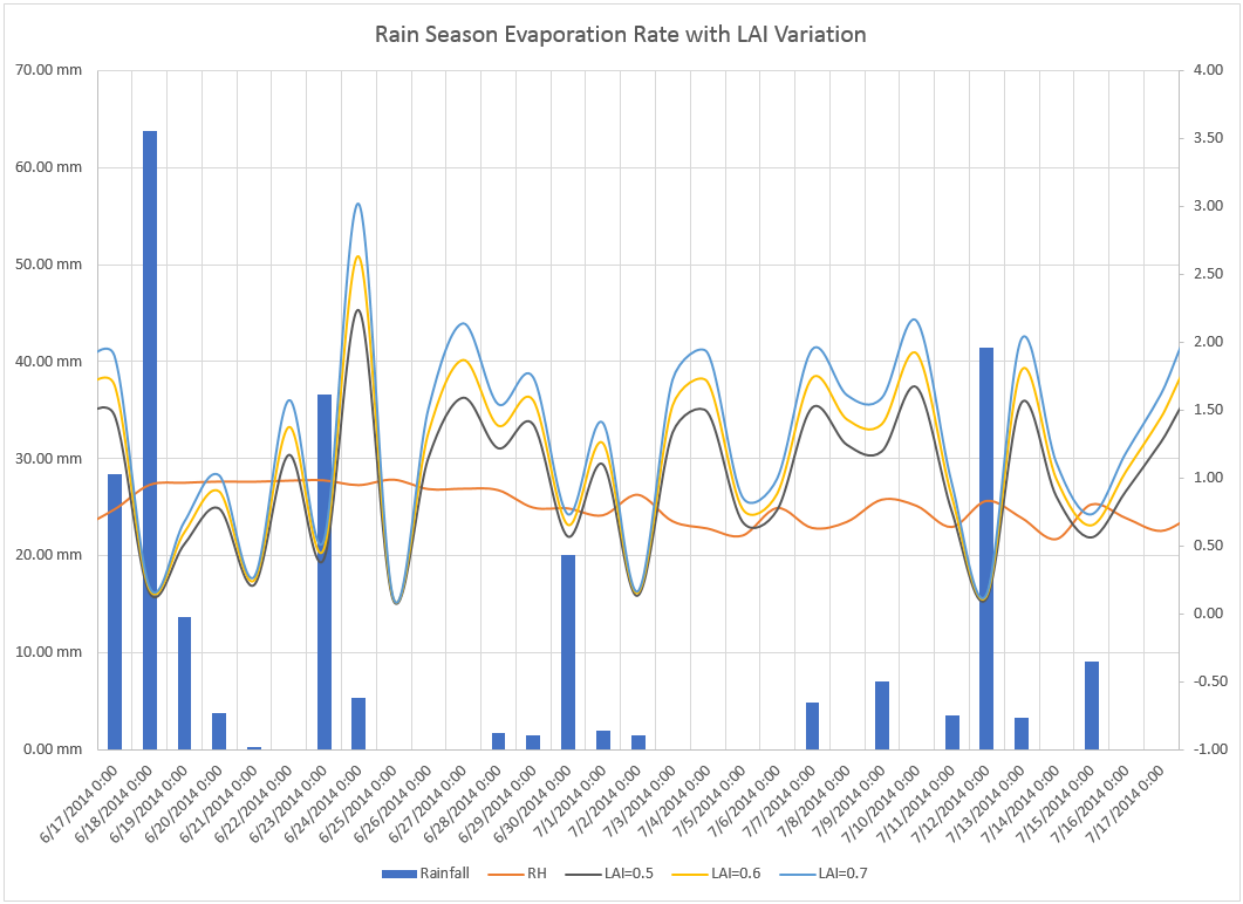

Figure 53. Evaporation rates with LAI= 0.5, 0.6 and 0.7 between June 17th and July 17th, 2014

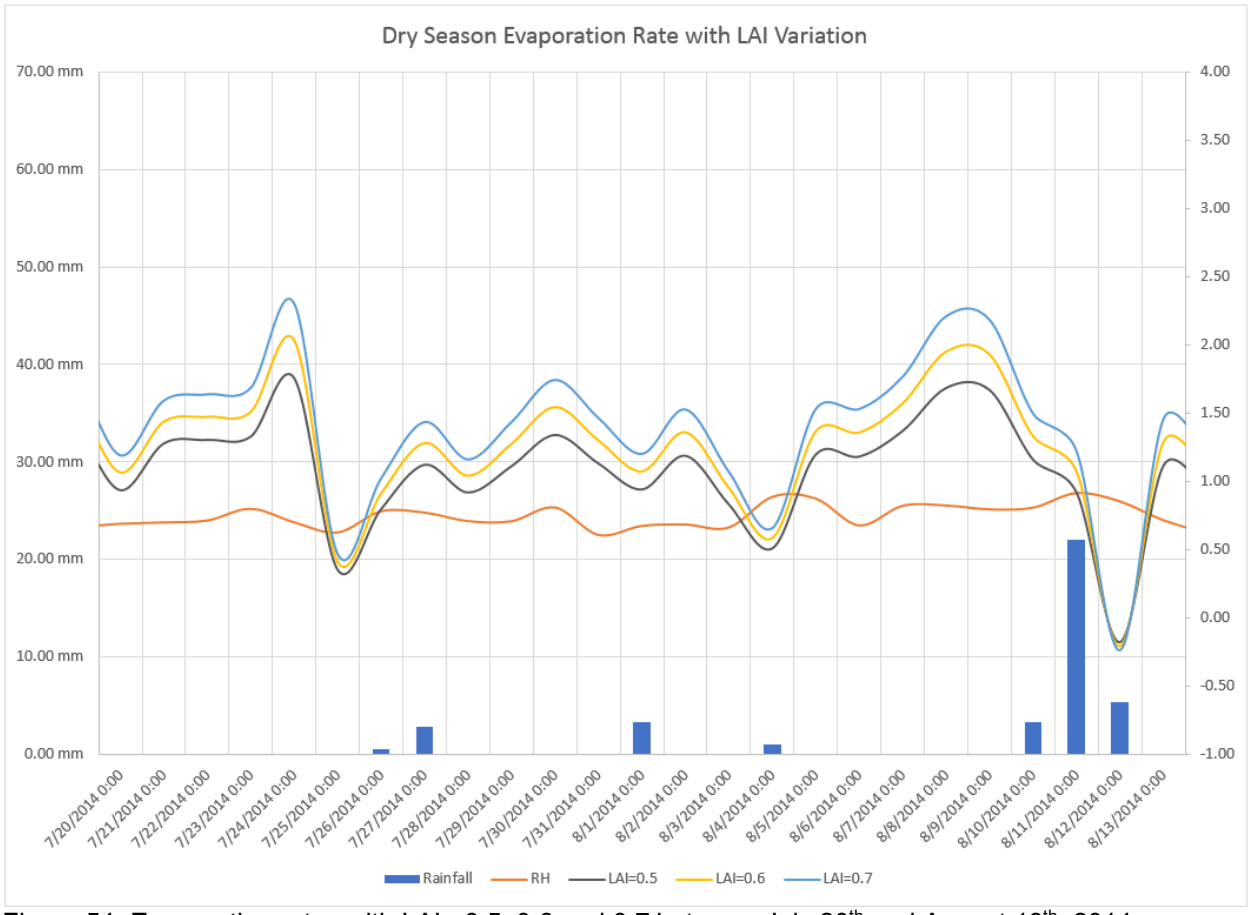

Figure 54. Evaporation rates with LAI= 0.5, 0.6 and 0.7 between July 20th and August 13th, 2014

In the evaporation rate equation, the internal leaf resistance r_l and the boundary-layer resistance r_a are two properties of plants. In nature, usually leaves that have larger internal leaf resistance loss less moisture (Gates, 2012). The internal leaf resistance varies between and 2000 s/m. The most common internal leaf resistance is 200 s/m in nature.

Regarding to the water balance model validated in Chapter 3, the internal leaf resistance of the sedum is 360 s/m.

$$E_{total} = E_{veg} + E_{soil}$$

$$= LAI \cdot \frac{\rho_a \cdot \frac{BP_{w,l}}{\left(P_{total} - P_{w,l}\right)} - h \cdot \rho_a \cdot \frac{BP_{w,a}}{\left(P_{total} - P_{w,a}\right)}}{r_l - r_a} + (1 - LAI) \cdot \rho C_{(z)} \bar{u}_{(z)}$$

$$\cdot \frac{0.622}{P} 0.61078(\exp\left(\frac{17.27T_{soil}}{T_{soil} + 237.3}\right) - \exp\left(\frac{17.27T_{air}}{T_{air} + 237.3}\right)$$

(4.13)

$$r_a = k_2 \frac{W^{0.2} D^{0.3}}{V^{0.5}}$$

(4.14)

The width and length for the leaves are described as W and D in Equation 4.14. To better describe the size of the leaves, I assumed a variable of effective area, which is equal to $W^{0.2}D^{0.3}$.

Therefore, the effective areas $A_{effective}$ for grass, native plants and sedum are calculated as below:

$$A_{grass} = W^{0.2}D^{0.3} = (0.005)^{0.2}(0.08)^{0.3} = 0.162 \text{ m}^{1/2} \quad (4.15)$$

$$A_{native} = W^{0.2}D^{0.3} = (0.03)^{0.2}(0.08)^{0.3} = 0.232 \text{ m}^{1/2} \quad (4.16)$$

$$A_{sedum} = W^{0.2}D^{0.3} = (0.01)^{0.2}(0.01)^{0.3} = 0.1 \text{ m}^{1/2} \quad (4.17)$$

Figures 55, 56 and 57 show the comparison of evaporation rates of the plants with different internal leaf resistances and boundary-layer resistances (leaf size). The comparison shows that the evaporation of the native plants is the largest among the tested plants, and that grass has the second-largest. Sedums have the least evaporation.

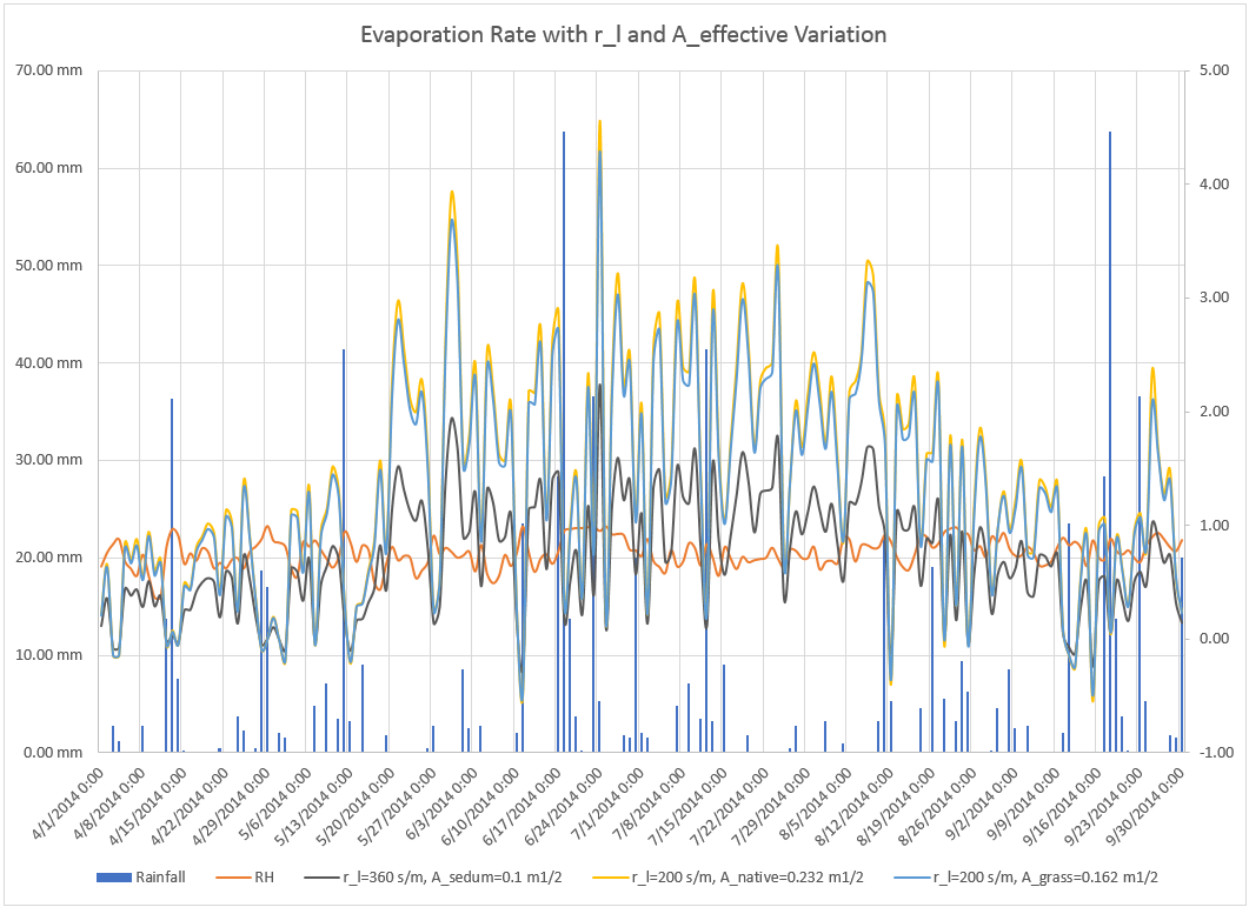

Figure 55. Evaporation rates with internal leaf resistance and leaf size variation from April to September, 2014

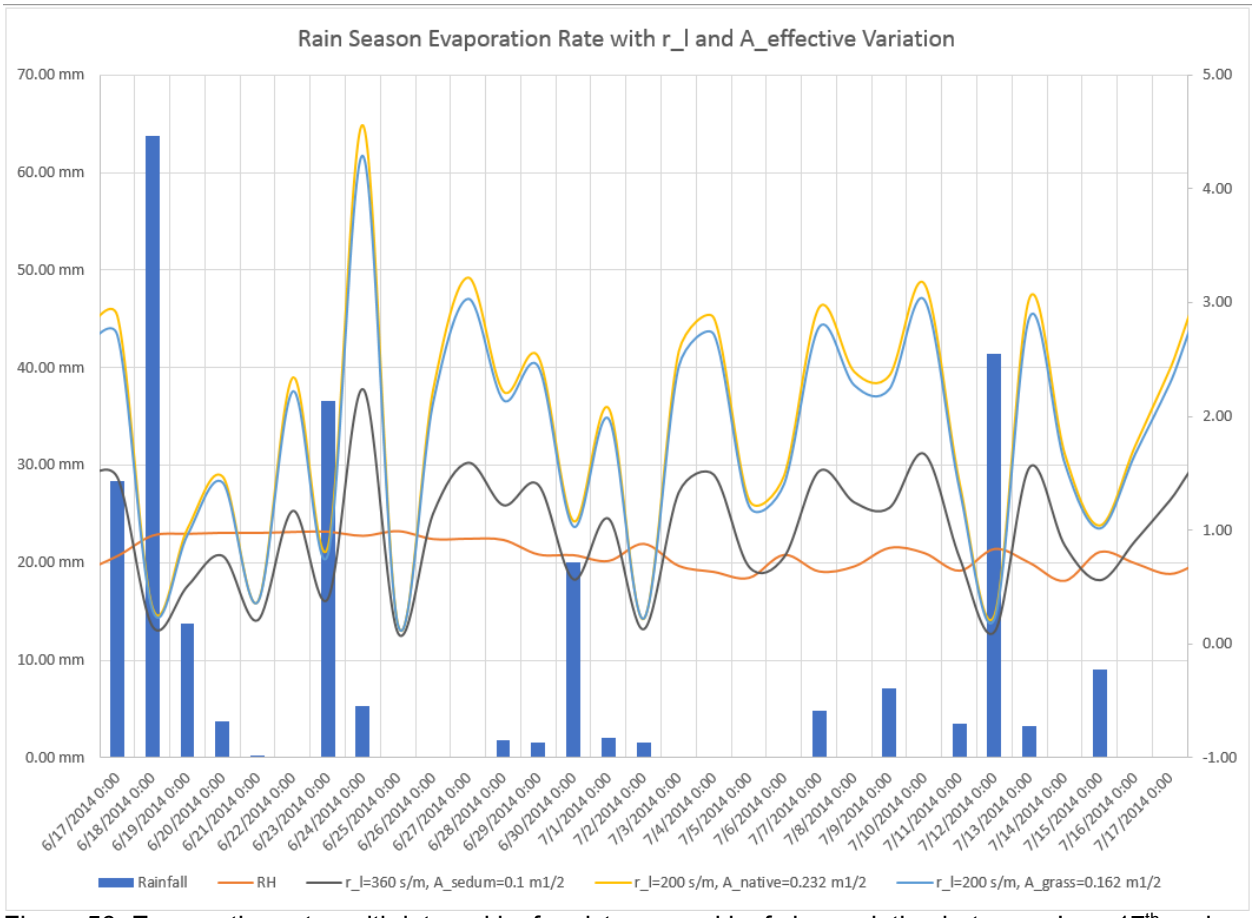

Figure 56. Evaporation rates with internal leaf resistance and leaf size variation between June 17th and July 17th, 2014

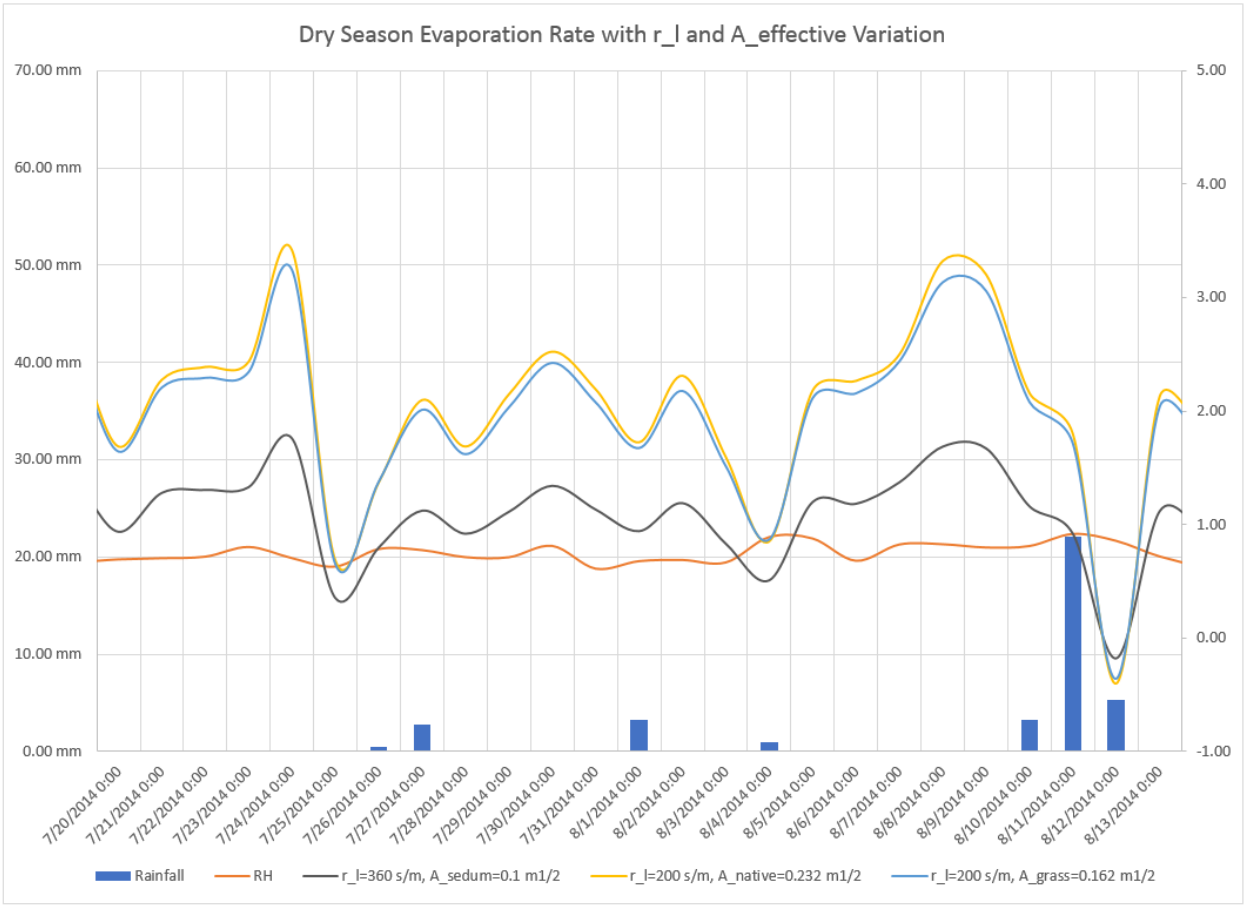

Figure 57. Evaporation rates with internal leaf resistance and leaf size variation between July 20th and August 13th, 2014.

Another element that has impact on the water runoff is the property of soil. As shown in Equation 4.18, porosity and the depth of the soil determine how much runoff there will be. The absorption of soil relies on its porosity, and the water content is proportional to the porosity. Because the water content is a ratio between water depth and soil depth, the soil depth determines the water depth in the soil.

$$\Delta r_i = \begin{cases} 0, & p_i = 0 \\ 0, & w_{i-1} < 0.028 \\ p_{i+1}, & \sum_{i=1}^{n} p_i \geq (0.383 - w_{i-1})\, d \\ 0.89p_i, & \sum_{i=1}^{n} p_i \geq (0.30 - w_{i-1})\, d \\ 0.3p_i, & \sum_{i=1}^{n} p_i \geq (0.20 - w_{i-1})\, d \\ 0.1p_i, & \sum_{i=1}^{n} p_i < (0.20 - w_{i-1})\, d \end{cases}$$

(4.18)

To examine the effects of soil porosity and depth of soil on water runoff, I simulated the water runoff with increased porosity and soil depth, which are both 50% higher than the original setting, as shown in Equation 4.19.

$$\Delta r_i{}' = \begin{cases} 0, & p_i = 0 \\ 0, & w_{i-1} < 0.028 \times 1.5 \\ p_{i+1}, & \sum_{i=1}^{n} p_i \geq (0.383 \times 1.5 - w_{i-1} \times 1.5)\, (d \times 1.5) \\ 0.89p_i, & \sum_{i=1}^{n} p_i \geq (0.30 \times 1.5 - w_{i-1} \times 1.5)\, (d \times 1.5) \\ 0.3p_i, & \sum_{i=1}^{n} p_i \geq (0.20 \times 1.5 - w_{i-1} \times 1.5)\, (d \times 1.5) \\ 0.1p_i, & \sum_{i=1}^{n} p_i < (0.20 \times 1.5 - w_{i-1} \times 1.5)\, (d \times 1.5) \end{cases}$$

(4.19)

The comparison of the effects of different porosity and depth of soil on reducing water runoff is shown in Figures 58, 59, 60, 61, and 62.

Figure 58 shows a year-long water runoff comparison with different soil porosity and depth. There are periods of heavy rain and light rain, and dry periods during a year. To study how different soil conditions reacted to different rain conditions, I studied the effect of soil porosity and depth under different rain conditions separately.

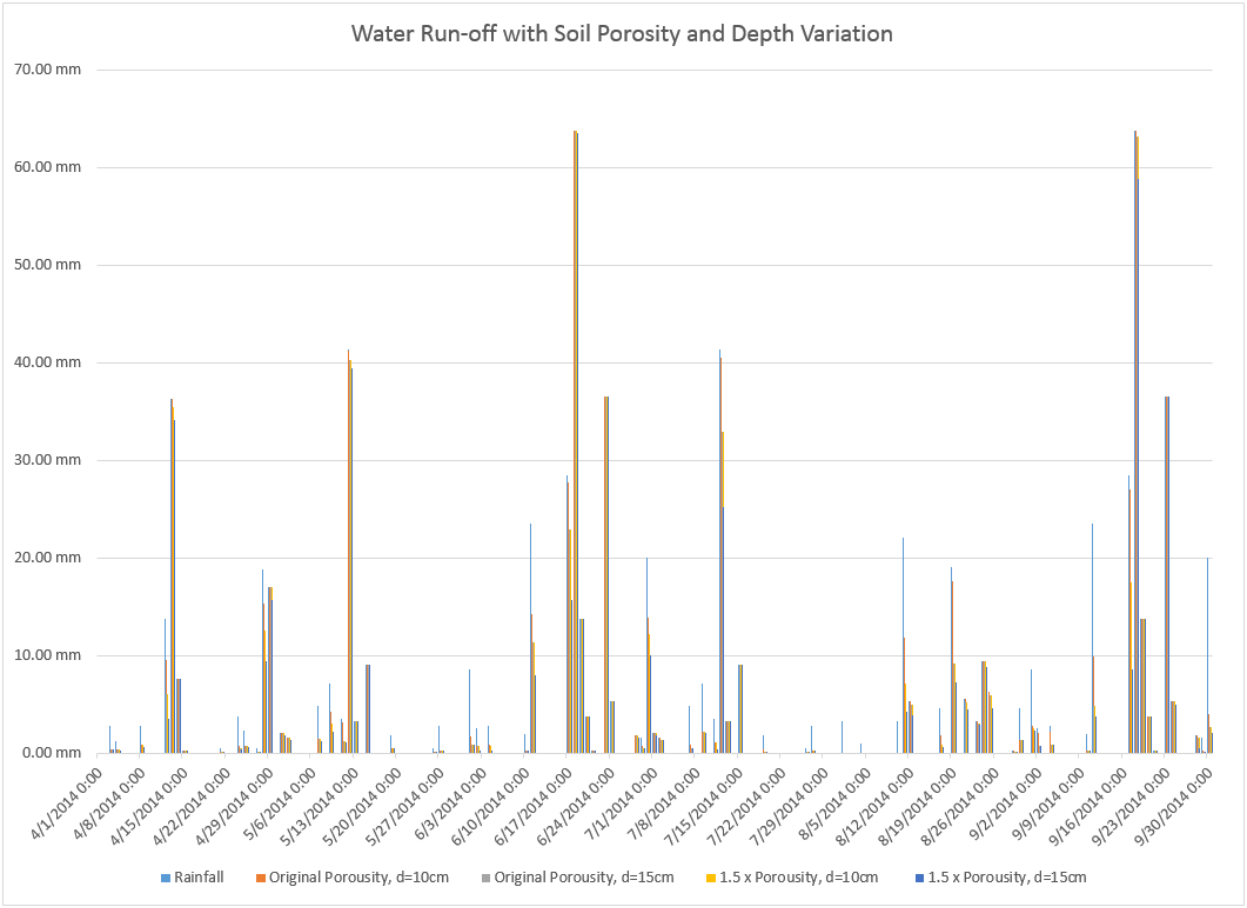

Figure 58. Water runoff comparison with different soil porosity and depth from April to September, 2014.

Figure 59 shows the water runoff comparison after a 5-day dry period. On the first day of rain, the original soil type had little water absorption. The original porosity with 15 cm of soil and the 1.5 × porosity with 10 cm of soil have similar water runoff. The 1.5 × porosity with 15 cm of soil had the least runoff, which is about 60% of the rainfall. When it continuously rained, all the soil types had the same 100% runoff.

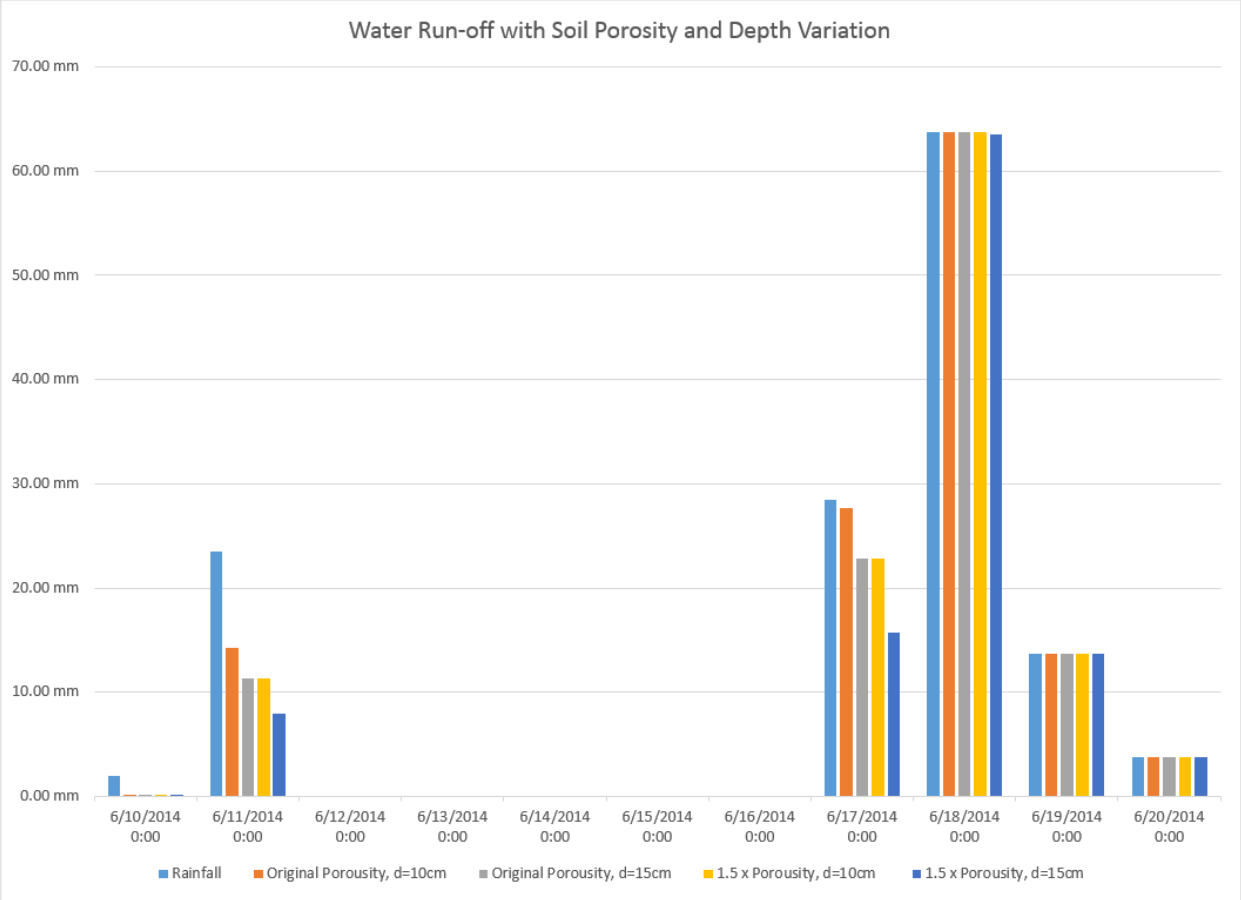

Figure 59. Water runoff comparison with different soil porosity and depth between June 10th and June 20th, 2014.

Figure 60 shows the water runoff comparison after a long dry period. Between July 27th and August 10th, there was no rain that yielded more than a depth of 5 mm, and they were completedly absorbed by all four types of soil . On August 11th, the first day of an over 20mm rain, the original soil type had approximatedly 50% of runoff, the

original porosity with 15cm of soil and 1.5 x porosity with 10cm of soil had approximately 32% runoff, and 1.5 x porosity with 15cm of soil had approximately 20% runoff. On August 12th, the second day of a 5mm rain, 1.5 x porosity with 15cm soil showed 20% less water runoff than the other three types of soil. The other three types of soil had similar water runoff amounts and were close to the rainfall amount.

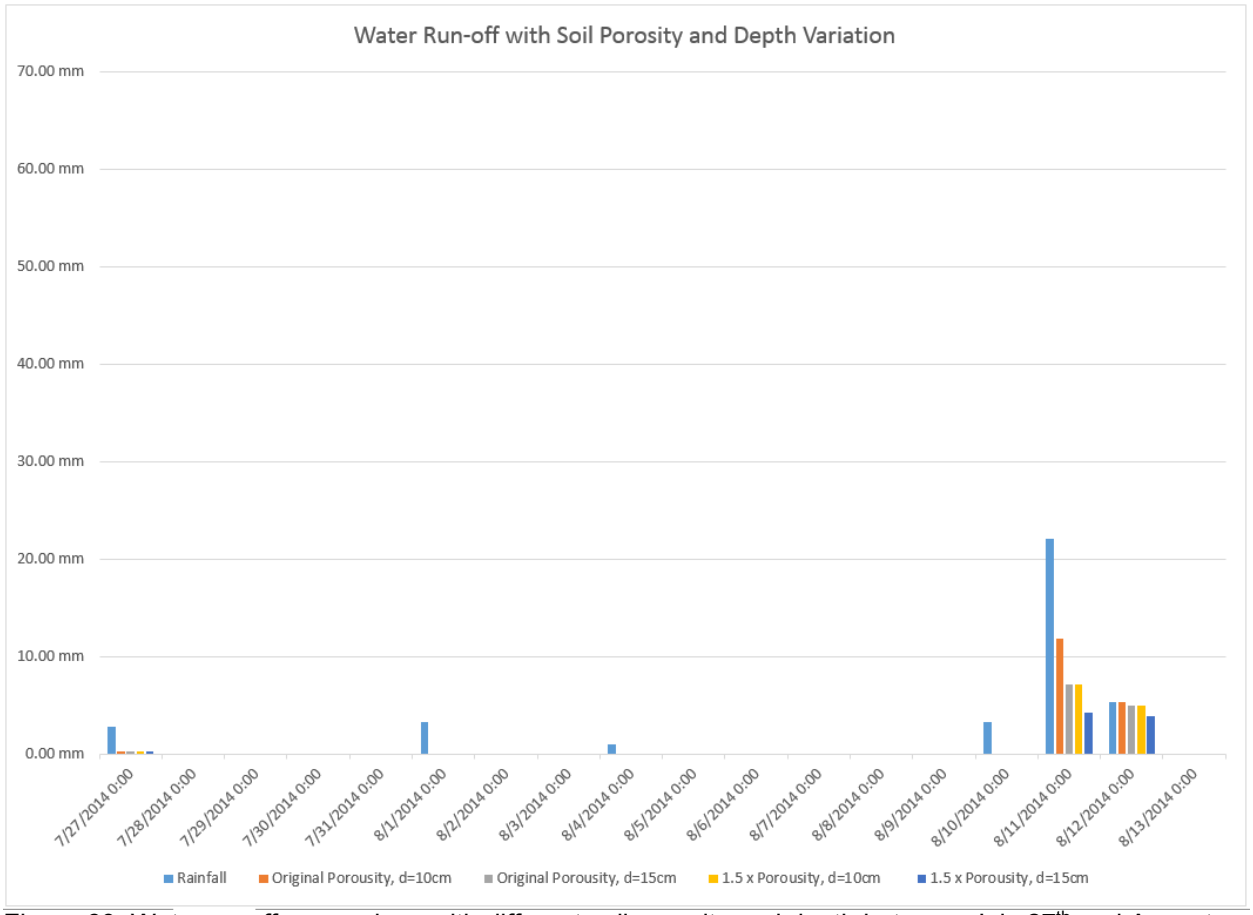

Figure 60. Water runoff comparison with different soil porosity and depth between July 27th and August 13th, 2014.

Figure 60 shows another runoff comparison after a five-day dry period. The rain water runoff situation during this time was very similar to that of June 17th to June 20th. On the first day of a series of rain showers, the 1.5 x porosity with 15cm of soil absorbed the most rain, the original porosity with 15cm of soil and 1.5 x porosity with

10cm of soil had similar performances on reducing water runoff, and the original soil type had the most water runoff. When rain continued and all the soil types got their maximum content, all the rain ran off the roof no matter what type of soil they were.

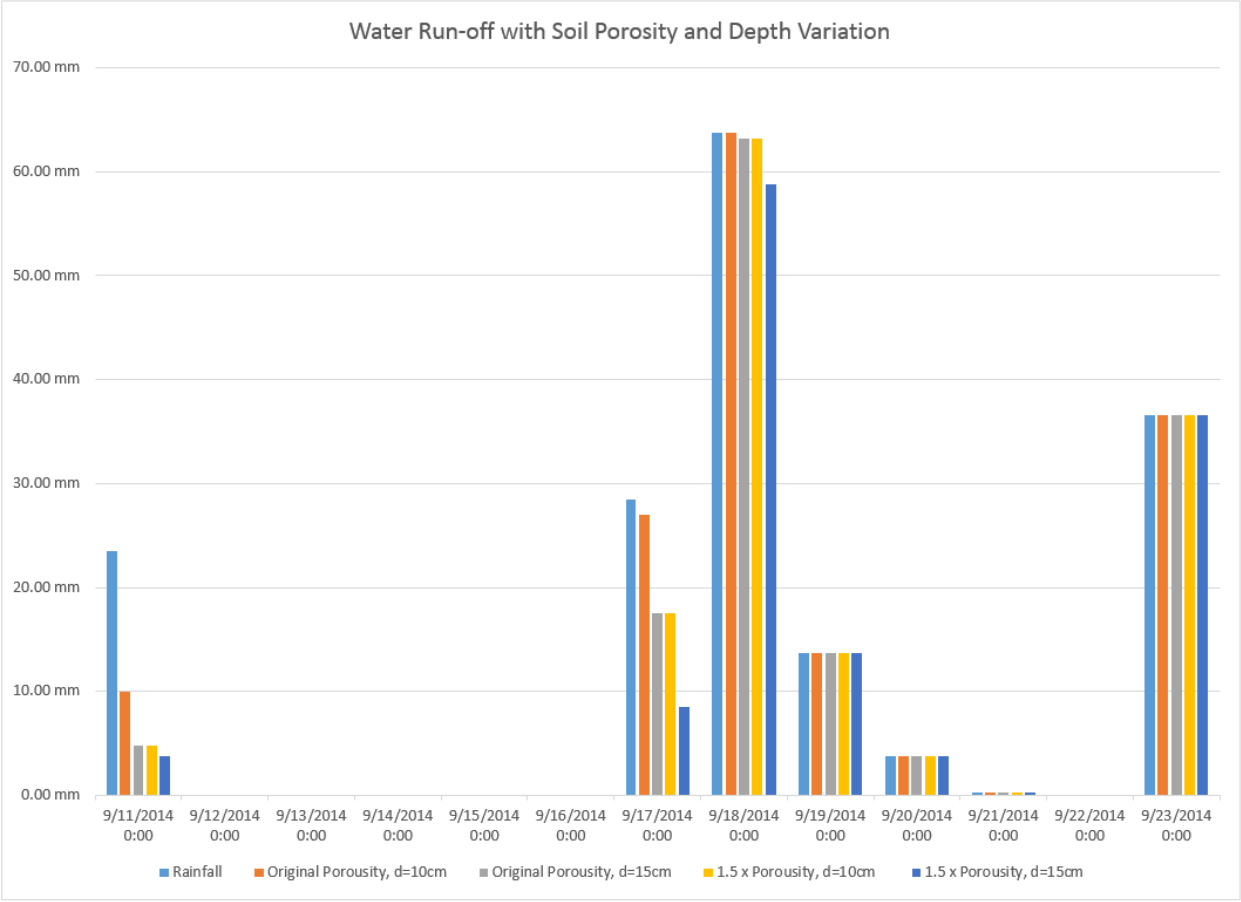

Figure 61. Water runoff comparison with different soil porosity and depth between September 11th and September 23rd, 2014.

Figure 62 shows the runoff comparison in spring. During the period of April 25th to May 19th, there were multiple small amounts of rain. Unlike the summer rain, the rain in spring was more frequent and in small amounts. The soil with larger porosity and depth still showed higher absorption rates during rain events. And the original soil type was still the poorest in reducing water runoff.

In sum, increasing 50% of porosity of the soil, can reduce approximately 40% more runoff, and increasing 50% of soil depth can reduce 40% more runoff. Therefore, increasing porosity or soil depth are equally effective strategies to reduce storm water runoff.

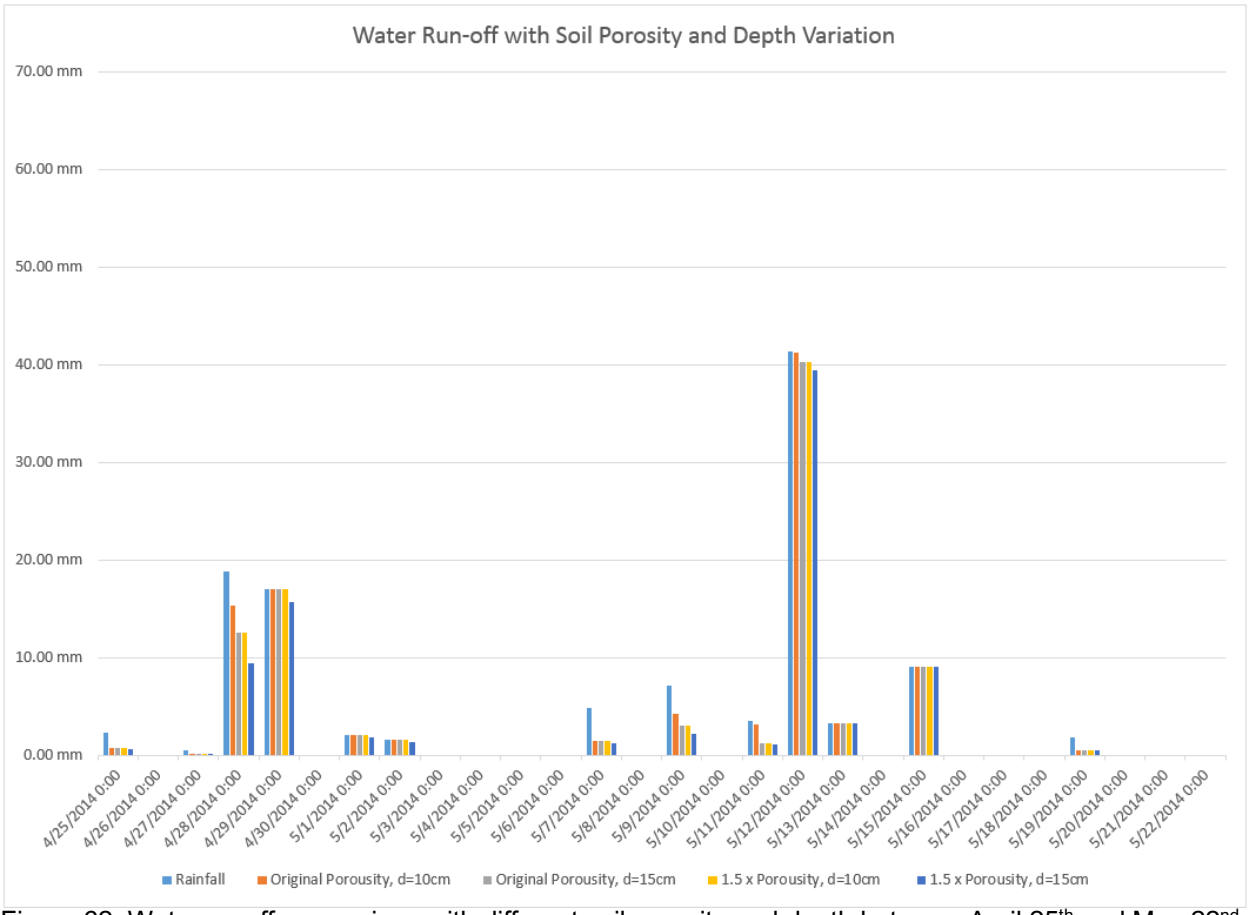

Figure 62. Water runoff comparison with different soil porosity and depth between April 25th and May 22nd, 2014.

5 Conclusions and Discussion

5.1 Conclusion

5.1.1 Surface Temperature

Three elements, surface color, soil depth and plant type were analyzed in relation to the green roof surface temperature. For each element, the following conclusions are drawn from these results.

(A) Surface Color

Reducing the solar absorption of a roof surface is the key in reducing the surface temperature during daytime. Usually, the solar absorption is decided by the color of the surface. Therefore, the surface color is a significant element impacting the surface temperature, especially in a high-radiation environment. The lighter the color, the lower the surface temperature.

(B) Soil Depth

Minimizing the soil depth reduces the surface temperature in the summer. In a high-radiation environment, the surface temperature is higher than the soil temperature. Based on the thermodynamic law, heat is transferred from the higher temperature to the lower temperature. When the heat conductivity is a constant, a shorter transfer distance is more efficient for heat conduction transfer. This means that a deeper soil layer will slow down the drop of the surface temperature.

(C) Plant Types

The latent heat transferred by vegetation evaporation reduces the surface temperature of the vegetation, increasing the evaporation rate cools down the green roof surface. A plant with lower internal leaf resistance and larger leaf size has a higher evaporation rate. Regarding the three types of plants I compared in Chapter 4, the native plants perform best in reducing surface temperature; the grass performs second-best, and the worst is the sedum.

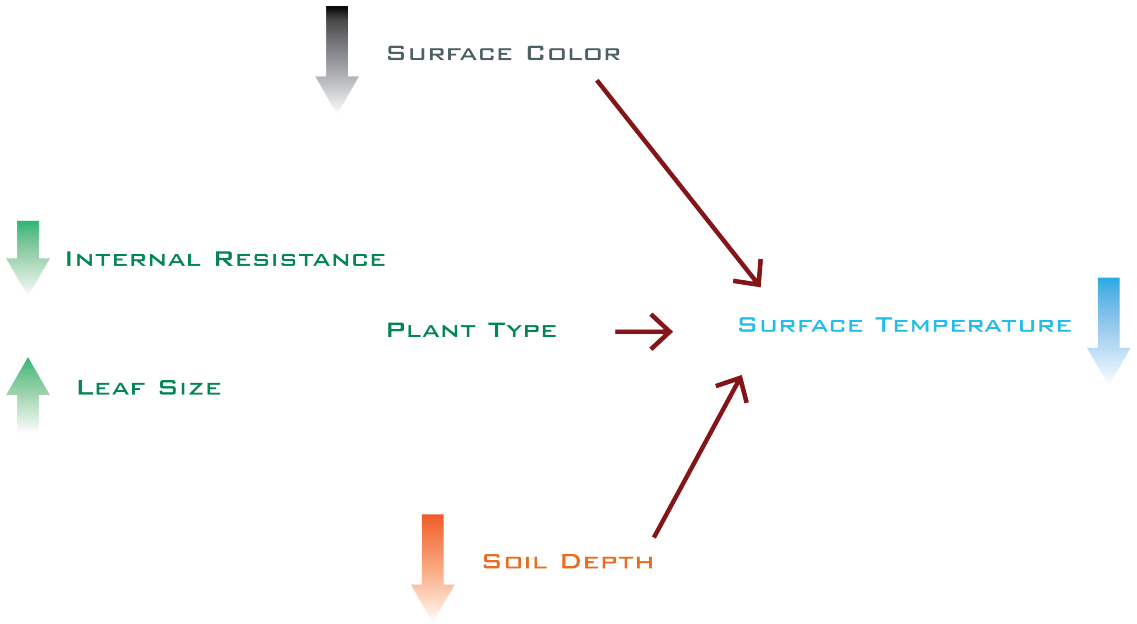

Figure 63. The effect of surface color, plant type and soil depth on reducing surface temperature.

In summary, a lighter color, shallow soil layer, and a lower internal leaf resistance with larger leaf plants will be more beneficial in reducing the heat island effect.

5.1.2 Storm Water Runoff

Three elements, vegetation coverage, soil depth and plant type were analyzed in relation to the storm water runoff. For each element, the following conclusions are drawn from these results.

(A) Vegetation Coverage

Increasing the vegetation coverage and minimizing the bare soil areas helps increase the total evaporation rate of a green roof and decreases the water content in the soil. Therefore, a larger vegetation coverage can increase the green roof's ability to absorb water during rain.

(B) Plant Types

Although vegetation has minimal effect on water retention, the water evaporated by vegetation reduces the soil water content ratio, which increases the capacity of soil absorption. To increase the evaporation rate, a plant with low internal leaf resistance and large leaf size is recommended. In the three types of plants I compared in Chapter 4, the native plants perform best in increasing evaporation rate; followed by the grass, with the worst being the sedum.

(C) Soil Porosity

Increasing the soil porosity can increase the soil absorption. This means that selecting a high absorption soil type can efficiently reduce water runoff. However, increasing soil porosity has limitations. Therefore, some artificial green roof growing medium was produced to replace the real soil.

(D) Soil Depth

Increasing soil depth is a way to increase the volume of a rain “container”. An increased soil depth can multiply its potential to absorb water. However, in reality, an oversized soil layer for a green roof will increase the burden on a building structure. Therefore, increasing soil depth to reduce storm water runoff is not recommended.

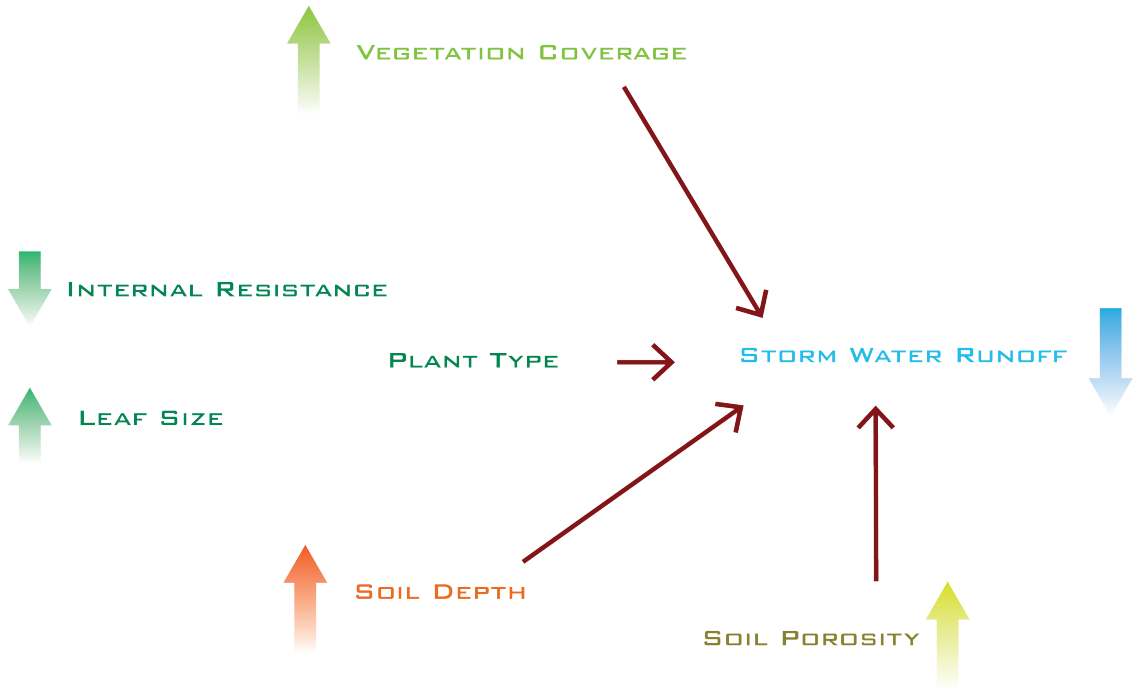

Figure 64. The effect of vegetation coverage, plant type, soil depth and soil porosity on storm water runoff reduction.

To sum up, a higher vegetation coverage, high absorption soil, deeper soil layer, and native plants will be more beneficial in reducing storm water runoff. Increasing soil porosity and soil depth have similar outcomes in reducing the runoff.

5.2 Discussion

As shown in Figure 65, the performance of green roofs is impacted by comprehensive environmental conditions. The energy balance includes solar and

atmosphere radiation, convection and conduction heat transfer, evapotranspiration, and soil heat storage. The mass balance includes precipitation, soil water absorption, evapotranspiration and runoff. All of those components were setup in the Golda Meir Library green roof in Milwaukee, Wisconsin. If other weather data from green roofs in other regions can be used to validate the proposed mathematical mode, the accuracy of the proposed mathematical model can be improved.

The goal of the proposed mathematical model is to help designers optimize their green roofs in the schematic phase in order to predict the reduction of the heat island effect and storm water runoff. There should be no absolute answer to what kind of green roof is the best. The designers need to consider aesthetical, economical and practical elements. When green roof designers use the mathematical models proposed in this dissertation to simulate their own projects, they need to accommodate the specific situation in which they are working to optimize their design. For example, for a location where the overcast days are common, and the radiation is always low, the surface color may not be as critical as it would be in a project located in a high-radiation area. This applies to other elements, such as the soil depth, plant type, and vegetation coverage.

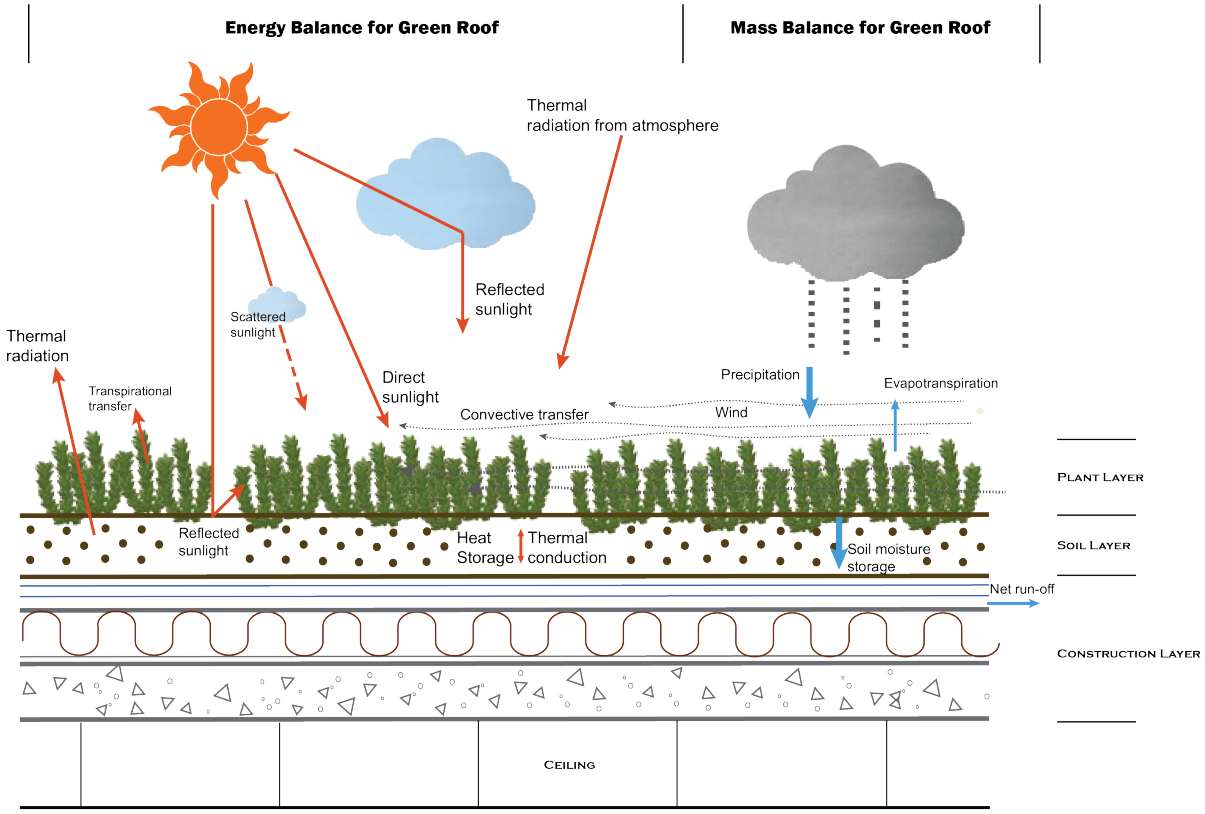

Figure 65. Energy balance and water balance in green roofs.

In Chapter 3, I mentioned that the irrigation system for the green roofs were broken since the winter of 2013. Prior to that, the sprinklers irrigated the sedum every other day when there was no rain. Figure 66 shows the regular soil moisture change every two days, which was the irrigation schedule.

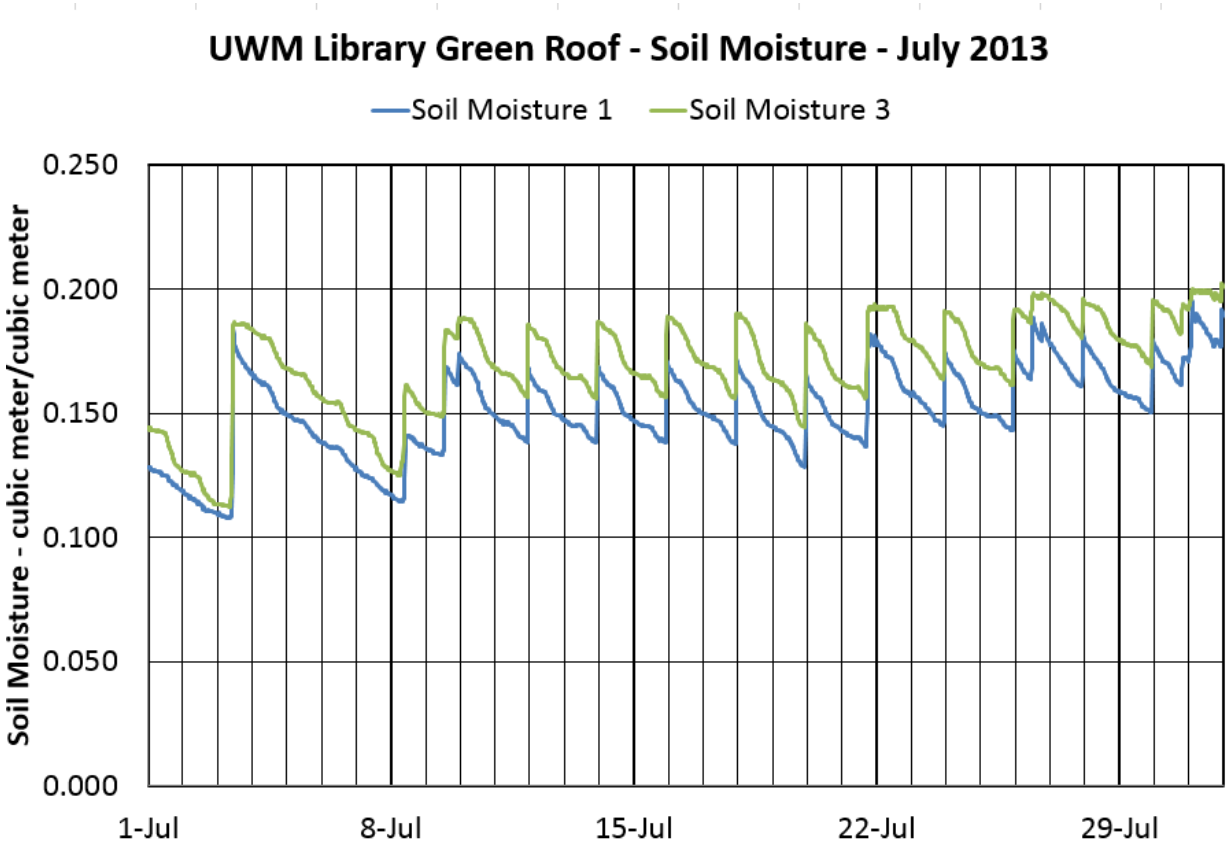

Figure 66. Soil moisture change in July, 2013.

Figure 19 shows the panorama of the north green roof in late August, 2017, when it had been 4 years without irrigation during summer. The sedum was healthy and lush. So, an irrigation system is not necessary for green roofs with sedum, and removing the irrigation system can also help reduce water consumption.

In Chapter 3, all the runoff experiments were done with soil only. If the plant roots sprawling in the soil were considered, the tested soil absorption of the green roof may be larger than then experiments.

The mathematical models proposed in Chapter 3 were solved in MATLAB, a numerical equation solver that guarantees it is adaptive to any simulation tools. To

program the mathematical models in a simulation tool, the coding language may be different, but the calculation methods and logical relationship will be the same.

Some of the green roof coefficients are estimated instead of being measured, as shown in Table 4. A measured coefficient may increase or decrease the validation errors.

Reference

Alassio, M., & Buchanan, P. (2005). Emilio Ambasz: Casa de Retiro Espiritual.

Alnefaie, K. A., & Abu-Hamdeh, N. H. (2013). Specific heat and volumetric heat capacity of some saudian soils as affected by moisture and density. In *International Conference on Mechanics, Fluids, Heat, Elasticity and Electromagnetic Fields* (pp. 139-143).

An, K., Wang, W., Wang, Z., Zhao, Y., Yang, Z., Chen, L., & Duan, L. (2017). Estimation of ground heat flux from soil temperature over a bare soil. *Theoretical and Applied Climatology*, *129*(3-4), 913-922.

Bass, B., Liu, K. K. Y., & Baskaran, B. A. (2003). Evaluating rooftop and vertical gardens as an adaptation strategy for urban areas.

Berndtsson, J. C. (2010). Green roof performance towards management of runoff water quantity and quality: a review. *Ecological Engineering*, 36(4), 351-360.

Berdahl, P., & Martin, M. (1982). Emissivity of clear skies.

Bhumralkar, C. M. (1975). Numerical experiments on the computation of ground surface temperature in an atmospheric general circulation model. *Journal of Applied Meteorology*, *14*(7), 1246-1258.

Brenneisen, S. (2003, May). The benefits of biodiversity from green roofs: key design consequences. In *Proceedings of the 1st North American Green Roof Conference pp323-329*.

Brenneisen, S. (2006). Space for urban wildlife: designing green roofs as habitats in Switzerland. *Urban habitats*, 4(1), 27-36.

California Academy of Science. (2009). *Project: California Academy of Sciences (SanFran).* Retrieved May 29, 2018, from http://www.solaripedia.com/13/102/919/california_academy_of_sciences_vegetated_roof_(usa).html

Castleton, H. F., Stovin, V., Beck, S. B., & Davison, J. B. (2010). Green roofs; building energy savings and the potential for retrofit. *Energy and buildings*, *42*(10), 1582-1591.

Currie, B. A., & Bass, B. (2008). Estimates of air pollution mitigation with green plants and green roofs using the UFORE model. *Urban Ecosystems*, 11(4), 409-422.

Del Barrio, E. P. (1998). Analysis of the green roofs cooling potential in buildings. *Energy and buildings*, *27*(2), 179-193.

Duffie, J. A., & Beckman, W. A. (1980). Solar engineering of thermal processes.

Dunnett, N., Nagase, A., & Hallam, A. (2008). The dynamics of planted and colonising species on a green roof over six growing seasons 2001–2006: influence of substrate depth. *Urban Ecosystems*, *11*(4), 373-384.

Farouki, O. (1982). Thermal properties of soils. US Army Corps of Engineers, Cold Regions Research and Engineering Laboratory.

Fuchs, M., & Tanner, C. B. (1968). Calibration and Field Test of Soil Heat Flux Plates1. *Soil Science Society of America Journal*, *32*(3), 326-328.

Gates, D. M., & Papian, L. E. (1971). Atlas of energy budgets of plant leaves. *Atlas of energy budgets of plant leaves.*

Gates, D. M. (2012). *Biophysical ecology*. Courier Corporation.

Gedge, D., & Kadas, G. (2005). Green roofs and biodiversity. *Biologist*, *52*(3), 161-169.

Henderson-Sellers, B. (1984). A new formula for latent heat of vaporization of water as a function of temperature. *Quarterly Journal of the Royal Meteorological Society*, *110*(466), 1186-1190.

Higginison, C. (2006, October). *Malcolm Wells: The Father of Earth-Sheltered Architecture.* Retrieved May 29, 2018, from https://www.motherearthnews.com/green-homes/malcolm-wells-earth-sheltered-architecture-zmaz06onzraw

Hou, J., & Wang, J. (1999). *Yao-dong in China*. Zhengzhou: Henan Technology and Science Press.

Hodo-Abalo, S., Banna, M., & Zeghmati, B. (2012). Performance analysis of a planted roof as a passive cooling technique in hot-humid tropics. *Renewable Energy*, *39*(1), 140-148.

Kaluvakolanu, P. (2006, December). *History of Green Roofs.* Retrieved May 29, 2018, from https://www.ltu.edu/water/greenroofs_history.asp

Kao, C. (2013). Dynamic data development analysis: A relational analysis. *European Journal of Operational Research*, *227*(2), 325-330

Knepell, P. L., & Arangno, D. C. (1993). *Simulation validation: a confidence assessment methodology* (Vol. 15). John Wiley & Sons..

Kuehn, T. H., Ramsey, J. W., & Threlkeld, J. L. (1998). *Thermal environmental engineering* (Vol. 188). Upper Saddle River, NJ: Prentice Hall.

Lazzarin, R. M., Castellotti, F., & Busato, F. (2005). Experimental measurements and numerical modelling of a green roof. *Energy and Buildings*, *37*(12), 1260-1267.

Lienhard, J. H. (2013). *A heat transfer textbook*. Courier Corporation.

Liesecke, H. J. (1998). Das retentionsvermögen von dachbegrünungen. *Stadt und Grün*, *47*(1), 46-53.

Lundholm, J., MacIvor, J. S., MacDougall, Z., & Ranalli, M. (2010). Plant species and functional group combinations affect green roof ecosystem functions. *PloS one*, *5*(3), e9677.

Mecanoo Architecten. (2007). *Library Delft University of Technology.* Retrieved May 29, 2018, from http://www.mecanoo.nl/Projects/project/27/Library-Delft-University-of-Technology?t=0

Mentens, J., Raes, D., & Hermy, M. (2006). Green roofs as a tool for solving the rainwater runoff problem in the urbanized 21st century?. Landscape and urban planning, 77(3), 217-226.

Minke, G., & Witter, G. (1982). Haeuser mit Gruenem Pelz, Ein Handbuch zur. *Hausbegruenung. Frankfurt: Verlag Dieter Fricke GmbH*.

Monteith, J., & Unsworth, M. (1998). *Principles of environmental physics*. Academic Press.

Moran, A., Hunt, B., & Jennings, G. (2003). A North Carolina field study to evaluate greenroof runoff quantity, runoff quality, and plant growth. In *World Water & Environmental Resources Congress 2003* (pp. 1-10).

Oke, T. R. (2002). *Boundary layer climates*. Routledge.

Oyj, V. (2013). HUMIDITY CONVERSION FORMULAS-Calculation formulas for humidity. *Humidity Conversion Formulas*, 16.

Pham, D. (2012). *Emilio Ambasz's Temple-Like Casa de Retiro Espiritual Rises from the Earth.* Retrieved May 29, 2018, from https://inhabitat.com/emilio-ambaszs-iconic-casa-de-retiro-espiritual-is-built-into-the-earth/

Qiu, B., Wang, F., Li, Y., & Zuo, W. (2012). Research on method of simulation model validation based on improved grey relational analysis. *Physics Procedia*, *25*, 1118-1125.

Sailor, D. J. (2008). A green roof model for building energy simulation programs. *Energy and buildings*, *40*(8), 1466-1478.

Santamouris, M., Synnefa, A., & Karlessi, T. (2011). Using advanced cool materials in the urban built environment to mitigate heat islands and improve thermal comfort conditions. *Solar Energy*, *85*(12), 3085-3102.

Schunck, E., Oster, H. J., Barthel, R., & Kiessl, K. (2003). *Roof construction manual: pitched roofs*. Walter de Gruyter.

Susca, T., Gaffin, S. R., & Dell'Osso, G. R. (2011). Positive effects of vegetation: Urban heat island and green roofs. *Environmental Pollution*, *159*(8), 2119-2126.

Takebayashi, H., & Moriyama, M. (2007). Surface heat budget on green roof and high reflection roof for mitigation of urban heat island. *Building and Environment*, *42*(8), 2971-2979.

Van Renterghem, T., & Botteldooren, D. (2009). Reducing the acoustical façade load from road traffic with green roofs. *Building and environment,* 44(5), 1081-1087.

Vandermeulen, V., Verspecht, A., Vermeire, B., Van Huylenbroeck, G., & Gellynck, X. (2011). The use of economic valuation to create public support for green infrastructure investments in urban areas. *Landscape and Urban Planning*, *103*(2), 198-206.

VanWoert, N. D., Rowe, D. B., Andresen, J. A., Rugh, C. L., Fernandez, R. T., & Xiao, L. (2005). Green roof stormwater retention. *Journal of environmental quality*, 34(3), 1036-1044.

Wells, M. (1981). *Gentle architecture*. New York: McGraw-Hill.

Wong, E., Akbari, H., Bell, R., & Cole, D. (2011). Reducing urban heat islands: compendium of strategies. *Environmental Protection Agency, retrieved May*, *12*, 2011.

Yan-yan, Z. H. O. U., Xiao-yan, W. U., & Gang, W. (2009). Study of model verification method based on neutral network. *Journal of Air Force Engineering University (Natural Science Edition*, 64-67.

Yang, J., Yu, Q., & Gong, P. (2008). Quantifying air pollution removal by green roofs in Chicago. *Atmospheric environment*, *42*(31), 7266-7273.

Zinzi, M., & Agnoli, S. (2012). Cool and green roofs. An energy and comfort comparison between passive cooling and mitigation urban heat island techniques for residential buildings in the Mediterranean region. *Energy and Buildings*, *55*, 66-76.

.

Appendix A: The U-value Calculation beneath Green Roof

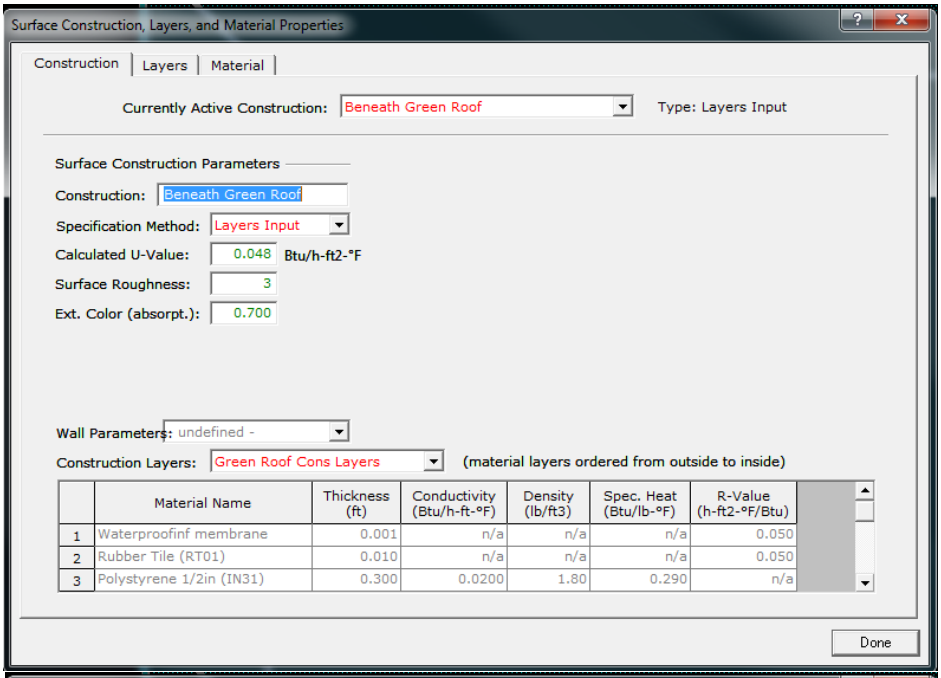

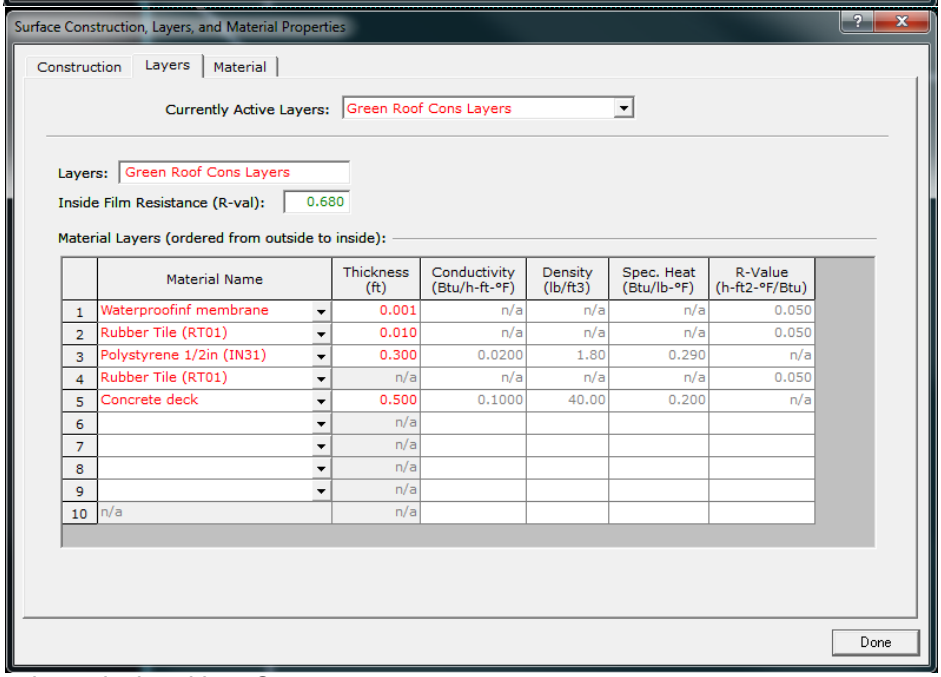

Figure 67. U-value calculated by eQuest

0.048 Btu/h·ft^2·°F=0.273 W/ (m^2·K)

Appendix B: Soil Calibration of Volumetric Water Content Sensors

Tools: Decagon soil moisture sensors (SN:10160937 and 10160939), soil sample, one volume sampler (tube), measuring cups, one mixing container (a bucket), one soil drier, and one scale.

Procedures:

1. Prepare soil

   Dehydrate the soil samples for 48 hours at 280˚F in oven.

2. Calibration

To calibrate the soil moisture sensor, we need to generate the formula of the real volumetric water content of soil mixed with varied amount of water along with the readings of the sensor. Following are the steps to obtain each of the data points and plotting them to create the formula:

a) Load the dry soil into the mixing container.

Figure 68. Dehydrated soil in bucket.

b) Vertically insert the probe into the soil.

Figure 69. Insert sensor into soil.

c) Record the average readings of sensors and include them in the tables.

d) Use the 50ml tube to take the sample, and put the sample in a number coded measuring cup. The sample represents the soil condition in the mixing container. The No. 1 sample is dry soil.

Figure 70. Take the sample with 50ml tube.

e) Use the measuring cup to pour some water into the mixing container. Make sure not to pour too much water to avoid soaking the soil to saturation immediately.

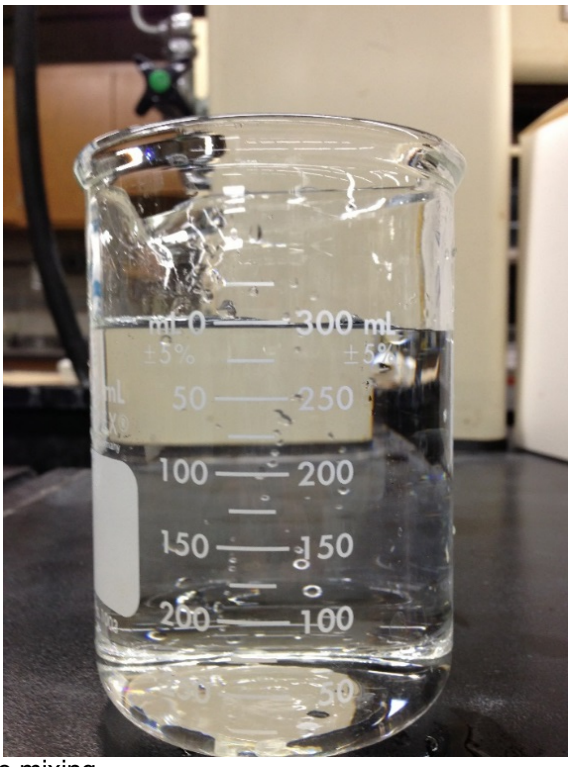

Figure 71. Pour water into the mixing

f) Repeat steps b) to d) to record all the sensor readings until the soil is saturated. This results in five samples with five levels of water content of soil.


Figure 72. Saturated soil

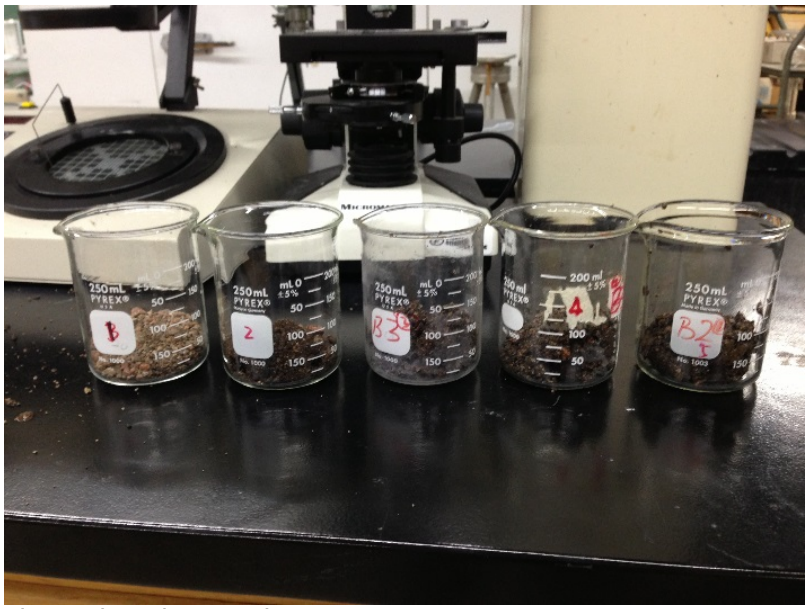

Figure 73. Samples in numbered measuring cups.

g) Weigh all the samples taken with the volume sampler. The weight of the samples are the soil with water (with the exception of the first sample). Input the weights in the row titled “mass of moist soil” in the excel table.

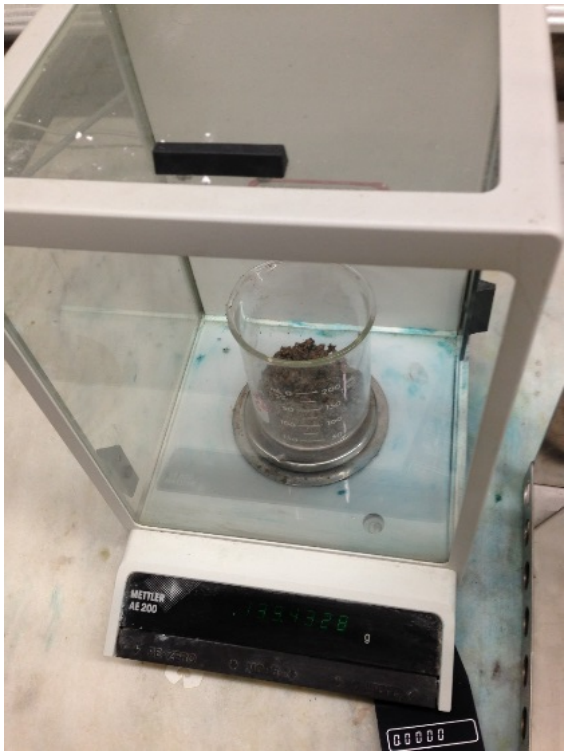

Figure 74. Weigh the samples

h) Load the samples in the oven at 105 F for 24 hours to dry.

Figure 75. Dry the samples in the oven

i) Weigh the samples again once they are dry. The difference between the weight before and after dehydration will be the mass of the water in the samples.

j) Calculate the VWC in excel.

Dry soil mass= (Mass of container+dry soil) - drying container tare mass

Mass of water= (Mass of container+moist soil) - (mass of container+dry soil)

Soil bulk density= Dry soil mass/ sample volume

VWC= Volume of water/ sample volume

Table 6. The readings of soil sensor 1060937 calibration.

Soil sensor 10160937										
Sample Number	Drying container tare mass (g)	Sample Volume (cm3)	mass of container+ moist soil (g)	Mass of Container+ dry soil (g)	Mass of water (g)	Dry soil mass (g)	Soil bulk density (g/cm3)	VWC (cm3/cm3)	Average (cm3/cm3)	Avg sensor reading (cm3/cm3)
1	109.7	50	145.55	144.42	1.13	34.72	0.6944	0.0226	0.0042	-0.0142
2	108.82	50	156.53	153.24	3.29	44.42	0.8884	0.0658	0.069	0.0722
3	102.86	50	148.14	139.44	8.7	36.58	0.7316	0.174	0.1496	0.1252
4	91.61	50	146.34	133.1	13.24	41.49	0.8298	0.2648	0.26875	0.2727
5	121.45	50	179.12	162.66	16.46	41.21	0.8242	0.3292	0.399	0.4688

Table 7. The readings of soil sensor 10160939 calibration.

Soil Sensor 10160939										
Sample Number	Drying container tare mass (g)	Sample Volume (cm3)	mass of container + moist soil (g)	Mass of Container +dry soil (g)	Mass of water (g)	Dry soil mass (g)	Soil bulk density (g/cm3)	VWC (cm3/cm3)	Average (cm3/cm3)	Avg sensor reading (cm3/cm3)
1	65.17	30	86.62	85.82	0.8	20.65	0.688333	0.02666667	0.0080333	-0.0106
2	66.87	30	91.1	89.56	1.54	22.69	0.756333	0.05133333	0.0672167	0.0831
3	67.46	30	94.43	88.89	5.54	21.43	0.714333	0.18466667	0.1647333	0.1448
4	68.05	30	99.97	91.58	8.39	23.53	0.784333	0.27966667	0.2601833	0.2407
5	68.56	30	103.08	92.59	10.49	24.03	0.801	0.34966667	0.4059333	0.4622

k) Make a graph. The X is sensor output and the Y is VWC. The blue curves in Figures 73 and 74 are the plots of average sensor readings and the measured volumetric water content.

3. Calculation and application

Engineering Equation Solution (EES) is adopted to get the most fitting function of sensor readings and the VWC. As shown in Appendix 1-4, assume the linear and quadratic equation with unknown coefficients a,b (linear) or a,b,c (quadratic) in EES for the calibration function, and input the sensor readings and VWC of the samples as the variable x and y. Also, define SRS, the sum of the squares of the residuals, to minimize the difference between the desired function and the actual plots (blue curve). The smaller the SRS, the closer the calibrated function to the real situation. For both of the

sensors, 10160937 and 10160939, quadratic functions have smaller SRS than the linear ones, so quadratic functions will be selected as the calibration functions, as following:

10160937:

$Y=-1.06X^2+1.15X+0.02553$

10160939:

$Y=-1.131X^2+1.265X+0.01341$

Their graph of the functions are shown as the orange curves in the Figure 73 and Figure 74.

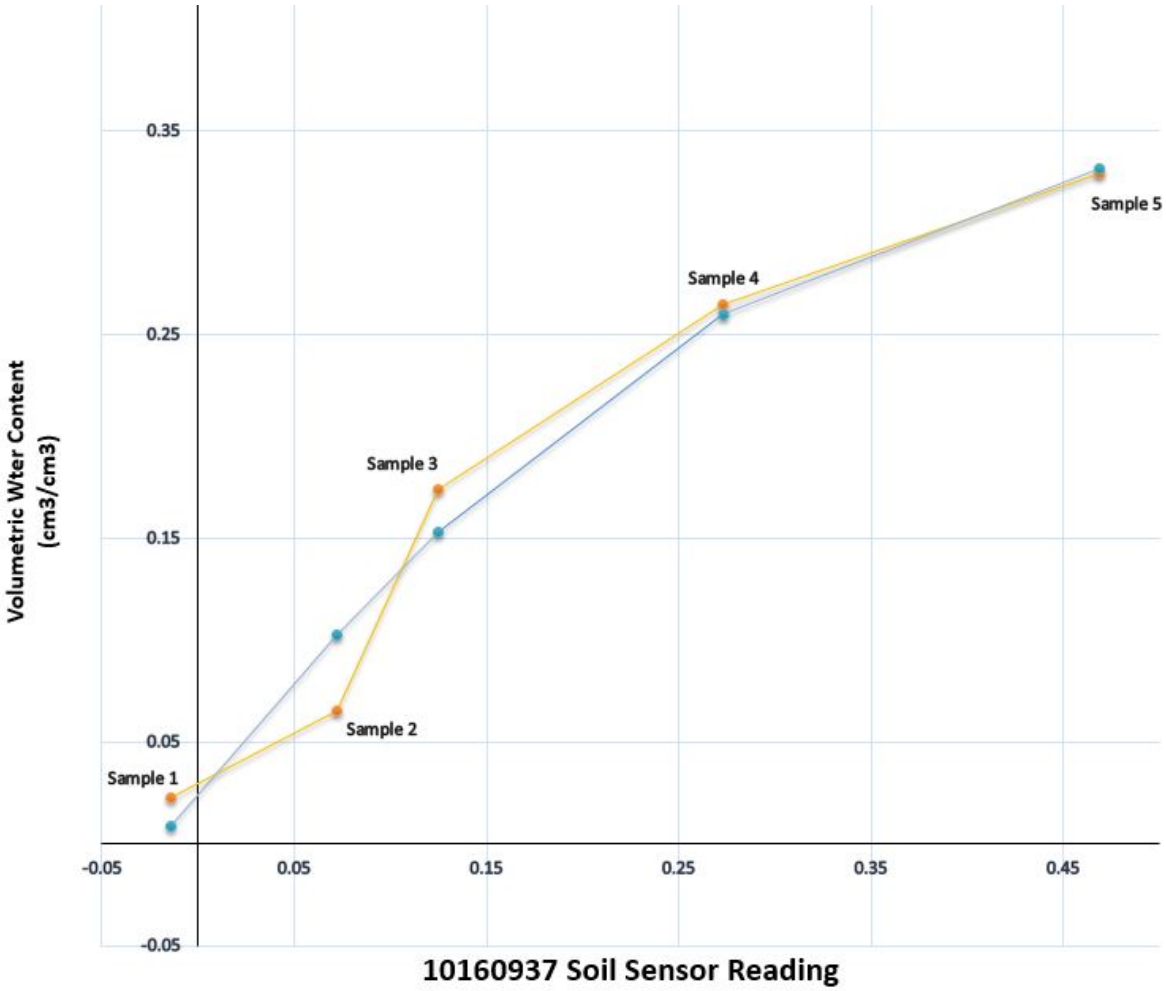

Figure 76. Soil moisture sensor 10160937. Orange line: the plot of the sensor reading and VWC. Blue line: Calibrated soil sensor function curve.

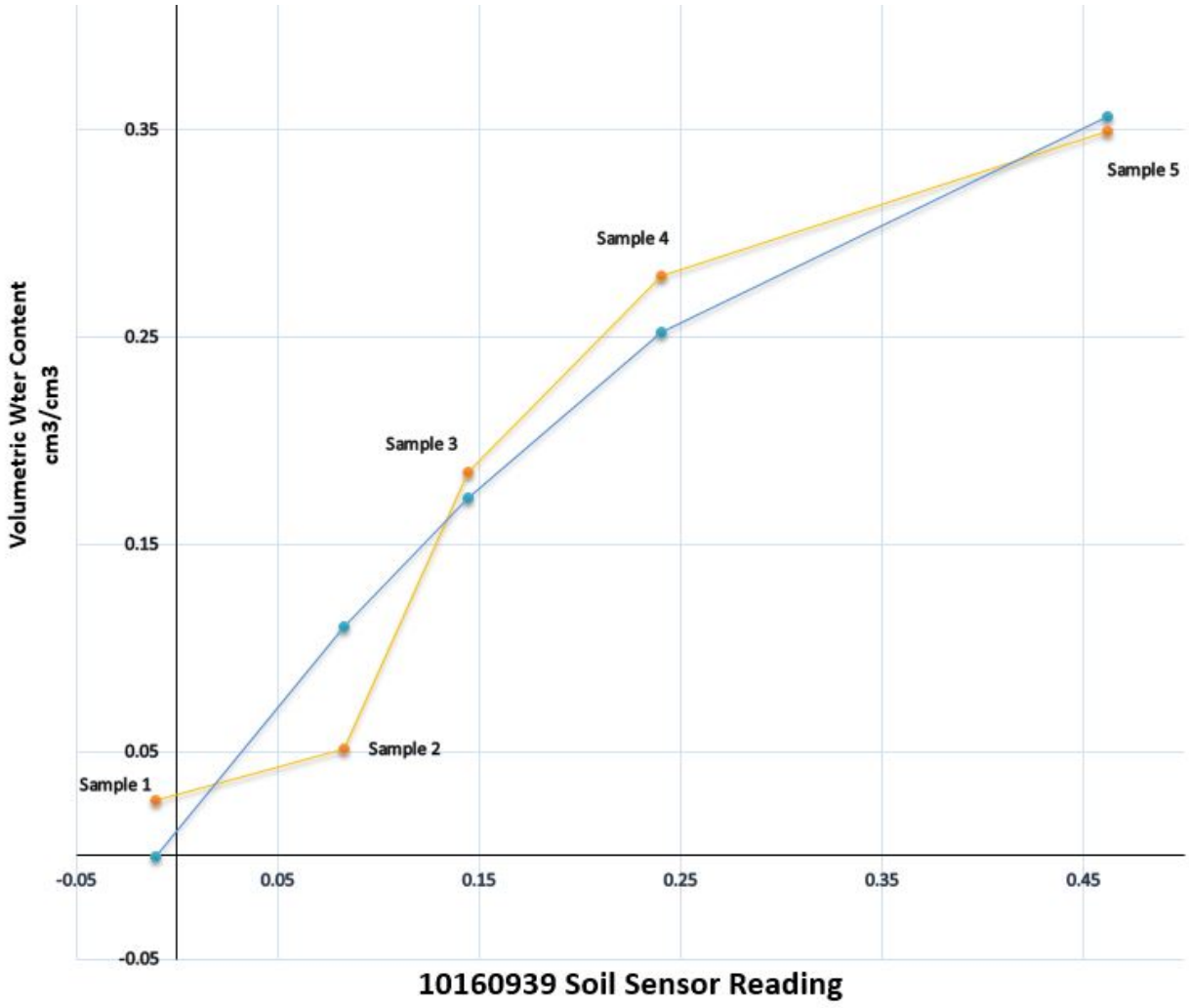

Figure 77. Soil moisture sensor 10160939. Orange line: the plot of the sensor reading and VWC. Blue line: Calibrated soil sensor function curve

Appendix C: Soil Maximum Water Content Measurement

Tools: One scale, measuring cups, dry soil sample, one mesh strainer.

Procedures:

1. Load dry soil into the measuring cup.
    a) Weight the empty cup.

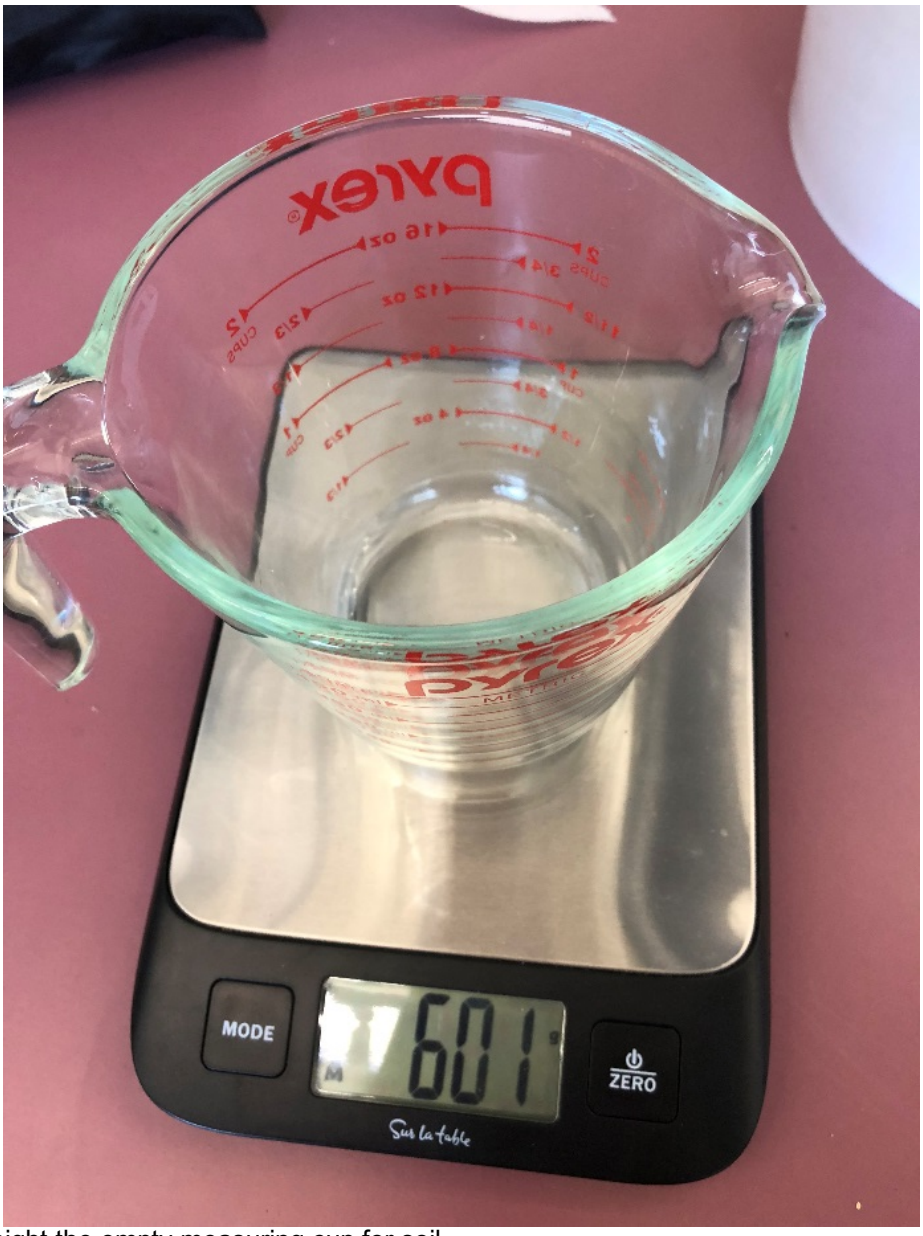

Figure 78. Weight the empty measuring cup for soil.

b) Weight the cup with 300 ml soil.

Figure 79. Measuring 300ml soil.

Figure 80. Weight the soil with the measuring cup.

2. Prepare 250ml water.

    a) Weight the empty cup.

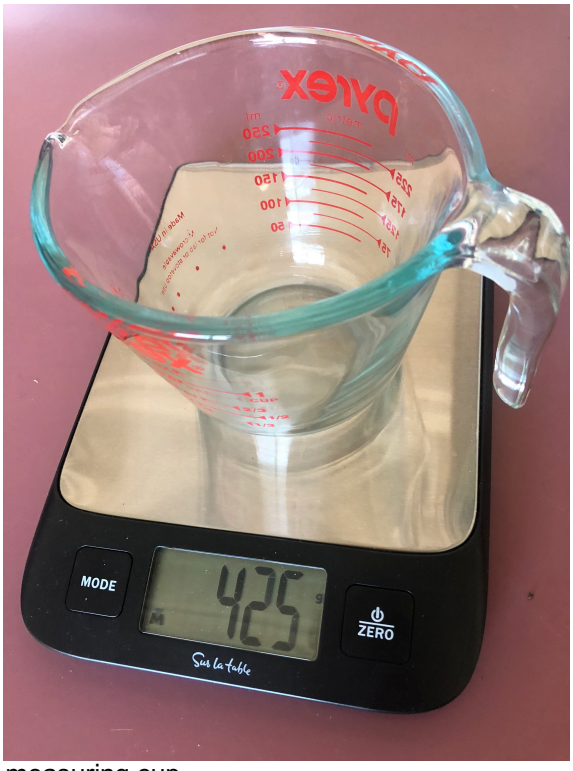

Figure 81. Weight the empty measuring cup.

    b) Weight the cup with 250 ml water

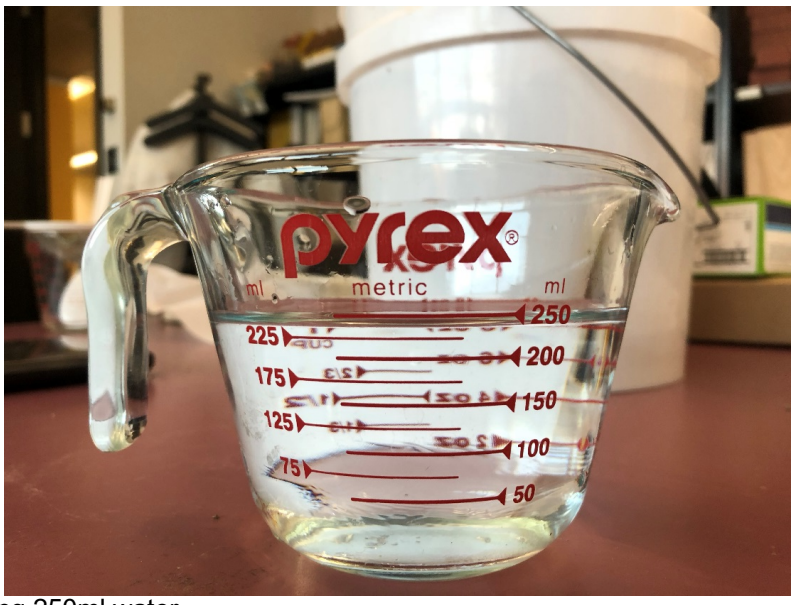

Figure 82. Measuring 250ml water.

Figure 83. Weight the water with the measuring cup.

3. Load soil into the strainer and place the strainer on the top of a measuring cup.

    a) Weight the empty cup.

Figure 84. Load soil into the strainer.

b) Weight an empty measuring cup.

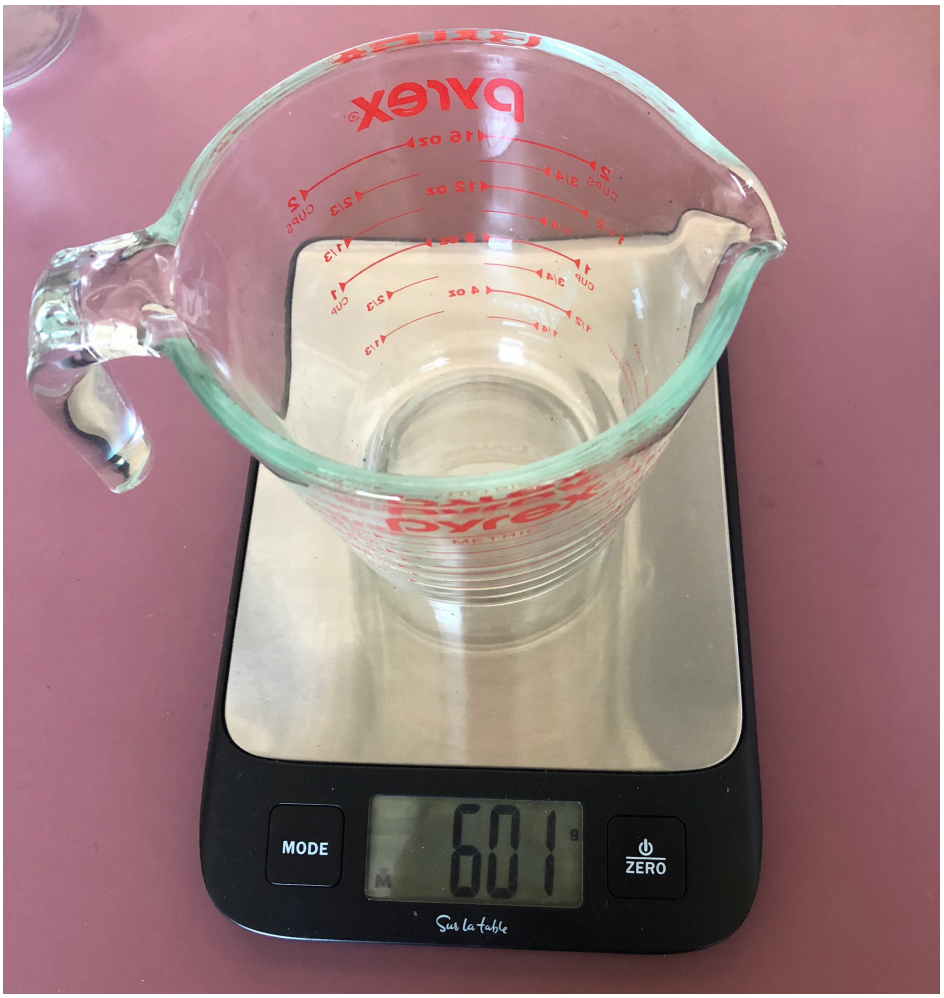

Figure 85. Weight the empty cup for runoff water.

c) Place the strainer containing soil on the top of the empty measuring cup.

Figure 86. Place the strainer containing soil on the top of the measuring cup.

4. Slowly pour all the prepared water into the soil in the strainer.

    a) Record the volume of water drain into the measuring cup when no more water flow into the measuring cup beneath the strainer.

Figure 87. Water drain into the measuring cup.

    b) Weight the runoff water with the measuring cup.

Figure 88. Weight the runoff water with the measuring cup.

5. Repeat procedure 1-4.

6. Calculate the maximum water content in excel.

Table 8. Maximum soil water content experiment record and calculation.

Sample	Empty Soil Cup Mass	Soil Volume	Soil+Cup Mass	Calculated Soil Volume	Empty Water Cup Mass	Water Volume	Water+Cup Mass	Calculated Water Volume	Empty Run-off Cup	Run-off Water Mass with Cup	Calculated Run-off Volume	Water Content
	g	cm^3	g	cm^3	g	cm^3	g	cm^3	g	g	cm^3	cm^3/cm^3
1	601	250	786	268.115942	426	250	672	246	601	746	145	0.376703
2	601	250	792	276.811594	892	300	1212	320	601	818	217	0.372094
3	601	250	779	257.971014	891	350	1267	376	601	877	276	0.38764
4	601	250	799	286.956522	893	400	1334	441	602	932	330	0.386818
5	425	250	628	294.202899	601	450	1040	439	891	1222	331	0.367094
6	426	250	619	279.710145	602	500	1096	494	892	1279	387	0.382539
7	425	250	621	284.057971	1026	550	1574	548	891	1321	430	0.415408
8	426	250	623	285.507246	1027	600	1627	600	893	1387	494	0.371269
9	426	250	624	286.956522	1027	700	1718	691	893	1479	586	0.365909
10	425	250	614	273.913043	1204	800	1989	785	892	1571	679	0.386984
11	425	250	620	282.608696	1203	900	2094	891	892	1679	787	0.368
12	426	250	633	300	1204	1000	2188	984	893	1750	857	0.423333
Average Maximum Soil Water Content												**0.384**

Appendix D: Soil Water Runoff Ratio Measurement

Tools: One scale, measuring cups, one lightweight plastic cup, dry soil sample, one mesh strainer.

Procedures:

1. Measure the soil sample mass and volume.
    a) Weight the empty measuring cup.

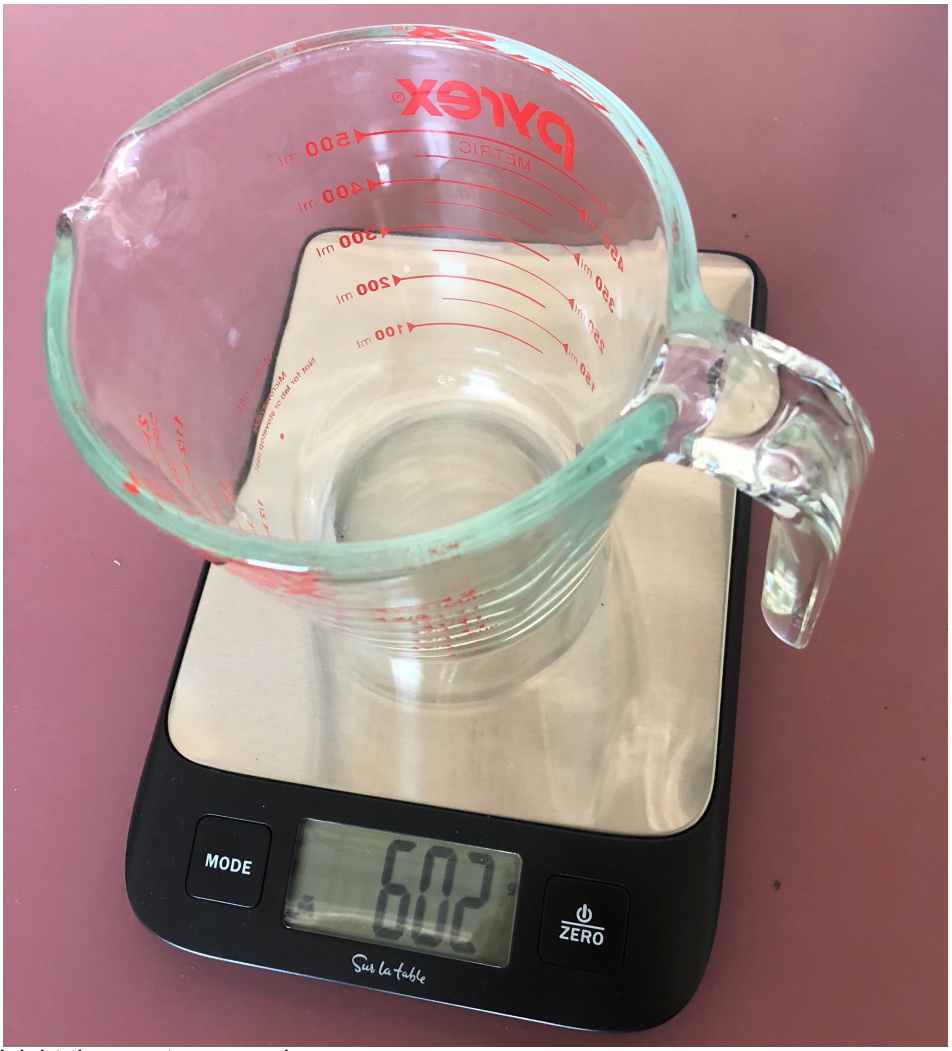

Figure 89. Weight the empty measuring cup.

    b) Weight the 250 ml soil sample with the measuring cup.

Figure 90. Weight the soil sample.


Figure 91. Load the soil sample in the strainer.

2. Prepare the measuring cup that going to retain runoff water.

    a) Weight the empty measuring cup.

Figure 92. Weight the empty measuring cup.

Figure 93. Place the strainer with soil on the top of the measuring cup.

3. Prepare the water that is going to be added into the soil.

    a) Weight the empty plastic cup.

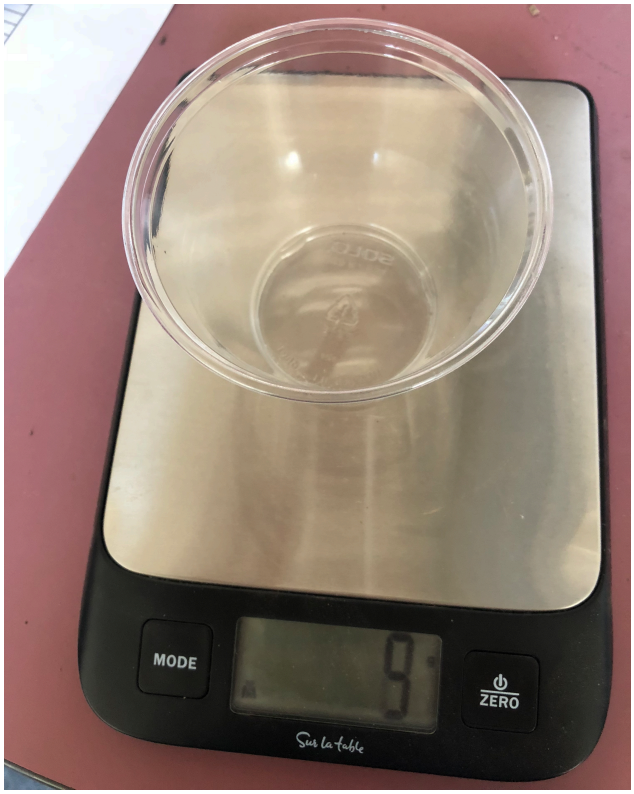

Figure 94. Weight the empty water cup.

b) Weight 10g water.

Figure 95. Weight the water with the cup.

4. Pour the prepared water into the soil sample

Figure 96. Pour the water into the soil.

5. Wait the water run off the soil and flow into the measuring cup until it stops.

Figure 97. Water run off the soil and retained in the measuring cup.

6. Weight the runoff water with the measuring cup.

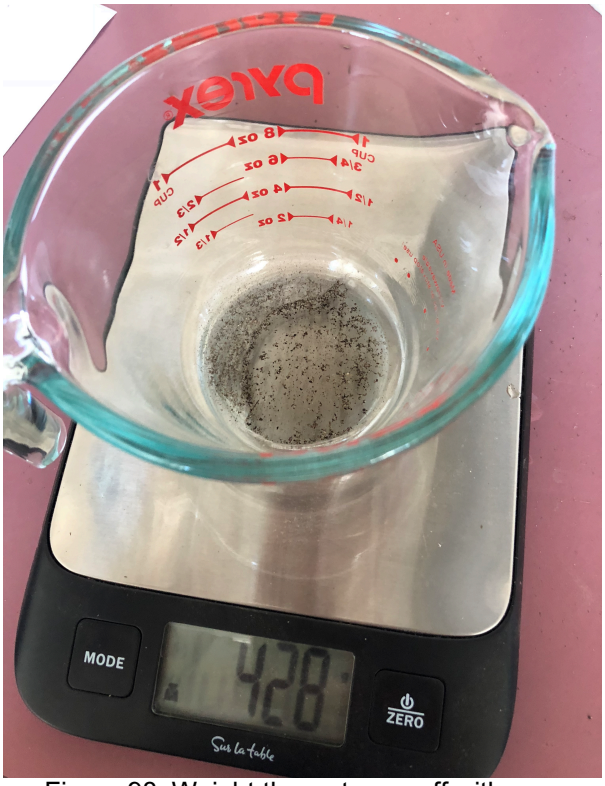

Figure 98. Weight the water runoff with cup.

7. Repeat step 3 to step 5 twenty-three times until the soil has received 240 g water. Record the whole procedures and the measurement.

Table 9. Runoff ratio experiment outcomes.

Sample Volume	Empty Soil Cup	Empty Water Cup	Empty Runoff Cup	Water Added in the Soil + Cup	Water Runoff + Cup
ml	g	g	g	g	g
250	602	9	425	19	428
		9	425	19	429
		9	425	19	431
		9	425	19	432
		9	425	19	433
		9	425	19	436
		9	425	19	439
		9	425	19	441
		9	425	19	444
		9	425	19	453
		9	425	19	462
		9	425	19	471
		9	425	19	481
		9	425	19	491
		9	425	19	501
		9	425	19	511
		9	425	19	521
		9	425	19	533
		9	425	19	543
		9	425	19	555
		9	425	19	566
		9	425	19	577
		9	425	19	589
		9	425	19	599

Appendix E: MATLAB Scripts for Green Roof Simulation

MATLAB scripts for bare soil temperature validation from April to September, 2014:

```
[T_soil] = SolveFunction(1,17568);
T = readtable('soiltemp2014.xlsx');
NewT =[table(T_soil')];
writetable(NewT, 'test7.csv');

function [T_soil]=SolveFunction(start,finish)
A = xlsread('soiltemp2014.xlsx');
v = A(start:finish,1);
len=size(v);
I_solar=A(start:finish,3);
X_f=A(start:finish,8);
Wind=A(start:finish,9);
P=A(start:finish,10);
T_air=A(start:finish,11);
H_c=A(start:finish,13);
T_sky=A(start:finish,15);
RHO_air=A(start:finish,16);



A_solar=0.6;
B=0.0000000567;
d=0.05;
k_s=0.15;
k_f=0.6;
Delta_t=900;
rho_dry=690;
c_w=4180;
c_d=950;
U=0.273;
T_bldg=22 + 273.16;
T_soil = 8.12;



for i=1:len

    x_f=X_f(i);
    h_c=H_c(i);
    t_air=T_air(i) + 273.16;
    i_solar=I_solar(i);
    t_sky=T_sky(i)+273.16;
    rho_air=RHO_air(i);
    u=Wind(i);
    p=P(i)*100;
```

```
    k = k_s*k_f/((1-x_f)*k_f+x_f*k_s);
    E_surf=0.92+0.03*x_f;
    C_z=0.0015;
    R=2430000;
    C_evp=R*rho_air*C_z*u*0.622*0.61078/p;



    C_v=rho_dry*(c_d*(1-x_f)+x_f*c_w);

    m=[t_sky,t_air];
    t_avg = mean(m);
    C_mean = t_avg^3;

    C_1= Delta_t / (2 * C_v * d);
    C_2= i_solar * A_solar + 4 * E_surf * B * C_mean * t_sky + h_c * t_air;
    C_3= h_c + 4 * E_surf * B * C_mean + k/d;
    C_4= 1 / ( d / k + 1 / U);
    C_5=exp(17.27*(t_air-273.16)/(t_air-273.16+237.3));


    T_soil(i+1) = (C_1 * (C_2-C_evp*(exp(17.27*T_soil(i)/(T_soil(i)+237.3))-
C_5)) * (k/d) / C_3  + C_1 * C_4 * T_bldg - (C_1 * (k/d) + C_1 * C_4 - C_1 *
(k/d)^2 / C_3  -1) * (T_soil(i)+273.16)) - 273.16;


end
end
```

MATLAB scripts for vegetation-covered soil temperature validation from April to September, 2014:

```
[T_soil] = SolveFunction(1,17568);
T = readtable('vegtemp2014.xlsx');
NewT =[table(T_soil')];
writetable(NewT, 'test8.csv');

function [T_soil]=SolveFunction(start,finish)
A = xlsread('vegtemp2014.xlsx');
v = A(start:finish,1);
len=size(v);
I_solar=A(start:finish,3);
X_f=A(start:finish,8);
Wind=A(start:finish,9);
T_air=A(start:finish,11);
H_c=A(start:finish,13);
T_sky=A(start:finish,15);
RHO_air=A(start:finish,16);
H=A(start:finish,17);
HumRat=A(start:finish,20);



A_solar=0.6;
B=0.0000000567;
d=0.05;
k_s=0.15;
k_f=0.6;
Delta_t=900;
rho_dry=690;
c_w=4180;
c_d=950;
U=0.273;
r_l=360;
R=2430000;
T_bldg=22 + 273.16;
T_soil = 3.722;



for i=1:len

    x_f=X_f(i);
    h_c=H_c(i);
    t_air=T_air(i) + 273.16;
    i_solar=I_solar(i);
    t_sky=T_sky(i)+273.16;
    rho_air=RHO_air(i);
    w=Wind(i);
    h=H(i);
    hr=HumRat(i);
```

```
    C_v=rho_dry*(c_d+x_f*c_w);

    k = k_s*k_f/((1-x_f)*k_f+x_f*k_s);
    E_canopy=0.97;
    h_a=5.4;


    m=[t_sky,t_air];
    t_avg = mean(m);
    C_mean = t_avg^3;
    R_canopy= 1 / ( d/k + 1/h_a);

    C_1= Delta_t / (2 * C_v * d);
    C_2= i_solar * A_solar + 4 * E_canopy * B * C_mean * t_sky + h_c * t_air;
    C_3= h_c + 4 * E_canopy * B * C_mean + R_canopy;
    C_4= 1 / ( d / k + 1 / U);
    C_5= R *((1-h)*rho_air*hr/(r_l+20/(w^0.5)));

    T_soil(i+1) = (C_1 * (C_2-C_5) * R_canopy / C_3 + C_1 * C_4 * T_bldg -
(C_1 * R_canopy + C_1 * C_4 - C_1 * R_canopy^2 / C_3  -1) *
(T_soil(i)+273.16)) - 273.16;


end
end
```

MATLAB scripts for water content validation from April to September, 2014:

```
[w] = SolveFunction(1,17568);
T = readtable('massbalance2014.xlsx');
NewT =[table(w')];
writetable(NewT, 'test1.csv');

function [w]=SolveFunction(start,finish)
A = xlsread('massbalance2014.xlsx');
v = A(start:finish,1);
len=size(v);
Rain=A(start:finish,2);
T_soil=A(start:finish,3);
T_leaf=A(start:finish,4);
Wind=A(start:finish,9);
P=A(start:finish,10);
T_air=A(start:finish,11);
Rho_air=A(start:finish,13);
RH=A(start:finish,14);
DELTA_R=A(start:finish,16);


d=100;
B=0.622;
C_z=0.0015;
LAI=0.5;
w=0.1765;
r_l=360;


for i=1:len
    u=Wind(i);
    t_air=T_air(i);
    t_soil=T_soil(i);
    t_leaf=T_leaf(i);
    delta_r=DELTA_R(i);
    p=P(i);
    rain=Rain(i);
    rho=Rho_air(i);
    rh=RH(i);


    P_wa=rh*6.116441*10^(7.591386*t_air/(t_air+240.7263));
    P_wl=rh*6.116441*10^(7.591386*t_leaf/(t_leaf+240.7263));
    E_soil=rho*C_z*u*0.622/p*0.61078*(exp(17.27*t_soil/(t_soil+237.3))-
exp(17.27*t_air/(t_air+237.3)));
    E_veg=(rho*B*P_wl/(p-P_wl)-rh*rho*B*P_wa/(p-P_wa))/(r_l-46.4/u^0.5);
    E_total=900*((1-LAI)*E_soil+LAI*E_veg);

%     w(i)=rain-E_total-delta_r;

    w(i+1)=(rain-E_total-delta_r)/d+w(i);

end
end
```

MATLAB scripts for bare soil surface temperature in August, 2014:

```
[t_surf] = SolveFunction(1,2976);
T = readtable('soilsurface201408.xlsx');
NewT = [T,table(t_surf)];
writetable(NewT, 'soilsurf201408.csv');

function [t_surf]=SolveFunction(start,finish)
A = xlsread('soilsurface201408.xlsx');
v = A(start:finish,1);
len=size(v);
I_solar=A(start:finish,3);
T_soil=A(start:finish,4);
X_f=A(start:finish,8);
Wind=A(start:finish,9);
P=A(start:finish,10);
T_air=A(start:finish,11);
H_c=A(start:finish,13);
T_sky=A(start:finish,15);
RHO_air=A(start:finish,16);



A_solar=0.60;
B=0.0000000567;
d=0.05;
k_s=0.15;
k_f=0.6;
C_z=0.0015;


t_surf=zeros(len);


for i=1:len
    x_f=X_f(i);
    h_c=H_c(i);
    t_air=T_air(i) + 273.16;
    i_solar=I_solar(i);
    t_soil=T_soil(i)+ 273.16;
    p=P(i)*100;
    u=Wind(i);
    t_sky=T_sky(i)+273.16;
    rho_air=RHO_air(i);



   %soil property%

    k = k_s*k_f/((1-x_f)*k_f+x_f*k_s);
    E_soil=0.93+0.03*x_f;
    R=2430000;
    C_evp=rho_air*C_z*u;
```

```
    m=[t_sky,t_air];
    t_avg = mean(m);
    C_mean = t_avg^3;
    delta_hum=0.622*0.61078/p*(exp(17.27*(t_soil-273.16)/((t_soil-
273.16)+237.3))-exp(17.27*(t_air-273.16)/((t_air-273.16)+237.3)));
    q_evp=R*C_evp*delta_hum;


    num = i_solar * A_solar + 4 * E_soil* B * C_mean* t_sky + h_c * t_air +
k/d * t_soil-q_evp ;
    dem = h_c + 4 * E_soil * B * C_mean + k/d;


    t_surf(i) = num/dem-273.16;


end
end
```

MATLAB scripts for vegetation-covered surface temperature in August, 2014:

```
[t_surf] = SolveFunction(1,2976);
T = readtable('vegsurface201408.xlsx');
NewT = [T,table(t_surf)];
writetable(NewT, 'vegsurf201408.csv');

function [t_surf]=SolveFunction(start,finish)
A = xlsread('vegsurface201408.xlsx');
v = A(start:finish,1);
len=size(v);
I_solar=A(start:finish,3);
T_soil=A(start:finish,4);
X_f=A(start:finish,8);
Wind=A(start:finish,9);
T_air=A(start:finish,11);
H_c=A(start:finish,13);
T_sky=A(start:finish,15);
RHO_air=A(start:finish,16);
H=A(start:finish,17);
HumRat=A(start:finish,20);


A_solar=0.6;
B=0.0000000567;
d=0.05;
k_s=0.15;
k_f=0.6;


r_l=360;
R=2430000;


t_surf=zeros(len);



for i=1:len
    x_f=X_f(i);
    h_c=H_c(i);
    t_air=T_air(i) + 273.16;
    i_solar=I_solar(i);
    t_sky=T_sky(i)+273.16;
    rho_air=RHO_air(i);
    w=Wind(i);
    h=H(i);
    hr=HumRat(i);



   %soil property%

    k = k_s*k_f/((1-x_f)*k_f+x_f*k_s);
```

```
    E_canopy=0.97;
    h_a=5.4;


    m=[t_sky,t_air];
    t_avg = mean(m);
    C_mean = t_avg^3;
    R_canopy= 1 / ( d/k + 1/h_a);


    num = i_solar * A_solar + 4 * E_canopy* B * C_mean* t_sky + h_c * t_air +
R_canopy * (T_soil(i)+273.16)-R * ((1-h) * rho_air * hr /(r_l-
(20/(w^0.52))));

    dem = h_c + 4 * E_canopy * B * C_mean + R_canopy;


    t_surf(i) = num/dem-273.16;



end
end
```

Curriculum Vitae

Jing Hong

PhD Candidate in Architecture, University of Wisconsin-Milwaukee —2018

Master of Science in Architecture, University of Texas at San Antonio —2011

Bachelor of Engineering, Shenyang University of Technology, China—2009